A<u>Development of a statistical model for global burntburned area model tailored for integration into Dynamic Global Vegetation Models</u>simulation within a DGVM-compatible framework

Blessing Kavhu<sup>1,3</sup>. Matthew Forrest<sup>1</sup>, Thomas Hickler<sup>1,2</sup>

<sup>1</sup>Senckenberg Biodiversity and Climate Research Centre (SBiK-F), Frankfurt am Main, Germany.

<sup>2</sup>Institute of Physical Geography, Goethe University Frankfurt am Main, Frankfurt am Main, Germany

<sup>3</sup>Environmental Studies, University of California, Santa Cruz, 1156 High 5th, Santa Cruz, 95064, California, United States.

<sup>4</sup>Finnish Geospatial Research Institute, National Land Survey of Finland, Vuorimiehentie, 02150 Espoo, Finland

Correspondence to: Blessing Kavhu (kavhublessing@gmail.com)

11 12

13

14

15

16

17

18

19

20

21

22

23

24

25

26

27

28

29

30

31 32

Abstract. Fire-enabled Dynamic Global Vegetation Models (DGVMs) play an essential role in predicting vegetation dynamics and biogeochemical cycles amid climate change, but modelling wildfires has been challenging in process-based biophysicsoriented DGVMs, regarding the role of socioeconomic drivers. In this study, we aimed to build a simple global statistical model that incorporates socioeconomic drivers of wildfire dynamics, together with biophysical drivers, tailored for integration within DGVMs.a DGVM-compatible framework. Using monthly burnt area (BA) data formfrom the latest global burned area product from GFED5 as our response variable, we developed Generalized Linear Models (GLMs) to capture the relationships between potential predictor variables (biophysical and socio-economic) that are simulated by DGVMs and/or available in future scenarios. We used predictors that represent aspects of fire weather, vegetation structure and activity, human land use and behavior and topography. Based on an iterative process of choosing various variable combinations that represent potential key drivers of wildfires, we chose a model with minimum collinearity and maximum model performance in terms of reproducing observations. Our results show that the-best performing (deviance explained 56.8%) and yet parsimonious model includes eight socio-economic and biophysical predictor variables encompassing the Fire Weather Index (FWI), a-Monthly Ecosystem Productivity Index (MEPI), Human Development Index (HDI), Population Density (PPN), Percentage Tree Cover (PTC), Percentage Non-Tree Cover (PNTC), Number of Dry Days (NDD), and Topographic Positioning Index (TPI). When keeping the other variables constant (partial residual plots), FWI, PTC, TPI and PNTC were positively related to BA, while MEPI, HDI, PPN, and NDD were negatively related to BA. While the model effectively predicted the spatial distribution of BA (Normalized Mean Error [NME] = 0.72), its standout performance lay in capturing the seasonal variability, especially in regions often characterized by distinct wet and dry seasons, notably southern Africa ( $R^2 = 0.72$  to 0.99), Australia ( $R^2 = 0.68$ ) and South America ( $R^2 = 0.75$  to 0.90). Our model reveals the robust predictive power of fire weather and vegetation dynamics emerging as reliable predictors of these seasonal global fire patterns. Finally, simulations with and without dynamically Formatted: Header

Formatted: Font color: Auto

changing HDI revealed HDI as an important driver of the observed global decline in BA. The model presented should be compatible with most, if not all, DGVMs used to develop future scenarios.

# 1 Introduction

33

34

35 36

37

38

39

40

41

42

43

44

45

46

47

48

49

50

51

52

53

54

55

56

57 58

59

60 61

62

63

Globally, the impacts of climate change continue to manifest through extreme weather events and changes in weather patterns (Clarke et al., 2019). Notably, climate change has led to more severe fire weather in large parts of the world and record fires have recently occurred in Australia and Canada, burning more than 15 million and 7 million ha (Jain et al., 2024; MacCarthy et al., 2024). Even though the effects of fires may be positive through contributing to selected natural ecosystem processes, large and frequent fires are often destructive and have far-reaching effects through loss of life, biodiversity, landscape aesthetic value, and increase in forest fragmentation and soil erosion (Bowman et al., 2017; Knorr et al., 2016; Nolan et al., 2022). The negative role of climate change in driving large and frequent burning has been well documented (Brown et al., 2023). However, climate change by itself does not fully account for the recent changes in global wildfire patterns as human activities are crucial drivers as well (Pausas and Keeley, 2021). For instance, recent empirical investigations have highlighted a notable 25% reduction in burnt area extent over the past two decades, explicitly attributing this decline to human activities (Andela et al., 2017). Wu et al. (2021) argue that future demographic and climate patterns will cause an increase in burnt areas, particularly in high latitude warming and tropical regions. However, Knorr et al. (2016) concluded that, under a moderate emissions scenario, global burnt areas will continue to decline, but they will begin to rise again around mid-century with high greenhouse gas emissions. Cunningham et al. (2024), on the other hand reported that although total burnt area is declining globally, extreme fire events are increasing as consequence of climate change especially in boreal and temperate conifer biomes. Future global fire dynamics are clearly driven by the overarching interaction between human activities (altered ignition patterns, surveill ance and management) and climate (Krawchuk et al., 2009). Accurately evaluating these factors through modelling could guide prescribing solutions that will ensure reliable fire management and attainment of Sustainable Development Goals (SDGs) (Koubi, 2019; Robinne et al., 2018).

Modelling continues to be an essential tool for comprehending and forecasting wildfire dynamics, founded on the intricate interplay among fire weather, vegetation, and human activities (Bistinas et al., 2014; Hantson et al., 2016). Models for wildfire can be process based or statistical. While process based models delve into the physics and dynamics of wildfires and vegetation, statistical models, on the other hand, tend to focus on analyzing historical data and identifying correlations to predict future wildfire events (Morvan, 2011; Xi et al., 2019). Process based models such as fire enabled DGVMs stand out in understanding interactions between climate, vegetation, and human activities in a mechanistic manner (Hantson et al., 2016;

Rabin et al., 2017). However, their predictive skill is often not yet satisfactory (Hantson et al., 2020). The predictive skill of process based models is often limited due to incomplete representation of fire drivers, uncertainty in parameterization, and difficulties in accurately simulating human fire interactions (Archibald, 2016; DeWilde and Chapin, 2006; Hantson et al., 2020). Hence statistical approaches have often been used to evaluate human impacts on wildfires, in combination with weather and vegetation drivers (Haas et al., 2022; Kuhn-Régnier et al., 2021). Statistical approaches can effectively quantify and evaluate empirical relationships between fire occurrences and diverse predictors, providing flexibility in handling diverse data from multiple spatial and temporal scales. However, some authors reported that the application of statistical models for ecosystems other than the ones used in their derivation is often not reliable (e.g. Perry, 1998). This is mainly because statistical models assume that the relationship between predictors and responses is stationery and context dependent, which is not typical of fires that are stochastic in nature. Integration of mechanistic process-based techniques and statistical methods remains one common way forward to advance our understanding of fire dynamics.

The integration of DGVMs and statistical models increasingly benefits from remote sensing data (Dantas De Paula et al.,

75 76

64

65

66

67

68

69

70

71

72

73

74

77 2020). Remote sensing provides spatially explicit observations, such as vegetation cover, leaf area index (LAI), and biomass, 78 which are used to initialize, calibrate, and validate DGVM simulations (Yang et al., 2020). Meanwhile, statistical models help 79 correct biases in DGVM outputs and enhance predictions by combining empirical relationships with mechanistic model results. 80 This integration enables more reliable modelling of global wildfires, offering a macroscopic perspective, and allowing 81 researchers to analyze large scale patterns across diverse ecosystems (Doerr and Santín, 2016; Flannigan et al., 2009). The 82 strength of modelling fires at a global scale lies in its ability to capture overarching patterns (spatial, seasonal and inter-annual) that might provide valuable insights for strategic wildfire control. While one can argue about the potential oversimplification

83 84 of local factors and the challenges in representing fine scale heterogeneity, global models do, on the other hand, excel in

85 capturing and understanding the effect of climate change, partly because they capture large climatic gradients (Robinne et al., 86 2018). The ability to capture the interconnectedness of ecosystems and fire regimes on a planetary scale contributes to a more

87 88 As such, studies on evaluating drivers of burnt areas at a global scale in the face of ongoing climatic shifts are crucial in 89 ensuring sustainable management of vulnerable ecosystems.

90 91

92

93

94

#### 1 Introduction

Globally, the impacts of climate change continue to manifest through extreme weather events and changes in weather patterns (Clarke et al., 2019). In Australia, the mean annual burned area in forested regions was about 1.8 million ha per year between

holistic approach to understanding global vegetation dynamics and carbon cycling (Bowman et al., 2013; Kelly et al., 2023).

1988-2001, increasing to 3.5 million ha per year between 2002-2018, before the 2019-2020 "Black Summer" fires burned over 15 million ha nationally (Australian Government, 2020; Canadell et al., 2021). Similarly, in Canada, the 1986–2022 mean annual burned area was about 2.1 million ha, compared with the record-breaking 15 million ha burned in 2023 (Curasi et al., 2024; Jain et al., 2024; MacCarthy et al., 2024). These multi-decadal increases in burned area in both countries are consistent with evidence that climate change has intensified fire-conducive weather over time. Even though the effects of fires may be positive through contributing to selected natural ecosystem processes, large and frequent fires are often destructive and have far-reaching effects through loss of life, biodiversity, landscape aesthetic value, and increase in forest fragmentation and soil erosion (Bowman et al., 2017; Knorr et al., 2016; Nolan et al., 2022). The negative role of climate change in driving large and frequent burning has been well documented (Brown et al., 2023). However, climate change by itself does not fully account for the recent changes in global wildfire patterns as human activities are crucial drivers as well (Pausas and Keeley, 2021). For instance, recent empirical investigations have highlighted a notable 25% reduction in burnt area extent over the past two decades, explicitly attributing this decline to human activities (Andela et al., 2017). Wu et al. (2021) argue that future demographic and climate patterns will cause an increase in burnt areas, particularly in high latitude warming and tropical regions. However, Knorr et al. (2016) concluded that, under a moderate emissions scenario, global burnt areas will continue to decline, but they will begin to rise again around mid-century with high greenhouse gas emissions. Cunningham et al. (2024), on the other hand reported that although total burnt area is declining globally, extreme fire events are increasing as consequence of climate change especially in boreal and temperate conifer biomes. Future global fire dynamics are clearly driven by the overarching interaction between human activities (altered ignition patterns, surveillance and management) and climate (Krawchuk et al., 2009). Accurately evaluating these factors through modelling could guide prescribing solutions that will ensure reliable fire management and attainment of Sustainable Development Goals (SDGs) (Koubi, 2019; Robinne et al., 2018).

115 116 117

118

119

120

121

122

123

124

125

126

127

128

129

130

95

96

97

98

99

100

101

102

103

104

105

106

107

108

109

110

111

112

113

114

Modelling continues to be an essential tool for comprehending and forecasting wildfire dynamics, founded on the intricate interplay among fire weather, vegetation, and human activities (Bistinas et al., 2014; Hantson et al., 2016). Models for wildfire can be process-based or statistical. While process-based models delve into the physics and dynamics of wildfires and vegetation, statistical models, on the other hand, tend to focus on analyzing historical data and identifying correlations to predict future wildfire events (Morvan, 2011; Xi et al., 2019). Process-based models such as fire-enabled DGVMs stand out in understanding interactions between climate, vegetation, and human activities in a mechanistic manner (Hantson et al., 2016; Rabin et al., 2017). However, their predictive skill is often not yet satisfactory (Hantson et al., 2020). The predictive skill of process-based models is often limited due to incomplete representation of fire drivers, uncertainty in parameterization, and difficulties in accurately simulating human-fire interactions (Archibald, 2016; DeWilde and Chapin, 2006; Hantson et al., 2020). Hence statistical approaches have often been used to evaluate human impacts on wildfires, in combination with weather and vegetation drivers (Haas et al., 2022; Kuhn-Régnier et al., 2021). Statistical approaches can effectively quantify and evaluate empirical relationships between fire occurrences and diverse predictors, providing flexibility in handling diverse data from multiple spatial and temporal scales. However, some authors reported that the application of statistical models for ecosystems other than the ones used in their derivation is often not reliable (e.g. Perry, 1998). This is mainly because statistical

models assume that the relationship between predictors and responses is stationery and context dependent, which is not typical of fires that are stochastic in nature. Integration of mechanistic process-based techniques and statistical methods remains one common way forward to advance our understanding of fire dynamics.

The integration of DGVMs and statistical models increasingly benefits from remote sensing data (Dantas De Paula et al., 2020). Remote sensing provides spatially explicit observations, such as vegetation cover, leaf area index (LAI), and biomass, which are used to initialize, calibrate, and validate DGVM simulations (Yang et al., 2020). Meanwhile, statistical models help correct biases in DGVM outputs and enhance predictions by combining empirical relationships with mechanistic model results. This integration enables more reliable modelling of global wildfires, offering a macroscopic perspective, and allowing researchers to analyze large-scale patterns across diverse ecosystems (Doerr and Santín, 2016; Flannigan et al., 2009). The strength of modelling fires at a global scale lies in its ability to capture overarching patterns (spatial, seasonal and inter-annual) that might provide valuable insights for strategic wildfire control. While one can argue about the potential oversimplification of local factors and the challenges in representing fine-scale heterogeneity, global models do, on the other hand, excel in capturing and understanding the effect of climate change, partly because they capture large climatic gradients (Robinne et al., 2018). The ability to capture the interconnectedness of ecosystems and fire regimes on a planetary scale contributes to a more holistic approach to understanding global vegetation dynamics and carbon cycling (Bowman et al., 2013; Kelly et al., 2023). As such, studies on evaluating drivers of burnt areas at a global scale in the face of ongoing climatic shifts are crucial in ensuring sustainable management of vulnerable ecosystems.

There is a growing recognition of the significance of exploring both inter-annual and seasonal variations to comprehensively understand the dynamics of fire across diverse ecosystems (Dwyer et al., 2000), (Dwyer et al., 2000), partly because of the strong seasonal dynamics of vegetation. Also, understanding seasonal cycles of fires helps to identify peak fire seasons, regions prone to seasonal outbreaks, potential shifts in fire regimes over time and facilitating adaptive management strategies (Carmona-Moreno et al., 2005). (Carmona-Moreno et al., 2005). Incorporating monthly data in global fire modelling helps researchers to accurately capture seasonal variations in fire activity. Hence, global models developed using monthly data are necessary.

Recent efforts have seen global burnt area models based on Convolution Neural Network (CNN)(Bergado et al., 2021), Random Forest (RF) and generalized additive models (GAM)(Chuvieco et al., 2021) which are currently not easily integrated into DGVMs, although we note that recent work from Son et al. (2024)

Recent efforts have seen global burnt area models based on Convolution Neural Network (CNN: Bergado et al., 2021), Random\*
Forest (RF) and Generalized Additive Models (GAM) (Chuvieco et al., 2021) which are currently not easily integrated into DGVMs, although we note that recent work from Son et al. (2024) is an important step towards integration of an advanced recursive neural network in a DGVM. GLMs are easier to implement into DGVMs, and their partial residual plots show the relationships of each predictor with the response variable when all other drivers are kept constant, which facilitates a discussion of potential underlying mechanisms. The risk of overfitting can be minimized by only choosing potential driver variables that

Formatted: Line spacing: Multiple 1,36 li

Formatted: Line spacing: Multiple 1,36 li

are mechanistically expected to play an important role and by choosing only a limited number of uncorrelated driver variables. Accordingly, Haas et al. (2022) Accordingly, Haas et al. (2022) developed a GLM for global burnt area with good model skill but without accounting for seasonal dynamics and without a focus on driver variables that can be predicted with DGVMs. Generally, most earlier fire modules in DGVMs such as the LPJ-LMfireLmfire (v1) were informally parameterized to predict seasonal fire cycles and do not consider the fuller range of predictors available in a more rigorous statistical framework (Fosberg et al., 1999; Pfeiffer et al., 2013). Nurrohman, et al., (2024)(Fosberg et al., 1999; Pfeiffer et al., 2013). Nurrohman et al. (2024) produced monthly fire predictions from downscaling of annual model outputs without building a statistical approach that is calibrated trained based on monthly inputs. This left an opportunity to improve burnt area models in DGVMs to accurately represent the detailed seasonal dynamics. To our knowledge, there haven't been any reports on a simpler and more efficient statistical model specifically crafted to capture the seasonal cycles of global burnt areas, while also being easily integrated into DGVMs. Closing this gap can best be facilitated by developing a statistical model based on variables pertinent to fire modelling, with the goal to later integrate it into DGVMs. This integration can efficiently enhance our comprehension of inadequately understood factors while leveraging the potential of finely detailed temporal resolution burnt area datasets.

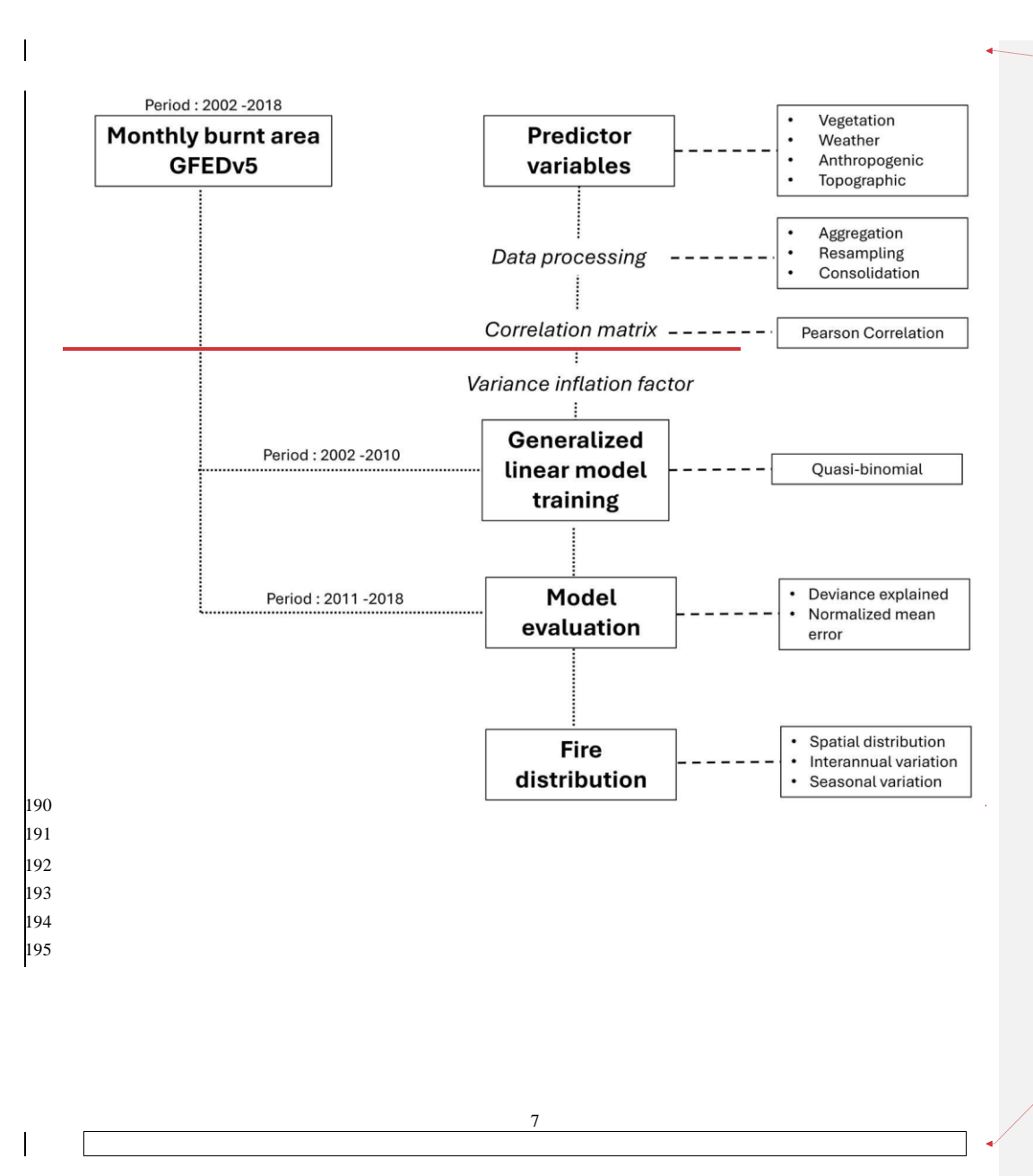
The main aim of this research is to build a parsimonious statistical model for global seasonal burnt areas that can be integrated into a DGVM. The specific objectives are to 1) to improve our understanding of major drivers of global burnt area dynamics, 2) to leverage a GLM for predicting global burnt areas using DGVM-integrablecompatible predictors and 3) to evaluate the interannual and seasonal cycles of burnt area extent, both globally and regionally.

#### 2 Data and Methods

In this study, we used GLM to assess the drivers and distribution of global wildfires based on a combination of vegetation, weather, anthropogenic and topographic predictors. The spatial and temporal variability (interannual and seasonality) was also evaluated. Fig. 1 provides an overview of the steps that were followed during modelling.

Formatted: Line spacing: 1,5 lines, Don't keep with i

Formatted: Line spacing: Multiple 1,36 li



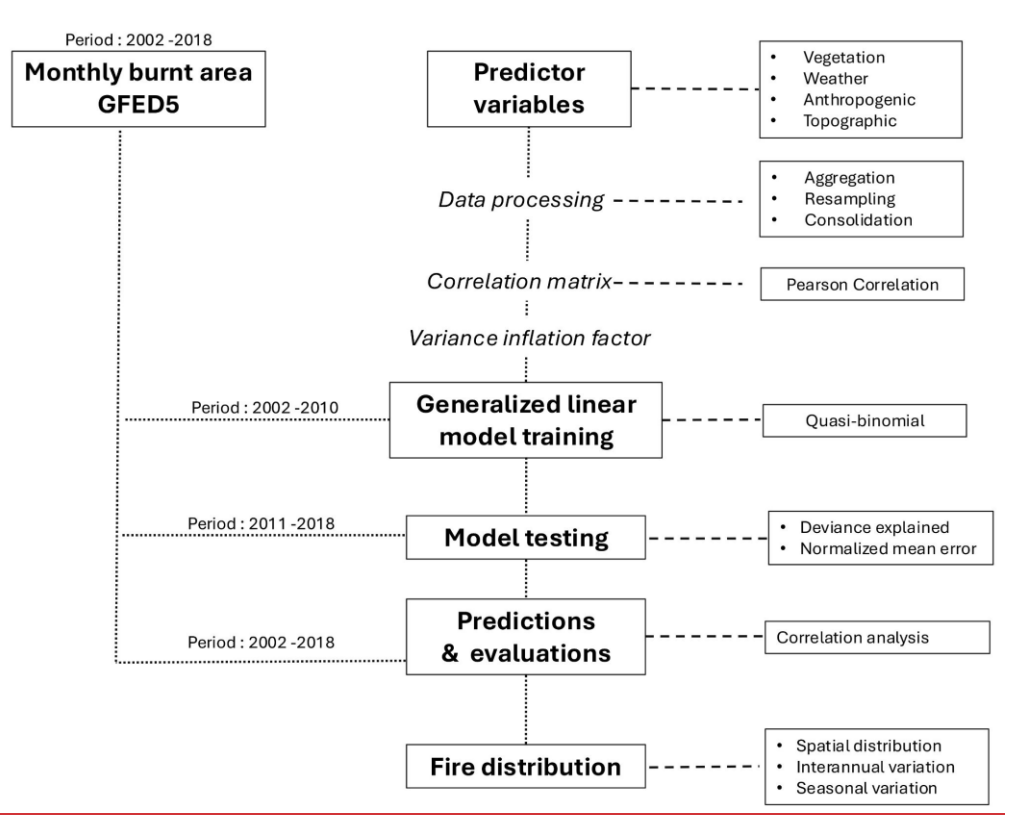


Figure 1: Study workflow showing an overview of steps followed in model ealibration training, testing, prediction and evaluation together with the outputs and time periods.

## 2.1 Fire data

196 197

198

199

200

201

202

203

204

205

Monthly BA data for the periodsperiod 2002 and 2018 were derived from monthly mean fractional BA from the GFED5. We selected this data because of their improved ability to detect burnt area scars (Chen et al., 2023). (C

8

Formatted: Header

Formatted: Line spacing: Multiple 1,36 li

Formatted: Line spacing: 1,5 lines, Don't keep with I

Formatted: Line spacing: Multiple 1,36 li

lands. We used data for the period 2002 to 2010 for model training and data for 2011 to 2018 for model testing. The BA data comes at a resolution of  $0.25^{\circ} \times 0.25^{\circ}$ , therefore we aggregated it by a factor of 2 to a resolution of  $0.5^{\circ}$ . This was done for ease of processing at a global scale and at the same time to ensure that our outputs are DGVM integrable since they are commonly applied at  $0.5^{\circ}$  globally.

#### 2.2 Predictor variables

206 207

208

209

210

211

212

213

214

215

216

217

218

219

220

221

222 223 In this study, we only used variables which don't prohibit the use of the model for future projections. Whilst there are many possible variables that could be tried as predictors of fire, especially in terms of socioeconomics predictors, we restricted our selection to variables where: climate and vegetation variables typically available in a DGVM framework; socioeconomic variables with future scenario projections; and time-invariant topographic variables. Previous studies used several variables that we couldn't include due to lack of future scenario projections such as nighttime lights, cattle density (Forkel et al., 2019a), Vegetation optical depth (Forkel et al., 2019b), Lightning (Rabin et al., 2017), Soil moisture (Mukunga et al., 2023), soil fertility (Aldersley et al., 2011). Consequently, we considered predictor variables that are compatible with DGVM integration to calibrate 2019), vegetation optical depth (Forkel et al., 2019), lightning (Rabin et al., 2017), soil moisture (Mukunga et al., 2023), soil fertility (Aldersley et al., 2011). Consequently, we considered predictor variables that are compatible with DGVM integration to train the model effectively. The chosen predictor variables were categorized based on their representational nature and their roles in fire modelling (See Table 1).

Predictor	Abbreviations	Classification category (Climate, vegetation, landcover, landscape fragmentation,	Original spatial resolution	Temporal resolution	Temporal coverage	Source
		ignition, suppression topographic effect)				
Percentage Grass cover	PGC	Vegetation	300m	Annual	2002-2018	ESA CCI landcoverESA Climate Change Initiative landcover(UC Louvain, 2017)

Formatted: Header

Formatted: Line spacing: 1,5 lines, Don't keep with i

Formatted: Line spacing: Multiple 1,36 li

Formatted: Line spacing: Multiple 1,15 li

Inserted Cells

Formatted: Line spacing: Multiple 1,15 li

Formatted: Font: Not Bold, Italic

Formatted: Line spacing: Multiple 1,15 li

Formatted: Line spacing: Multiple 1,15 li

Percentage non-tree vegetation cover PNTC		category (Climate vegetation, landcover, landscape fragmentation, ignition, suppression topographic effect).  Vegetation	resolution	Temporal resolution  Annual	Temporal coverage 2002-2018	MODIS - MOD44B (DiMiceli et al., 2011)
Topographic positioning index		Topography	90m	Static	2010 (product of the global GMTED20 10)	Digital elevation model products of global 250 m GMTED2010 (GMTE data 2010) and near-global 90 m SRTM v4 (Jarvis et al., 2008)
Predictor			Original spatia resolution	Temporal	Predictor	
Human Development Index	HDI	Ignition/suppression/ ragmentation	f subnational	Annual	2002-2018	Global data lab (Smits and Permanyer, 2019)
Road density	oad density RD Ignition/suppression/ragmentation		f 0.5° × 0.5°	Static	Average of the period 1979-2015	Global Roads Inventory Project (GRIP) database (Meijer et al., 2018)

Formatted: Header
Inserted Cells
Formatted: Line spacing: Multiple 1,15 li
Formatted: Line spacing: Multiple 1,15 li
Formatted: Font: Not Bold, Italic
Formatted: Swedish (Sweden)
Formatted: Line spacing: Multiple 1,15 li

Formatted: Line spacing: Multiple 1,15 li
Inserted Cells

Formatted: Line spacing: Multiple 1,15 li

Formatted: Line spacing: Multiple 1,15 li

Formatted: Line spacing: Multiple 1,15 li

Population density	PPN	Ignition/suppression/f		5-year	2000,	Socioeconomi
		ragmentation	minutes	intervals	2005,	c data and
					2010,2015	applications
						centre
						(SEDAC)
						(Klein
						Goldewijk et
						al., 2017)
Percentage crop	PCC	Fragmentation	5 arc minutes	Annual	2002-2018	HistorY •
cover						<del>Database of</del>
						the Global
						Environment
						(HYDE 3.3)
						(Klein
						<del>Goldewijk et</del>
						<del>al.,</del>
						<del>2017)</del> HistorY
						<u>Database</u> of
						the Global
						<u>Environment</u>
						(HYDE
						3.3)(Klein
						Goldewijk et
						<u>al., 2017)</u>
Percentage pasture	PPS	Vegetation	5 arc minutes	Annual	2002-2018	HistorY
cover						<del>Database of</del>
						the Global
						Environment
						<del>(HYDE</del>
						3.3)(Klein
						Goldewijk et
						<del>al.,</del>
						2017)HistorY
						Database of
						the Global
						<u>Environment</u>
						(HYDE
						3.3)(Klein
						Goldewijk et
						<u>al., 2017)</u>

Formatted: Line spacing: Multiple 1,15 li

Formatted: Line spacing: Multiple 1,15 li

Formatted: Line spacing: Multiple 1,15 li

Formatted: Font color: Auto

Formatted: Line spacing: Multiple 1,15 li

Formatted: Header

**Formatted:** Line spacing: Multiple 1,15 li **Formatted:** Line spacing: Multiple 1,15 li

								Formatted: Header
Precipitation	PS	Climate	$0.5^{\circ} \times 0.5^{\circ}$	Annual	2002-2018	Copernicus		Formatted: Line spacing: Multiple 1,15 li
seasonality						<del>climate</del> data		Formatted: Line spacing: Multiple 1,15 li
						store		
ļ						(Copernicus		
						Climate Change		
ļ						Service		
ļ						2018)Coperni		
						cus climate		
ļ						data store		
ļ						(Copernicus		
						Climate		
						Change		
ļ						<u>Service</u> , 2021)		
Fire weather index	FWI	Climate	$0.5^{\circ} \times 0.5^{\circ}$	Monthly	2002-2018	Copernicus		Formatted: Line spacing: Multiple 1,15 li
						<del>climate</del> data		Formatted: Line spacing: Multiple 1,15 li
						store		(
ļ						(Copernicus		
						Climate		
ļ						Change Service		
						2018)Coperni		
						cus climate		
						data store		
ļ						(Copernicus		
						Climate		
ļ						Change		
						Service, 2021)		
Precipitation of the	PPNQ	Climate	$0.5^{\circ} \times 0.5^{\circ}$	Annual	2002-2018	Copernicus		Formatted: Line spacing: Multiple 1,15 li
driest quarter						climate data		
						store		
						(Copernicus		
						Climate		
						Change Service 2018)		
						(Copernicus		
						<u>Climate</u>		Formatted: Line spacing: Multiple 1,15 li
						<u>Change</u>		
						Service, 2021)		
	l			1	l .		ı	

12

Number of dr days	y NDD PGZC	Climate	$0.5^{\circ} \times 0.5^{\circ}$	Annual	2002-2018	Copernicus climate data store (Copernicus Climate Change Service 2018)Coperni cus climate data store (Copernicus Climate change Service, 2021) HistorY
Percentage grazeland cover	PGZC	Vegetation	3 arc minutes	Annuai	2002-2018	Histor Y Database of the Global Environment (HYDE 3.3) (Klein Goldewijk et al., 2017) Histor Y Database of the Global Environment (HYDE 3.3) (Klein Goldewijk et al., 2017)
Predictor 2	: :	Classification category (Climate, vegetation, landcover, landscape fragmentation, ignition, suppression topographic effect)	Original spatial resolution	Temporal	Predictor	

Formatted: Line spacing: Multiple 1,15 li

Formatted: Line spacing: Multiple 1,15 li

Formatted: Header

Formatted: Line spacing: Multiple 1,15 li
Formatted: Line spacing: Multiple 1,15 li

Annual average AAP Climate 5 arc minutes Annual 2002-2018  Annual average recipitation  Annual average recipitation  AAP Climate 5 arc minutes Annual 2002-2018  Annual average recipitation  Annual average recipitation  AAP Climate 5 arc minutes Annual 2002-2018  Copernicus climate data store (Copernicus Climate Change Service 2018)Copernicus climate Change Service 2018/Copernicus climate data store (Copernicus Climate Change Service 2018)Copernicus climate data stor									
Annual average AAP  Climate  S are minutes  Annual 2002-2018  Annual average recipitation  Annual average recipitation  Annual average of the Global Environment (HYDE 3.3) (Klein Global Environmen									Formatted: Header
Annual average AAP  Climate  5 are minutes  Annual 2002-2018  Annual average recipitation  Cross primary  GPP  Vegetation  OSS NOSS  AGB  Vegetation  OSS NOSS  AGB  Vegetation  OSS NOSS  Longterm average  AGB  Vegetation  AGG  AGG  AGG  AGG  AGG  AGG  AGG  A	Percentage	PRC	Vegetation	5 arc minutes	Annual	2002-2018	HistorY		Inserted Cells
Annual average AAP Climate 5 arc minutes Annual 2002-2018 Copernicus (HYDE 3.3)K(kein Goldewijk et ein, 2017)History Database of the Global Environment (HYDE 3.3)K(kein Goldewijk et ein, 2017)History Database of the Global Environment (HYDE 3.3)K(kein Goldewijk et ein, 2017)History Database of the Global Environment (HYDE 3.3)K(kein Goldewijk et ein, 2017)History Database of the Global Environment (HYDE 3.3)K(kein Goldewijk et ein, 2017)History Database of the Global Environment (HYDE 3.3)K(kein Goldewijk et ein, 2017)History Database of the Global Environment (HYDE 3.3)K(kein Goldewijk et ein, 2017)History Database of the Global Environment (HYDE 3.3)K(kein Goldewijk et ein, 2017)History Database of the Global Environment (HYDE 3.3)K(kein Goldewijk et ein, 2017)History Database of the Global Environment (HYDE 3.3)K(kein Goldewijk et ein, 2017)History Database of the Global Environment (HYDE 3.3)K(kein Goldewijk et ein, 2017)History Database of the Global Environment (HYDE 3.3)K(kein Goldewijk et ein, 2017)History Database of the Global Environment (HYDE 3.3)K(kein Goldewijk et ein, 2017)History Database of the Global Environment (HYDE 3.3)K(kein Goldewijk et ein, 2017)History Database of the Global Environment (HYDE 3.3)K(kein Goldewijk et ein, 2017)History Database of the Global Environment (HYDE 3.3)K(kein Goldewijk et ein, 2017)History Database of the Global Environment (HYDE 3.3)K(kein Global Environment (	rangeland cover								
Annual average AAP Climate 5 arc minutes Annual 2002-2018  Annual average recipitation  Annual average recipitation  Climate 5 arc minutes Annual 2002-2018  Annual average recipitation  Annual average recipitation  Climate 5 arc minutes Annual 2002-2018  Annual average recipitation  Copernicus climate data store (Copernicus Climate Change Service 2018) Copernicus climate data store (Copernicus Climate Change Service 2018) Copernicus climate data store (Copernicus Climate Change Service 2018) Copernicus Climate Change Service 2018 Copernicus Climate Change Service 2021 Copernicus Change Change Cha									
Annual average crecipitation  Annual average precipitation  AAP  Climate  5 arc minutes  Annual  2002-2018  Cimate  Copernicus  Climate  Change Service 2013/ROpernicus  Climate Change Service 2013/Ropernicus  Climate Change Service 2013/Ropernicus  Climate Change Service 2013/Ropernicus  Climate Change Service 2013/Ropernicus  Climate Change Inserted Cells  Formatted: Line spacing: Multiple 1,15 li  Climate Change Inserted Cells  Formatted: Line spacing: Multiple 1,15 li  Climate Change Inserted Cells  Formatted: Line spacing: Multiple 1,15 li  Climate Change Inserted Cells									Formatted: Line spacing: Multiple 1,15 II
Annual average AAP Climate 5 arc minutes Annual 2002-2018									
Annual average AAP Climate 5 arc minutes Annual 2002-2018 Copernicus Climate Change Service 2018/Copernicus Climate Change Chan							× .		
Annual average AAP Climate 5 are minutes Annual 2002-2018 Copernicus climate Change Service 2018/Copernicus Climate Change Service 2019/2002 2018 Aboveground AGB Vegetation 0.5° × 0.5° Longterm average  Database of the Global Environment (HYDE 3.3)tKlein Goldewijk et al., 2017 Formatted: Line spacing: Multiple 1,15 li Inserted Cells									
Annual average recipitation  Annual average recipitation  Climate  5 arc minutes  Annual  2002-2018  Copernicus elimate data store (Copernicus Climate Change Service 2018) Copernicus climate data store (Copernicus Climate Change Service)  (Copernicus Climate Change Serv							2017)HistorY		
Annual average recipitation  Annual average recipitation  Annual average recipitation  Climate  5 arc minutes  Annual  2002-2018  Cepernicus elimate—data store (Copernicus Climate Change Service 2018/Copernicus Climate data store (Copernicus Climate Change Service 2018/Copernicus Climate Change Service 2019/2002 2018  Aboveground  AGB  Vegetation  0.5° × 0.5°  Longterm average  2010  JSA Biomass  Climate Change Inserted Cells  Formatted: Line spacing: Multiple 1,15 li Inserted Cells  Formatted: Line spacing: Multiple 1,15 li Inserted Cells  Formatted: Line spacing: Multiple 1,15 li Inserted Cells									
Annual average recipitation  AAP  Climate  5 arc minutes  Annual  2002-2018  Copernicus climate data store (Copernicus Climate Change Service 2011)  Gross primary orductivity  Gross primary orductivity  Gross primary orductivity  ABO Vegetation  AGB  Vegetation  O.5° × 0.5°  ABO Vegetation  O.5° × 0.5°  ABO Vegetation  O.5° × 0.5°  Longterm average  AAP  Climate  Change Service 2021  ABOUT7A2H  Goriginally (originally Rand—Than and Than and									
Annual average AAP Climate 5 arc minutes Annual 2002-2018 Copernicus climate data store (Copernicus Climate Change Service, 2021)  Gross primary GPP Vegetation 0.5° × 0.5° Longterm average AGB Vegetation 0.5° × 0.5° Longterm average AGB Vegetation 0.5° × 0.5° Longterm average Change Change AGB Vegetation 0.5° × 0.5° Longterm average Change Chan							·		
Annual average precipitation  AAP  Climate  5 arc minutes  Annual  2002-2018  Copernicus climate data store (Copernicus Climate  Change Service 2018)Coperni cus climate data store (Copernicus Climate  Change Service 2018)Coperni cus climate data store (Copernicus Climate Change Service 2018)Coperni cus climate data store (Copernicus Climate Change Service 2018)Coperni cus climate data store (Copernicus Climate Change Service 2021)  ABOUTA2H (Running and Zhao, 2019)2002- 2018  ABOVeground AGB  Vegetation  O.5° × 0.5°  Longterm average  AGB  Vegetation  O.5° × 0.5°  Longterm average  AGB  Formatted: Line spacing: Multiple 1,15 li  Formatted: Line spacing: Multiple 1,15 li  Inserted Cells  Formatted: Line spacing: Multiple 1,15 li  Inserted Cells  Formatted: Line spacing: Multiple 1,15 li  Inserted Cells									
Annual average precipitation  Annual average precipitation  AAP  Climate  5 are minutes  Annual  2002-2018  Copernieus climate data store (Copernieus Climate Change Service 2018) Copernieus Climate Change Service 2018 (Running and Zhao, 2019) 2021  Aboveground  AGB  Vegetation  O.5° × 0.5°  Longterm average  AGB  Vegetation  O.5° × 0.5°  Longterm average  AGB  Vegetation  O.5° × 0.5°  Longterm average  AGB  Formatted: Line spacing: Multiple 1,15 li  Inserted Cells  Formatted: Line spacing: Multiple 1,15 li  Inserted: Line spacing: Multiple 1,15 li  Inserted Cells									
Gross primary oroductivity  GPP  Vegetation  O.5° × Monthly originally 8 days)  Aboveground piomass  AGB  Vegetation  O.5° × 0.5°  Longterm average  AGB  Vegetation  O.5° × 0.5°  Longterm average  Formatted: Line spacing: Multiple 1,15 li  Inserted Cells  Formatted: Line spacing: Multiple 1,15 li  Inserted: Line spacing: Multiple 1,15 li  Inserted: Line spacing: Multiple 1,15 li  Formatted: Line spacing: Multiple 1,15 li  Inserted: Line spacing: Multiple 1,15 li  Inserted: Line spacing: Multiple 1,15 li  Formatted: Line spacing: Multiple 1,15 li  Inserted: Line spacing: Multiple 1,15 li  Formatted: Line spacing: Multiple 1,15 li  Formatted: Line spacing: Multiple 1,15 li  Formatted: Line spacing: Multiple 1,15 li  Inserted Cells									
Store (Copernicus Climate Change Service 2018)Coperni cus climate data store (Copernicus Climate Change Service 2018)Coperni cus climate data store (Copernicus Climate Change Service 2021)  Gross primary GPP Vegetation 0.5° × Monthly originally 8 days)  Aboveground piomass  AGB Vegetation 0.5° × 0.5° Longterm average  AGB Vegetation 0.5° × 0.5° Longterm average  Store (Copernicus Climate Change Service 2021)  MOD17A2H (Running and Zhao, 2019)2002- 2019  GF(Running and Zhao, 2019)2002- 2019  ESA Biomass Climate Change Initiative v4 (Santoro and Service 2019)	_	AAP	Climate	5 arc minutes	Annual	2002-2018			Formatted: Line spacing: Multiple 1,15 li
Gross primary productivity  GPP  Vegetation  0.5° × 0.5°  Aboveground piomass  AGB  Vegetation  0.5° × 0.5°  Climate Change Service 2018)Coperni cus climate data store (Copernicus Climate Change Service, 2021)  Rooting Change Service, 2021  Rooting Change Serv	precipitation								Formatted: Line spacing: Multiple 1,15 li
Climate Change Service 2018/Coperni cus climate data store (Copernicus Change Service, 2021)  Gross primary oroductivity  GPP Vegetation  O.5° — × Monthly (Originally Running and Zhao, 2019)2002-2018  Aboveground piomass  AGB Vegetation  O.5° × 0.5° Longterm average  AGB Vegetation  O.5° × 0.5° Longterm average  Climate Change Service 2021)  MOD17A2H (Running and Zhao, 2019)2002-2018  Formatted: Line spacing: Multiple 1,15 li Inserted Cells  Formatted: Line spacing: Multiple 1,15 li Inserted Cells									
Service 2018)Coperni cus climate data store (Copernicus Climate Change Service, 2021) Gross primary oroductivity  GPP  Vegetation  0.5° × Monthly (originally 8 days)  Aboveground promass  AGB  Vegetation  0.5° × 0.5°  Longterm average  AGB  Vegetation  0.5° × 0.5°  Longterm average  AGB  Formatted: Line spacing: Multiple 1,15 li Inserted Cells  Formatted: Line spacing: Multiple 1,15 li Inserted: Line sp									
Gross primary oroductivity  GPP  Vegetation  O.5° × Monthly (originally 8 days)  Aboveground piomass  AGB  Vegetation  O.5° × 0.5°  Longterm average  AGB  Vegetation  O.5° × 0.5°  Longterm average  AGB  Vegetation  O.5° × 0.5°  Longterm average  Climate data store (Copernicus Climate data store) (Copernicus Climate Climate Change Inserted: Line spacing: Multiple 1,15 limate Change Initiative v4 (Santoro and Change Init									
Gross primary oroductivity  GPP  Vegetation  O.5° × Monthly (originally 8 days)  Aboveground piomass  AGB  Vegetation  O.5° × 0.5°  Longterm average  O.5° × 0.5°  Longterm average  Climate Change Service, 2021)  (originally (originally 8 days)  AGB  Vegetation  O.5° × 0.5°  Longterm average  Climate Change Initiative v4 (Santoro and Change Init							Service		
Gross primary oroductivity  GPP  Vegetation  O.5° \times Monthly (originally 8 days)  Aboveground originals  AGB  Vegetation  O.5° \times 0.5° \times									
Gross primary oroductivity  GPP  Vegetation  O.5° × Monthly (originally 8 days)  Aboveground piomass  AGB  Vegetation  O.5° × 0.5°  Longterm average  O.5° × 0.5°  O.5°									
Gross primary oroductivity  GPP  Vegetation  O.5° × Monthly (originally 8 days)  Aboveground biomass  AGB  Vegetation  O.5° × 0.5°  Longterm average  O.5° × 0.5°  Longterm average  Climate Change Service, 2021)  (originally (Running and Zhao, 2019)2002- 2018  Longterm average  Formatted: Line spacing: Multiple 1,15 li  Inserted Cells  Formatted: Line spacing: Multiple 1,15 li  Inserted: Line spacing: Multiple 1,15 li  Formatted: Line spacing: Multiple 1,15 li  MOD17A2H (Running and Zhao, 2021)  Climate Change Initiative v4 (Santoro and									
Gross primary oroductivity  GPP  Vegetation  O.5° × Monthly (originally 8 days)  Aboveground biomass  AGB  Vegetation  O.5° × 0.5°  Longterm average  O.5° × 0.5°  Longterm average  Change Service, 2021)  MOD17A2H (Running and Zhao, 2019)2002-2018  Longterm average  Formatted: Line spacing: Multiple 1,15 linested Cells  Formatted: Line spacing: Multiple 1,15 linested Cells									
Gross primary oroductivity  GPP  Vegetation  O.5° × Monthly (originally 8 days)  Aboveground piomass  AGB  Vegetation  O.5° × 0.5°  Longterm average  O.5° × 0.5°  Longterm average  Service, 2021)  MOD17A2H  (Running and Zhao, 2019)2002- 2018  Service, 2021)  MOD17A2H  (Formatted: Line spacing: Multiple 1,15 linested Cells  Formatted: Line spacing: Multiple 1,15 linested Cells							' <del></del> '		
Aboveground biomass  O.5°500m  Originally 8 days)  AGB  Vegetation  O.5° × 0.5°  Longterm average  O.5° × 0.5°  AGB  Formatted: Line spacing: Multiple 1,15									
Aboveground biomass  AGB  Vegetation  O.5° × 0.5°  AGB  Vegetation  O.5° × 0.5°  Longterm average  AGB  Vegetation  O.5° × 0.5°  Longterm average  Climate Change Initiative v4 (Santoro and v		GPP	Vegetation	* * * *					Formatted: Line spacing: Multiple 1,15 li
Aboveground biomass  AGB  Vegetation  O.5° × 0.5°  Longterm average  Old ESA Biomass Climate Change Initiative v4 (Santoro and Control and	productivity			<del>0.5</del> ° <u>500m</u>					Inserted Cells
Aboveground biomass  AGB  Vegetation  O.5° × 0.5°  Longterm average  Climate Change Initiative v4 (Santoro and)  Formatted: Line spacing: Multiple 1,15 lines are consistent to the spacing of the space o					o days)				
Aboveground oiomass  AGB  Vegetation  0.5° × 0.5°  Longterm average  Climate Change Initiative v4 (Santoro and							<u> </u>		
average Climate Change Initiative v4 (Santoro and	Aboveground	AGB	Vegetation	$0.5^{\circ} \times 0.5^{\circ}$	Longterm		ESA Biomass	-	Formatted: Line spacing: Multiple 1,15 li
Initiative v4 (Santoro and	oiomass				average				
(Santoro and									
<u>Cartus, 2023)</u>									
						1	<u>Cartus, 2023)</u>		

Percentage T	ree	PTC	Vegetation	250m	Annual	2002-2018	MODIS -
cover							MOD44B
							(DiMiceli et
							al.,
							2011)MODIS
							- MOD44B
							(DiMiceli et
							al., 2011)
Fraction	of	FAPAR	Vegetation	500m	Monthly	2002-2018	MODIS
Absorbed					(originally		MOD15A2H
Photosynthetica	ally				8 days)		(Running and
Active Radiatio	n						<del>Zhao,</del>
							2019)MODIS
							- MOD15A2H
							(Running and
							Zhao, 2021)

**Table 1:** List of predictor variables that were considered in this study including their classifications, resolution (spatial **♣** temporal) and the respective data sources.

## 2.2.1 Vegetation-related predictors

225

226

227

228

229

230

231

232

233

234

235

236

237

238

239

240

241 242

243

244

We used eightnine vegetation predictor variables to comprehensively evaluate their role on global fire distribution. These variables encompass Percentage Grass Cover (PGC), Percentage Non-Tree Cover (PNTC), Percentage Crop Cover (PCC), Percentage Graze Cover (PGZC), Percentage Rangeland Cover (PRC), and Percentage Tree Cover (PTC). Previous work emphasizes the important role of vegetation on burnt area dynamics. For example, Thonicke et al. (2010), Percentage Tree Cover (PTC), Fraction of Absorbed Photosynthetically Active Radiation (FAPAR), Aboveground Biomass (ABG), and Gross primary productivity (GPP). Previous work emphasizes the important role of vegetation on burnt area dynamics. For example, Thonicke et al. (2010), discussed the crucial role of vegetation structure in shaping fire occurrence, spread and intensity. PGC defines the land covered by grass, influencing fuel availability, while PNTC considers non-tree vegetation such as grass and shrubs, contributing to overall fuel dynamics. PCC reflects the presence of cultivated crops which have been found to suppress fire occurrence as they fragment the landscape acting and so act as a barrier to fire spread (Haas et al., 2022).(Haas et al., 2022).

PGZC, PRC, PTNC and PTC were used to evaluate the relationship between landcover and burnt area distribution. Previous studies reported that land use/cover type has made a significant contribution to wildfire distribution (Gallardo et al., 2016; Villarreal and Vargas, 2021). GPP, AGB, and FAPAR were proxies for vegetation productivity and type, and fuel load. Also,

Formatted: Header

Inserted Cells

Formatted: Line spacing: Multiple 1,15 li

Formatted: Line spacing: Multiple 1,15 li

Formatted: Swedish (Sweden)

Formatted: Line spacing: Multiple 1,15 li

Formatted: Line spacing: Multiple 1,15 li

Formatted: Line spacing: Multiple 1,15 li

Formatted: Font color: Auto

Formatted: Line spacing: Multiple 1,15 li, Border: To (No border), Bottom: (No border), Left: (No border), Right: (No border), Between: (No border)

Formatted: Line spacing: 1,5 lines, Don't keep with I

Formatted: Line spacing: Multiple 1,36 li

some studies emphasized the varying effects of vegetation parameters on fire events (Bowman et al., 2020; Kuhn-Régnier et al., 2021).

To evaluate the role of fuel accumulation from the previous year on the burnt area, we derived the Monthly Ecosystem Productivity Index Index (MEPI) using monthly Gross Primary Productivity (GPP) data following Eq. (1). MEPI was originally defined in the work by Forrest et al. (2024). This index allowed us to quantify the relationship between vegetation growth, fuel accumulation and subsequent fire activity, providing a more nuanced understanding of the factors influencing fire dynamics.

$$\underline{\text{MEPI}} = \underbrace{\frac{GPP_m}{max_{1}GPP_{m_k}GPP_{m_{k-13}}}} \tag{1}$$

Where GPPm is the month's GPP, and the denominator is the maximum GPP of the past 13 months. Furthermore, we calculated additional metrics including GPP12 (the mean gross primary productivity over the previous 12 months), (FAPAR12) (the mean fraction of absorbed photosynthetically active radiation over the past 12 months), and FAPAR6 (the mean FAPAR over the last 6 months). These metrics serve to capture average vegetation productivity, serving as refined indicators of fuel accumulation. We used PGZC, PRC, PTNC and PTC to evaluate the relationship between landcover and burnt area distribution. Previous studies reported that landcover change has made a significant contribution to wildfire distribution (Gallardo et al., 2016; Villarreal and Vargas, 2021).

We used Gross Primary Productivity (GPP), Aboveground Biomass (AGB), and Fraction of Absorbed Photosynthetically Active Radiation (FAPAR) as proxies for vegetation health and productivity. Previous studies emphasized the varying effects of vegetation parameters on fire events (Bowman et al., 2020; Kuhn-Régnier et al., 2021).

Kuhn-Régnier et al. (2021) highlighted the important role of antecedent vegetation as a key driver for global fires.

## 2.2.2 Topographic-related predictors

245

246

247 248

249

250

251

252

253 254

255

256 257

258

259

260

261

262

263

264

265 266

267

268

269

270

271

272

273

274

275

276

277

We used topographic positioning index (TPI) to To evaluate how topography can influence the occurrence and spread of fires. we incorporated Topographic Positioning Index (TPI). Topography has been reported to be more influential in regions with complex terrain and microclimatic conditions (Blouin et al., 2016; Fang et al., 2015; Oliveira et al., 2014). (Blouin et al., 2016; Fang et al., 2015; Oliveira et al., 2014), Some studies used slope (Cary et al., 2006) (Cary et al., 2006) and surface area ratio (Parisien et al., 2011)(Parisien et al., 2011) in their models and reported topography to marginally contribute to wildfire dynamics. However, recent studies reported some significant contributions of topography to global burnt area distribution when using the TPI (Haas et al., 2022). (Haas et al., 2022). TPI is designed to encompass and evaluate the complex influence

Formatted: Header

Formatted: Finnish

Formatted: Finnish

Formatted: Finnish

Formatted: Indent: First line: 0.04 cm. Line spacing:

Multiple 1,36 li

Formatted: Finnish

Formatted: Finnish

Formatted: Finnish

Formatted: Finnish

Formatted: Finnish

Formatted: Line spacing: 1,5 lines, Don't keep with i

Formatted: Line spacing: Multiple 1,36 li

Formatted: English (United States)

**Formatted Table** 

16

of terrain features, such as elevation and slope, on the distribution of burnt areas. Thus, TPI goes beyond simplistic representations of landscapes and offers a more nuanced perspective on how terrain characteristics contribute to the occurrence and extent of wildfires. Given the role of terrain on fire behavior and propagation patterns, the inclusion of TPI in this study allows for a comprehensive examination of wildfire distribution.

#### 2.2.3 Anthropogenic Influence Predictorsinfluence predictors

278

279

280

281

282

283

284

285

286

287

288

289

290

291

292

293

294

295

296

297

298

299

300

301

302

303

304

305

306

307

308

309

We used To capture the impact of anthropogenic factors on both fire ignition and suppression, we adopted the Human Development Index (HDI), Population Density (PPN), and Road Density (RD) to capture the impact of anthropogenic factors on both fire ignition and suppression.). The inclusion of HDI aims to encapsulate human influence on ecological landscapes, thereby affecting the dynamics of both ignition and suppression processes. HDI is a composite index developed by the United Nations Development Program (UNDP) to assess long-term progress in three basic dimensions of human development, including health (life expectancy at birth), education (mean years of schooling and expected years of schooling), and standard of living (gross national income per capita) (Uddin, 2023). (Uddin, 2023). HDI values range from 0 to 1, with higher values indicating higher levels of human development. Although HDI itself may not directly relate to fire occurrence, it stands as a valuable socio-economic indicator that significantly influences overall fire dynamics and management, like how Gross Domestic Product (GDP) has been used in other fire models (Perkins et al., 2022), Perkins et al., 2022). To address the limitations of using GDP as a proxy for human development in predicting global fires, we opted for HDI. Previous research has utilized GDP for this purpose (Zhang et al., 2023), however, GDP is an indicator of a country's economic performance (Callen, 2008). In contrast, HDI is rather broad socioeconomic indicator, which we assume acts as a proxy for factor such as investments and advancements in fire control methods, surveillance, technology, and outreach strategies increasing awareness. HDH(Zhang et al., 2023), however, GDP is an indicator of a country's economic performance (Callen, 2008). In contrast, HDI is a broader socioeconomic indicator which evaluates a country or other administrative region's development status based on the critical factors of life expectancy, education, and income, We assume it acts as a proxy for factors such as investments and advancements in fire control methods, surveillance, technology, and outreach strategies increasing awareness, thus providing a more nuanced understanding of the socio-economic context shaping fire behavior (Teixeira et al., 2023) than GDP. To evaluate model sensitivity to inclusion of HDI, we trained our model based on the three settings: including, excluding and holding HDI constant.

## 2.2.4 Weather-Related Predictors related predictors

We employed the Canadian Fire Weather Index (FWI) to capture the impact of fire weather on the distribution of wildfires. FWI is renowned for its comprehensive framework integrating diverse meteorological parameters to evaluate potential fire behavior and danger (de Jong et al., 2016). The FWI is widely adopted by fire management agencies facilitating informed decisions on fire prevention, preparedness, and suppression strategies, and global context has been shown to correlate well with burnt areas across the globe (Jones et al., 2022). We used the number of dry days (NDD) as a proxy for biomass production

Formatted: Header

Formatted: Line spacing: 1,5 lines, Don't keep with I

Formatted: Line spacing: Multiple 1,36 li

Formatted: Line spacing: 1,5 lines, Don't keep with I

limitations. While it falls in the category of weather-related fire predictors, in this study it's an indirect indicator of how moisture availability can affect available combustible vegetation. We incorporated additional covariates capturing seasonal and annual weather dynamics that influence fires, including Precipitation Seasonality (PS), and Annual Average Precipitation (AAP). The selection of these predictors was informed by their significance in previous global fire modelling studies (Chuvieco et al., 2021; Joshi and Sukumar, 2021; Le Page et al., 2015; Mukunga et al., 2023; Saha et al., 2019), as well as insights from seminal works such as that by Pechony and Shindell, (2010).

We employed the Canadian Fire Weather Index (FWI) to capture the impact of fire weather on the distribution of wildfires.

FWI is renowned for its comprehensive framework integrating diverse meteorological parameters to evaluate potential fire behavior and danger (de Jong et al., 2016). The FWI is widely adopted by fire management agencies facilitating informed decisions on fire prevention, preparedness, and suppression strategies. It has been shown to correlate well with burnt areas across the globe (Jones et al., 2022). We used the number of dry days (NDD) as a proxy for biomass production limitations. While it falls in the category of weather-related fire predictors, in this study it's an indirect indicator of how moisture availability can affect available combustible vegetation. We incorporated additional covariates capturing seasonal and annual weather dynamics that influence fires, including Precipitation Seasonality (PS), and Annual Average Precipitation (AAP). The selection of these predictors was informed by their significance in previous global fire modelling studies (Chuvieco et al., 2021; Joshi and Sukumar, 2021; Le Page et al., 2015; Mukunga et al., 2023; Saha et al., 2019), as well as insights from seminal

## 2.3 Data Processing processing

works such as that by Pechony and Shindell (2010).

We harmonized the spatial and temporal resolution of the predictor dataset to conform to our analytical framework, which had a spatial resolution of 0.5° and a temporal resolution of one month. This involved employing techniques such as aggregation, resampling, and consolidation. For instance, while the native temporal resolution of FAPAR wasand GPP were 8 days, we transformed it into a monthly temporal resolution to align with our primary variable. Most predictors originally possessed an annual temporal resolution, except for FWI, GPP, and FAPAR, which werewas also available every month. For annual predictors, we replicated the same data for each month. Similarly, long-term variables like AGB, RD, and TPI were utilized every month to synchronize with the shorter-resolution predictors. PPN, which was available at a 5-year interval, was used monthly over the represented 5-year span. Kuhn-Régnier et al. (2021) highlighted the important role of antecedent vegetation as key driver for global fires. To evaluate the role of fuel accumulation from the previous year on the burnt area, we derived the Monthly Ecosystem Productivity Index Index (MEPI) using monthly Gross Primary Productivity (GPP) data following Eq. (1). MEPI was originally defined in the work by Forrest et al. (2024). This index allowed us to quantify the relationship between vegetation growth, fuel accumulation and subsequent fire activity, providing a more nuanced understanding of the factors influencing fire dynamics.

Formatted: Header

Formatted: Line spacing: 1,5 lines, Don't keep with i

Formatted: Line spacing: Multiple 1,36 li

 $\frac{GPP_{max}}{A} = \frac{GPP_{max}}{A}$  (1)

Where GPPm is the month's GPP, and the denominator is the maximum GPP of the past 13 months. Furthermore, we calculated additional metrics including GPP12 (the mean gross primary productivity over the previous 12 months), (FAPAR12) (the mean fraction of absorbed photosynthetically active radiation over the past 12 months), and FAPAR6 (the mean FAPAR over the last 6 months). These metrics serve to capture average vegetation productivity, serving as refined indicators of fuel accumulation.

### 2.4 Statistical modelling and final predictor choice

#### 2.4 Variable selection

344

345

346

347

348

349

350

351

352

353

354

355

356

357

358

359

360

361

362

363 364

365

366

367

368

369

370

371

372

373

374

To address variable collinearity, we conducted pairwise correlation analyses among predictor variables using the R statistical package (CoreTeam, 2014). (CoreTeam, 2014). Following established guidelines by Dormann et al. (2013). Dormann et al. (2013), we applied the conventional threshold of R > 0.5 to enhance the model's efficiency. Moreover, we employed the Variance Inflation Factor (VIF) to evaluate collinearity among predictor variables, removing those with VIF values surpassing 5, as recommended by O'brien, (2007). O'brien, (2007). Post collinearity tests, an additional 3 parameters were adopted to progressively select the best model, namely: 1) a simple (~ parsimonious) model which comprise of a full suite of categories of covariate combinations (i.e. vegetation, climate, topography, ignitions), 2) the deviance explained value and 3) the normalised mean square error Normalised Mean Square Error (NME) value as illustrated in the making of Burnt Area Simulator Forfor Europe (BASE) (Forrest et al., 2024). The variables include the MEPI, FWI, PNTC, HDI, PTC, TPI, NDD: Forrest et al., 2024).

## 2.5 Model training and PPN. testing

of transference to other modelling framework's ability to generate partial residual plots, i.e., the effect of each predictor in the model while the others are held constant (Bistinas et al., 2014; Haas et al., 2022; Lehsten et al., 2016), Residual plots were utilized to examine the magnitude and nature of each predictor's relationship with wildfire burnt area distribution.

A quasi-binomial GLM was selected for modelling BA due to its capability to handle non Gaussian error distributions, seamless integration into DGVMs and ability to generate partial residual plots, i.e. the effect of each predictor in the model while the others are held constant (Bistinas et al., 2014; Haas et al., 2022; Lehsten et al., 2016). Calibration of the model utilized data from 2002 to We used data from the period 2002–2010 for model training, the period 2011–2018 for model testing, and the full period 2002–2018 dataset for predictions and model evaluation. These time periods were chosen to ensure

A quasi-binomial GLM was selected for modelling BA due to its capability to handle non-Gaussian error distributions, ease

Formatted: Header

Formatted: Finnish

Formatted: Indent: First line: 0,04 cm, Line spacing:

Multiple 1,36 li

Formatted: Line spacing: Multiple 1,36 li

Formatted: Font: Bold

Formatted: Font: Not Bold

Formatted: English (United States)

timeframe to enhance the robustness of the analysis and evaluation. The essence of splitting training vs testing is to train the model on training data, and then check that the results are similarly good on the testing data (for example, no overfitting to the training data) before making predictions on the full dataset. Hence, during model testing we compared the performance of the model on training data vs testing data to assess model robustness.

## 2.6 Model selection

 We employed a sequential model-building approach, beginning with additive structures (M1–M12) to estimate the independent contribution of climate, vegetation, and human variables on burned area (Table 2). This approach aligns with established fire risk modelling practices (e.g., Forrest et al., 2024). Additional predictors were introduced if they represented ecologically meaningful processes (e.g., drought severity, vegetation productivity) and improved model fit (deviance explained and Normalised Mean Error). Multiplicative interaction terms (M13 onward) were added only when fire ecology theory suggested synergistic effects (e.g., human ignitions under extreme weather, vegetation dryness and temperature) and retained if deviance explained improved. This stepwise approach ensures both statistical rigor and ecological interpretability rather than ad hoc formula selection.

Formatted: Head	

Model(s)	Formula type	Deviance explained (range)	NME (range)	Rationale for additive / interaction terms
<u>M1–M2</u>	Additive, baseline predictors (FWI, GPP, HDI, PTC, RD) ± PGC)	0.35-0.37	0.74-0.75	Start with core fire-weather, vegetation, and human variables widely used in fire risk modelling (e.g., FWI, HDI). Summation quantifies independent effects and provides a baseline for deviance explained.
<u>M3–M9</u>	Additive, extended predictors (e.g., PNTC, FAPAR, PCC)	0.52-0.54	0.72-0.71	Additional vegetation productivity and phenology metrics tested to capture fuel continuity and biomass effects. Additive inclusion based on ecological theory (fuel load $\rightarrow$ fire extent) and retained if deviance $\uparrow > 1 - 2\%$ .
M10-M12	Additive, polynomial + seasonal predictors	0.52-0.55	0.71-0.72	Added nonlinear terms (e.g., poly(PTC,2)) to test curvilinear effects of vegetation productivity on fire risk, seasonal indices (e.g., FAPAR12) reflect lagged vegetation—fire relationships.
M13-M20	Additive + interaction terms (HDI×PCC, MEPI×PNTC, etc.)	0.55-0.57	0.71-0.72	Interaction terms introduced where ecological or anthropogenic synergies are expected (e.g., human density × vegetation affects ignition; drought × fuel load affects spread). Retained if deviance > 2 and NME improves 2%.
M21-M26	Full interactions, topographic + climate covariates	0.56-0.57	0.71-0.72	Topography (TPI) and drought indices (NDD) interact with vegetation to capture compound effects on fire behavior; final models balance explanatory power with ecological plausibility and parsimony.

Table 2: Summary of models (M1–M26) with corresponding formulas, performance metrics, and rationale for predictor inclusion or interaction terms. Predictor additions were guided by ecological theory (e.g., fuel load, climate extremes, anthropogenic factors) and retained based on statistical improvements.

#### 2.7 Model performance evaluation

392

393

394

395 396

397

398

399 400

401

402

403

404

405 406

407 408

409

410

411

412

413

414

415

416

417

418

419

420

421

422

423

424

 $\underline{2010 \ while \ testing \ utilized \ data \ from \ 2011 \ to \ 2018}_{\textbf{a}} \underline{Residual \ plots \ were \ utilized \ to \ examine \ the \ magnitude \ and \ nature \ of \ each}$ 

predictor's relationship with wildfire burnt area distribution.

Model performance was assessed using the Normalized Mean Error (NME) following Kelley et al. (2013). Kelley et al. (2013).

NME serves as a standardized metric for evaluating global fire-model performance, facilitating direct comparison between predictions and observations. The NME was calculated following Eq. (2).

$$NME = \frac{\sum Ai I obs_i - sim_i I}{\sum Ai I obs_i - obs I}$$
(2)

The NME score was computed by summing the discrepancies between observations (obs) and simulations (sim) across all cells (i), weighted by the respective cell areas (Ai), and then normalized by the average distance from the mean of the observations. A lower NME value reflects superior model performance, with a value of 0 indicating a perfect alignment between observed and simulated values. BA fractions were treated as a probability ranging from 0 to 1, following a quasibinomial distribution. We applied the logit link function based on the methodology outlined by Haas et al. (2022). After conducting a collinearity test, the models were systematically evaluated using various combinations of predictor variables. A total of 2526 model runs were conducted, each incorporating different sets of variables while iteratively excluding some, to discern the extent to which each predictor explained variance when others were not included (see Table A1). We followed the stepwise approach of variable inclusion, exclusion, interaction terms, log transformations, and polynomial transformations as described by Forrest et al. (2024). While their analysis focused on Europe, our objective was to replicate and apply Forrest et al. (2024). While their analysis focused on Europe, our objective was to replicate and test the method at a global scale. To evaluate the reliability of the predicted interannual variability and seasonal cycles, we applied a regression function to determine the relationship (R<sup>2</sup>) between the observed and predicted trends, using annual average data for the period 2002-2018. An R<sup>2</sup> of 1 shows good performance in our predictions and an R<sup>2</sup> of 0 shows poor performance in our predictions. To assess the trend in predicted interannual variability, we used the Mann-Kendall test (Kendall, 1975; Mann, 1945). (Kendall, 1975; Mann, 1945). This widely used method detects monotonic trends in environmental data. Being non-parametric, it works for all distributions, does not require normality, but assumes no serial correlation.

3 Results

Formatted: Header

Formatted: English (United States)

Formatted: Line spacing: Multiple 1,36 li

**Formatted:** Indent: First line: 0,04 cm, Line spacing: Multiple 1,36 li

Formatted: Line spacing: Multiple 1,36 li

Formatted: Line spacing: 1,5 lines, Don't keep with i

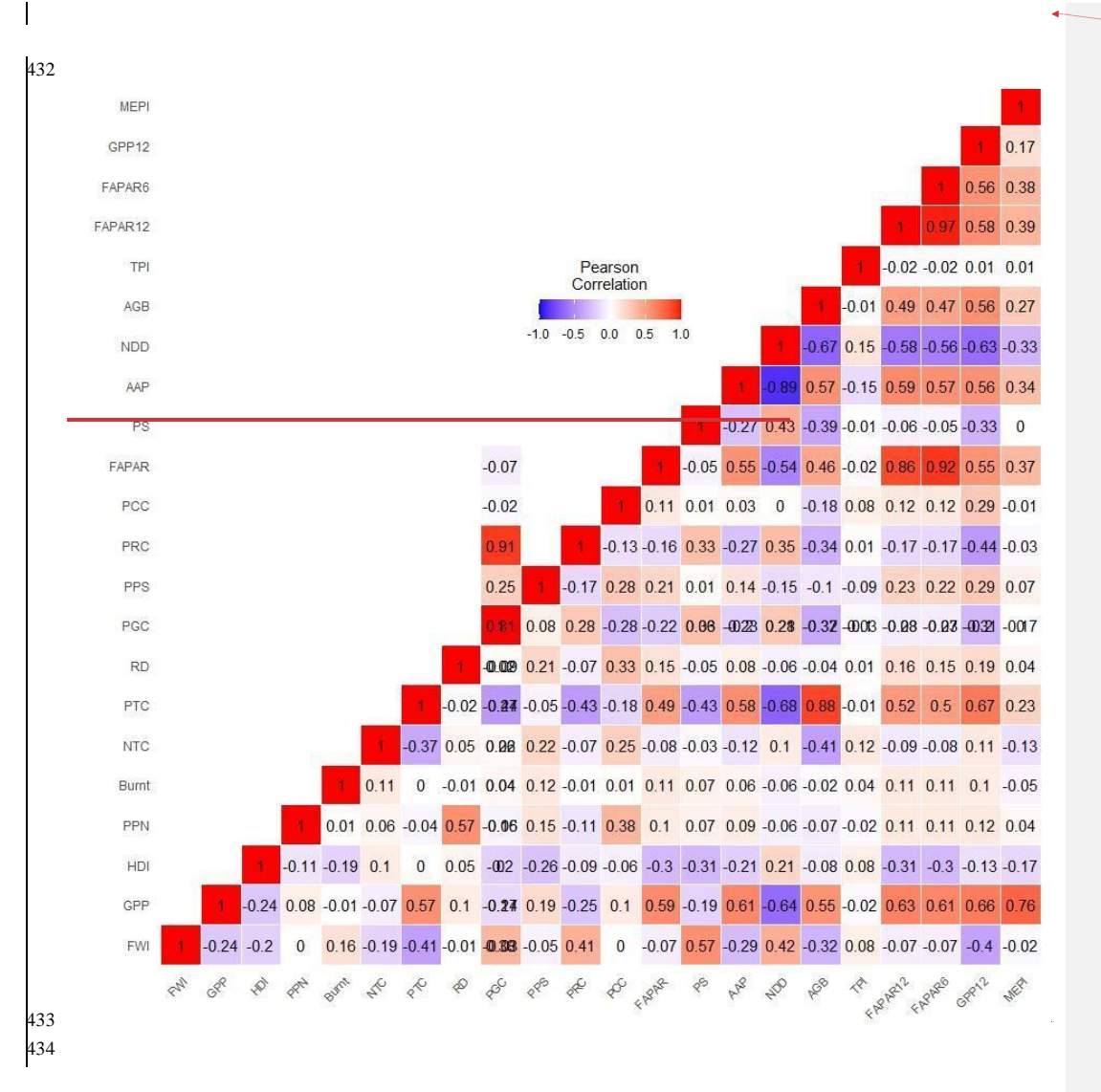
## 3.1 Correlation between variables

We found correlated variables that we had to exclude from the analysis. Specifically, variables such as AGB, FAPAR12, FAPAR6, AAP, and RD were excluded due to their strong correlations with other variables (see Fig. 2). There were however some variables that correlated but had to be returned to the model due to their significant contribution to fire modelling and model performance. For example, NDD was strongly correlated to PTC (-0.68), but both increased the variance explained by the full model.

Formatted: Header

Formatted: Line spacing: Multiple 1,36 li





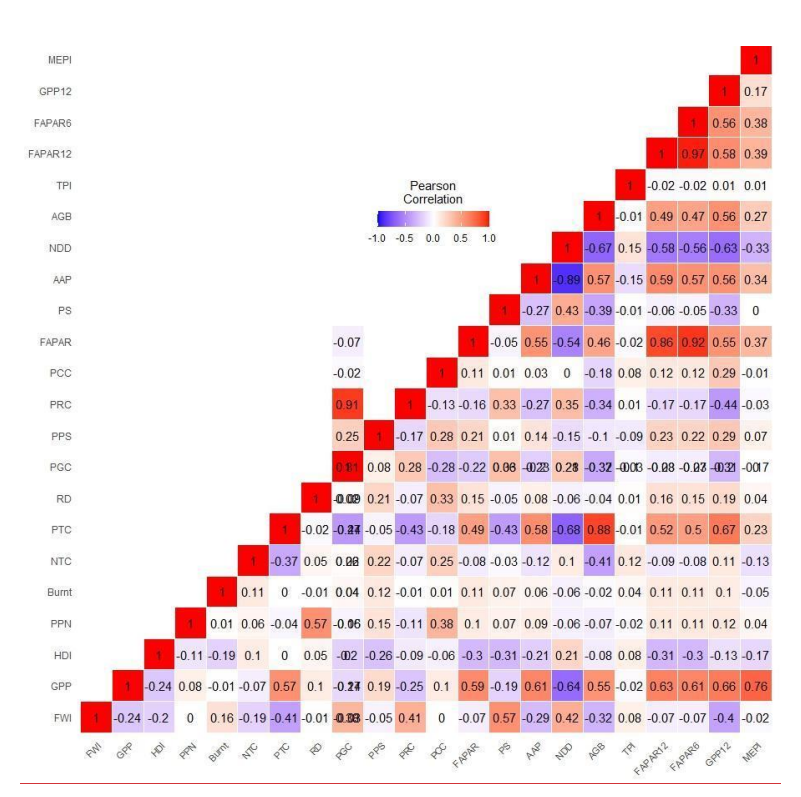


Figure 2: Correlation matrix of all the variables that were considered for modelling in this investigation.

## 3.12 Optimal model selection and GLM results.

The initial models (model 1 to model 3) progressively include more variables, however, a noticeable jump and substantial improvement is observed in deviancemodel 3 which explained when 52.98% following the inclusion of PNTC is added (Model 3: 0,5298). Models 4 to 8 involve adding vegetation (FAPAR) and various land use types (PCC, PPS, PRC, PGC). This is accompanied by marginal improvement in deviance explained, indicating these factors provide some additional predictive power but are not as impactful as existing vegetation covariates (such as GPP). Models 10 to 12 introduce polynomial terms for PTC. This results in an increase in deviance explained, peaking at around 0.558836 performance explaining 55.88% in Modelmodel 12. Models 13 to 16 incorporate interactions between HDI and land use types (e.g., PCC and PRC), resulting in

Formatted: Header

Formatted: Line spacing: Multiple 1,15 li

Formatted: Line spacing: Multiple 1,36 li

marginal increaseimprovement in deviance explained performance with the highest recorded in Modelmodel 15(~0.5664789). which explained 56.65%. Models 19 to 2526 fine-tune the overall performance by incorporating various variables and their interactions. Model 24, which includes a comprehensive set of climatic, vegetation, human, and topographic variables along with their interactions, achieves the highest devianceperformance as it explained (~0.5720048).57.20%. The marginal improvements observed in subsequent models indicate that while additional variables contribute to the model, the primary influencing factors were already identified by Modelmodel 19, however it was not the simplest model (~ parsimonious), and eonsisted of other included variables that we don't have for which future projections for are currently unavailable (e.g., RD)-), due to the lack of established projection models or datasets. Since the main objective of the study was to produce a DGVM-compatible model, availability of future projections for these datasets was indispensable to model building. We removed some of the redundant variables till Modelmodel 24 (~11 variables), however, it was not as parsimonious as Modelmodel 25 (~8 variables). Therefore, Modelmodel 25, which offers a balance of parsimony, simplicity, high deviance explained, and low NME, was selected as the best model in this analysis.

446

447

448 449

450

451

452

453

454

455

456

457

458 459

460

461

462

463

\_Our results reveal that each predictor variable incorporated in the final analysis significantly predicted the distribution of wildfires (p < 0.05), as outlined in Table  $\frac{23}{2}$ .

-	Estimate	Std.Error	T value	Pr(> t )
(Intercept)	- 6.159e+00	2.349x10^-02	-262.17	< 0.00001
FWI	9.296e-01	1.948x10^-03	477.28	< 0.00001
MEPI	-2.270e+00	8.974x10^-03	-252.96	< 0.00001
HDI	-1.680e+00	1.235x10^-02	-135.99	< 0.00001
PNTC	5.170e-02	2.270x10^-04	227.78	< 0.00001
poly(PTC,2)1	2.135e+03	1.114x10^01	191.55	< 0.00001
poly(PTC,2)2	-9.783e+02	6.975	-140.27	< 0.00001
TPI	2.225e-01	3.946x10^-03	56.39	< 0.00001
NDD	-9.550e-03	4.757x10^-05	-200.78	< 0.00001
PPN	-1.075e-03	1.808x10^-05	-59.48	< 0.00001

Table 23. Summary of GLM coefficients for the final model, presenting t-values and p-values for predictors. The results indicate that all predictors in the final model were statistically significant for wildfire distribution (p < 0.05).

Formatted: Line spacing: Multiple 1,36 li

465 466

472 473

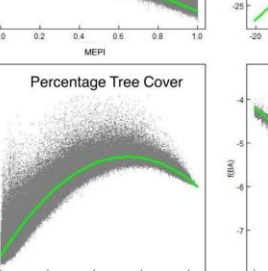
471

474 475

wildfire dynamics.

476

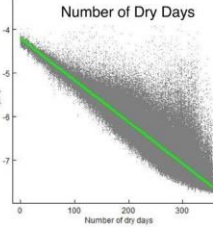




Monthly Ecosystem

Productivity Index





Fire Weather Index



Our analysis results revealed the relationship between various predictors and BA distribution, as depicted in Fig. 3. Among

the predictors studied, FWI, PNTC, PTC and TPI showed a positive relationship with BA distribution. Notably, FWI and

PNTC showed particularly strong relationships, underscoring the substantial role of fire weather, fuel availability on the

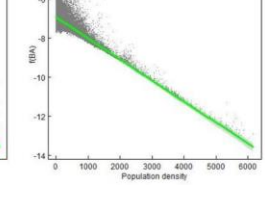
expansion of BA extent. Conversely, several predictors showed a negative relationship with BA distribution, including the

Overall, our observations highlight the critical role of factors such as fire weather, fuel availability, vegetation cover, climate

conditions, and landscape characteristics in shaping BA distribution patterns. Fig.3 visually represents the differential

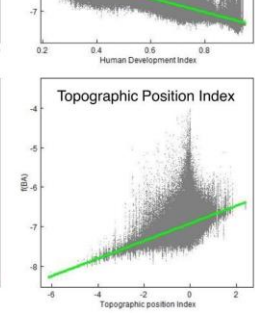
relationship of these predictors on BA distribution, offering a comprehensive overview of the underlying mechanisms driving

MEPI, HDI, PPN and NDD. A polynomial of PTC shows a slightly bell-shaped relationship with burnt area fraction.



Population Density

Percentage Non Tree Cover



Human Development Index

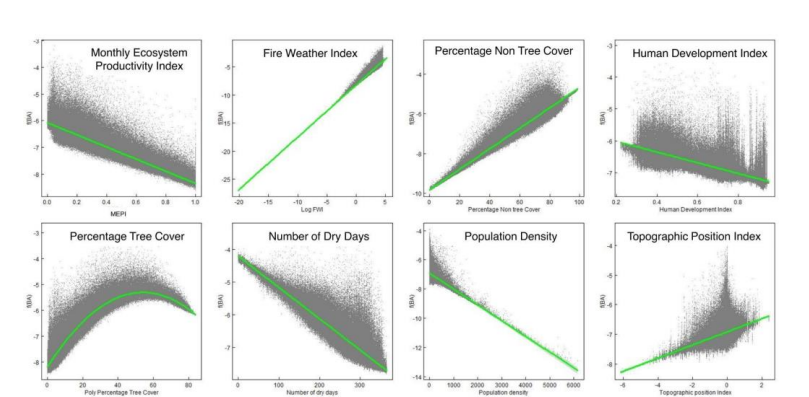


Figure 3: Partial Residual Plots illustrating the relationship between burnt Areas (BA) and the eight final predictor variables. These plots show the effect of each predictor while the others are held constant (Larsen and McCleary, 1972). Predictor variables were <a href="Gross Primary ProductionMonthly Ecosystem Productivity">Gross Primary ProductionMonthly Ecosystem Productivity</a> Index (GPPMEPI), Fire Weather Index (FWI), Percentage Non-Tree Cover (PNTC), Human Development Index (HDI), Percentage Tree Cover (PTC), Topographic Position Index (TPI), Population Density (PPN) and Number of Dry Days (NDD).

## 3.3 Performance evaluation

Afte model demonstrated comparable performance across the training and testing datasets. Specifically, the training data yielded a deviance explained of 0.57 and an NME of 0.73, while the testing data yielded a deviance explained of 0.56 and an NME of 0.70. The close agreement between training and testing performance supports the robustness of the model and justifies its application to the full dataset, which we subsequently evaluated with respect to both spatial and temporal predictive capability.

The full dataset model demonstrated strong performance in predicting BA, accounting for over 50 as it explained 56.83% of the variability in burnt areas (Deviance explained = 0.568). While our results slightly lagged those of a global fire distribution model by Haas et al. (2022), who found a deviance explained of 0.69, it's noteworthy that their model incorporated a broader array of variables (16 predictors) and operated at a coarser temporal resolution (annual). area. Our model's performance, based on eight predictors and operating at a finer temporal resolution (monthly), is considered satisfactory and parsimonious.

Formatted: Header

Formatted: Line spacing: Multiple 1,36 li

Formatted: Font: Not Bold

Assessment of Overall, the model accuracy yielded an NME of 0.718, indicating a generally close correspondence between observed and predicted burnt area patterns (see Fig. 4). This level of accuracy is comparable to that reported by previous global fire models, such as Haas et al. (2022) and Hantson et al. (2016) which reported NMEs ranging from 0.60 to 1.10.

The correlation analysis further shows significant variation in the strength of relationship between observed and predicted burnt area extent across the 14 GFED regions annually (Fig. 4a) and seasonally (Fig. 4b). These include: Boreal North America (BONA), Temperate North America (TENA), Central America (CEAM), Northern Hemisphere South America (NHSA), Southern Hemisphere South America (SHSA), Europe (EURO), Middle East (MIDE), Northern Hemisphere Africa (NHAF), Southern Hemisphere Africa (SHAF), Boreal Asia (BOAS), Central Asia (CEAS), Southeast Asia (SEAS), Equatorial Asia (EQAS) and Australia and New Zealand (AUST).

Our model overall performed poorly in predicting interannual variability as exhibited by a poor strength of relationship between the predicted trend when compared to the observed ( $R^2$ = 0.24). This poor relationship was exhibited across most of the GFED regions ( $R^2$  < 0.50, Fig. 4a), except for the NHSA which showed strong similarities between the predicted trend and observed trend ( $R^2$  = 0.55). This observation suggests that the combination of covariates that we incorporated in this model has limited strength in capturing global interannual variability in burnt areas.

Unlike the global interannual trends, there was a strong strength of similarity between observed and predicted seasonal cycles in most GFED regions (refer to Fig. 4b and Fig. A4). The model predicted better in GFED regions that are situated in Southern Africa, South America, Australia and Asia ( $R^2 > 0.50$ ). However, a few poor seasonal predictions were recorded in GFED regions situated in North America, North Africa and Europe as indicated by a poor relationship between observed burnt area and predicted burnt area ( $R^2 < 0.50$ ).

Formatted: Header

Formatted: Line spacing: Multiple 1,36 li

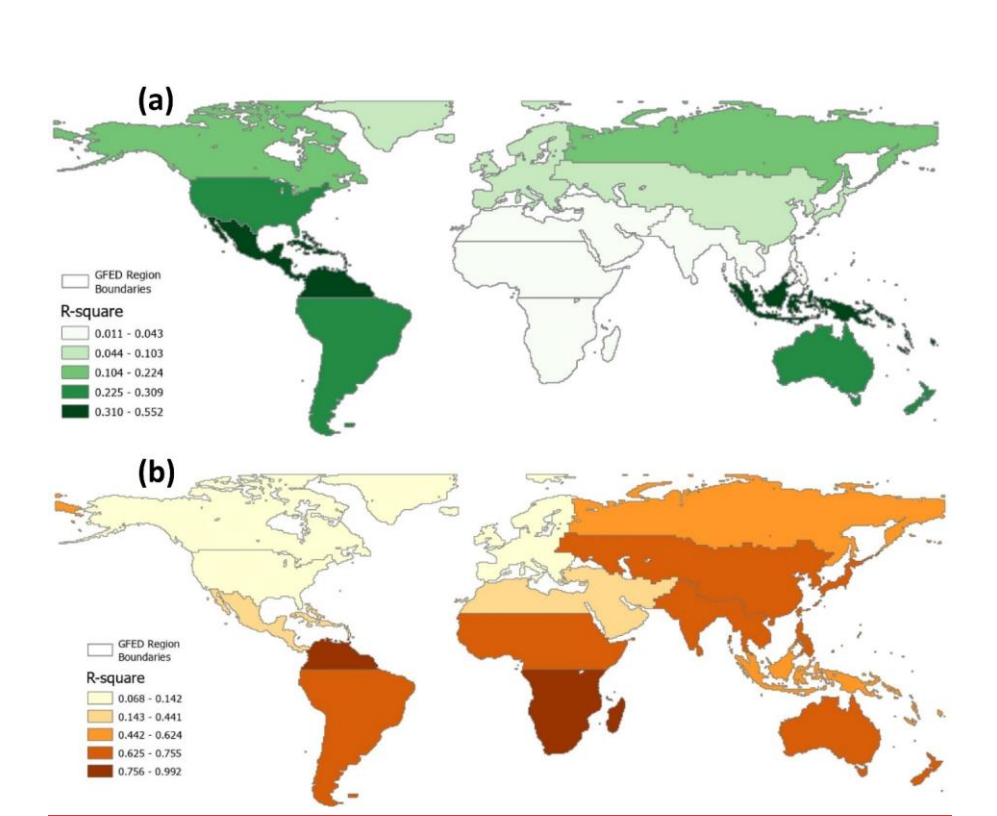


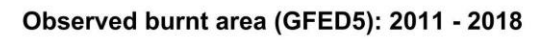
Figure 4: Evaluation of the selected model using observed burned area data from GFED5 predicted data (2011-2018). The maps show r-square values highlighting the model's performance for interannual (a) and seasonal variability (b) per GFED region.

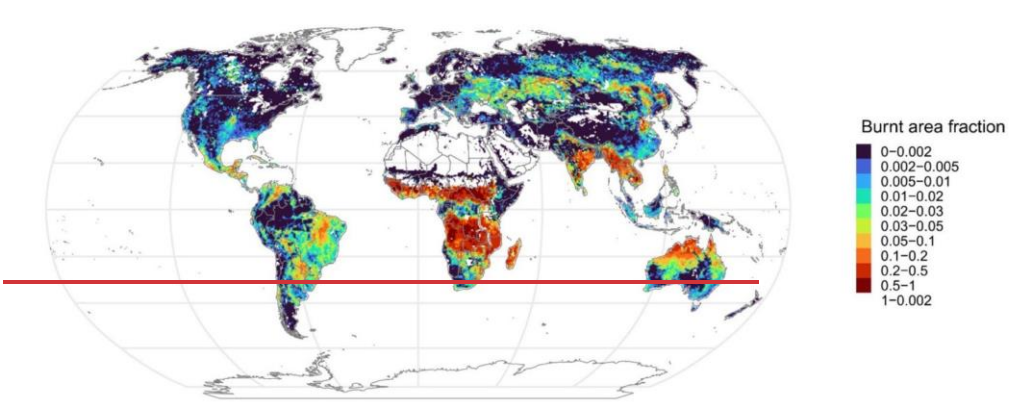
Spatially, our model effectively captured the distribution of BA in the tropics and the southern hemisphere, demonstrating notable similarities between observed and predicted burnt area fractions on an annual basis (see Fig. 45). However, in extratropical regions, particularly in the northern hemisphere, instances of over prediction overprediction were observed. This discrepancy is evident in the inconsistencies between observed annual distribution patterns and those predicted by the model.

Formatted: Header

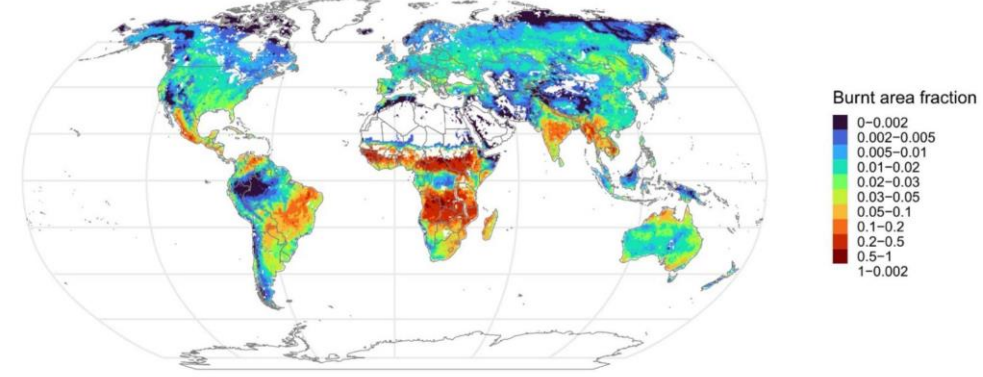
Formatted: Line spacing: Multiple 1,36 li







# Predicted burnt area: 2011 - 2018





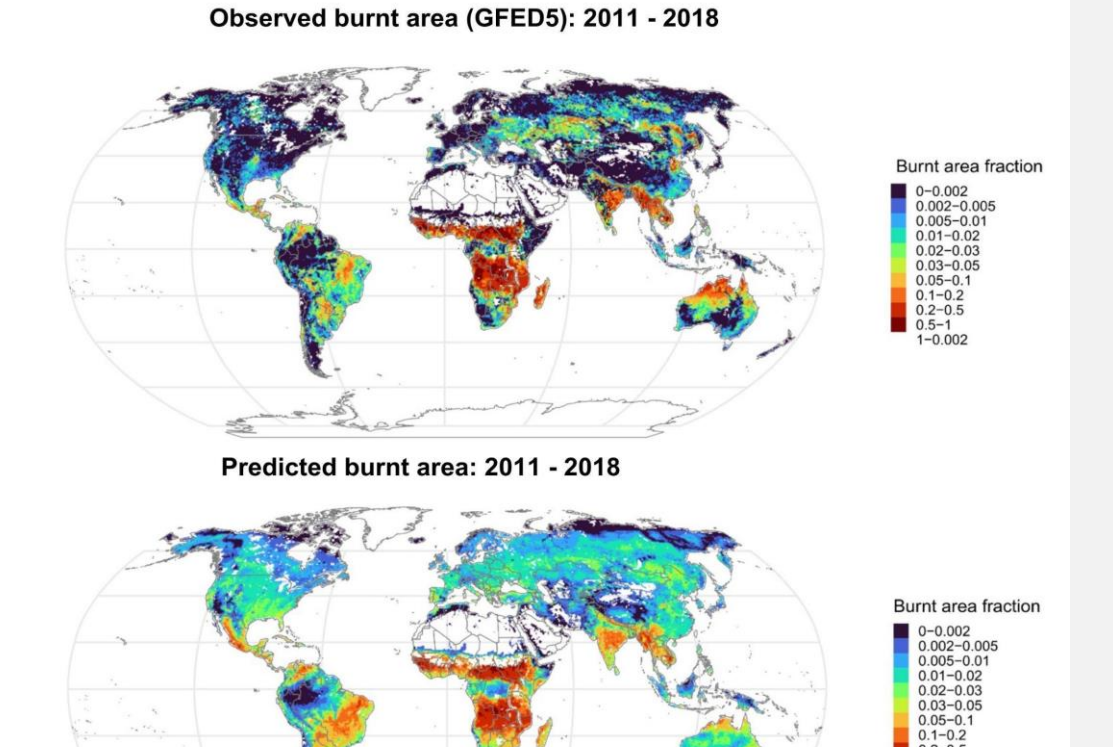


 Figure 45: Annual burnt area fraction distribution map with the observed burnt area (top) and predicted burnt area (bottom).

Formatted: Line spacing: Multiple 1,36 li

Formatted: Line spacing: Multiple 1,36 li

## 3.24 Interannual variability distribution

543

544

545

546

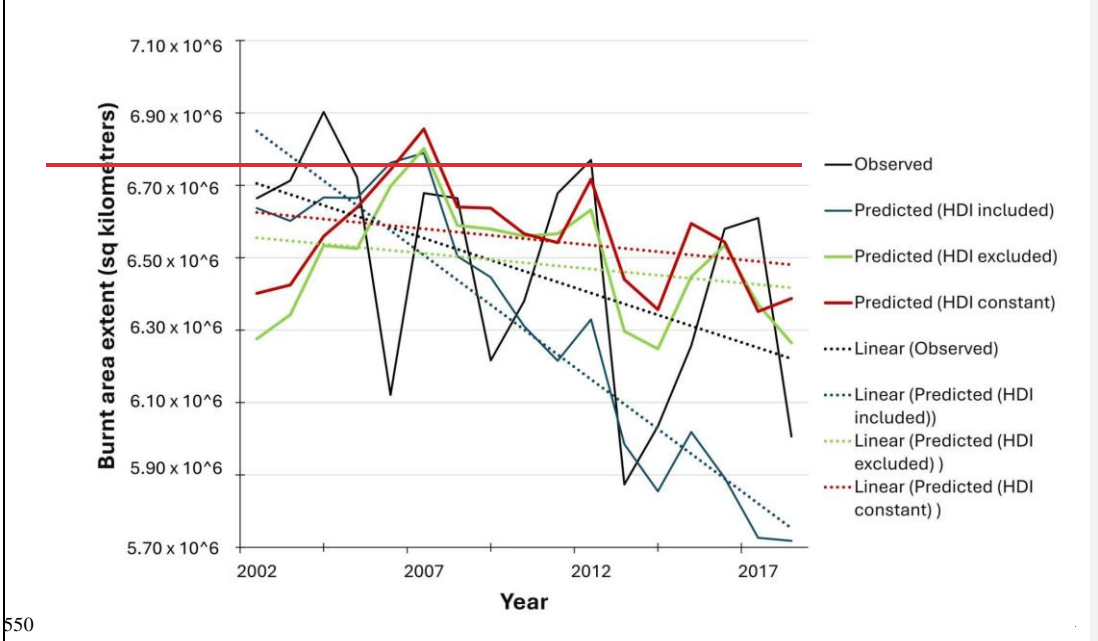
547

548

549

551

Our analysis results revealed a substantial global decrease in burnt areas exceeding 1 million square kilometers from 2002 to 2018, with the peak decline observed in 2004 (see Fig. 56). This downtrend was reproduced by the model, but the model underestimated the interannual variability and the model-predicted decline was stronger than observed. However, it aligns with the decreasing patterns reported in garlier studies (Andela et al., 2017; Jones et al., 2022). (Andela et al., 2017; Jones et al., 2022). Excluding and holding HDI constant in the model made the projected trend remain steady, suggesting the role of anthropogenic developments (increasing HDI over time) driving a downward trend in wildfire distribution.



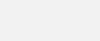
Formatted: Header

Formatted: Line spacing: 1,5 lines, Don't keep with i

Formatted: Line spacing: Multiple 1,36 li

Formatted: English (United States)

Formatted: English (United States)



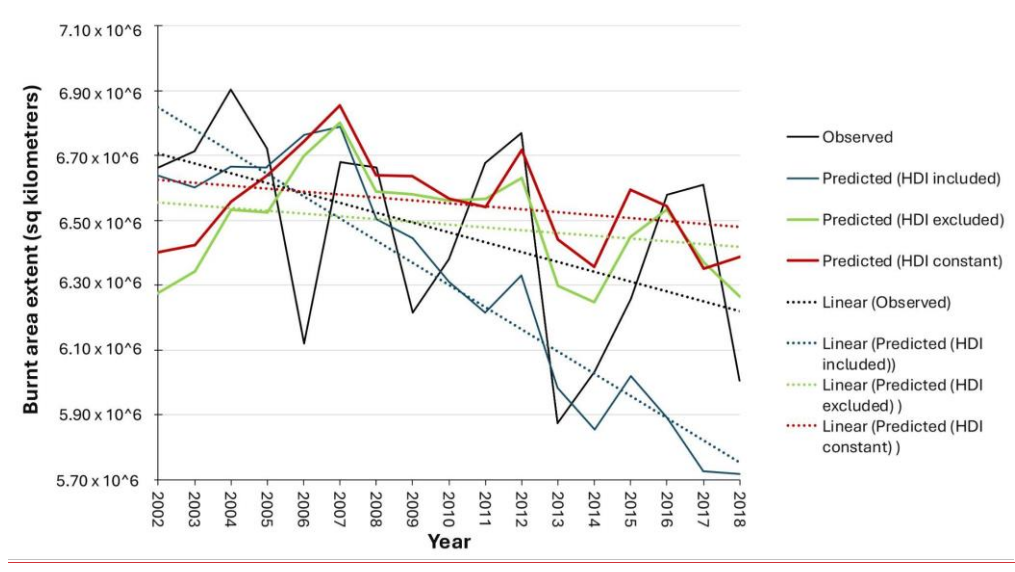


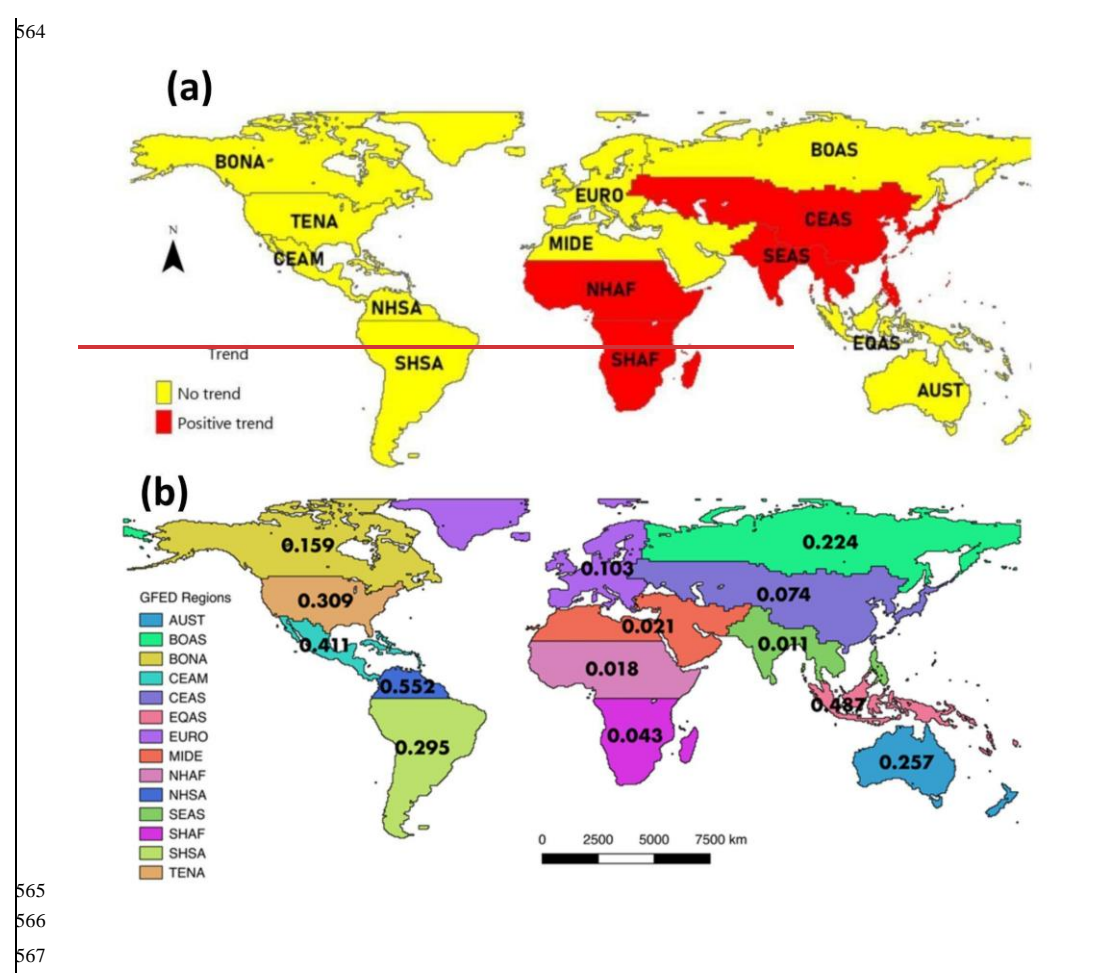
Figure 56: Interannual variability in burnt area extent showing the observed trend (based on GFED5 burnt estimates detection for the period 2002-2018 and model projections of the respective period under different HDI treatments: when HDI was excluded, included and held constant from the value of the first year in the model.

The Mann Kendall trend analysis further shows significant variation in the magnitude and direction of predicted burnt area extent across the 14 GFED regions (refer to Fig. 647 and Table A2). Five regions (SHAF, SHSA, NHAF, CEAS) predicted a significantly positive trend (p < 0.05) in burnt area extent, while the other regions predicted no significant trends (NHSA, SHSA, MIDE, TENA, AUST, EURO, EQAS, CEAM, BONA, BOAS). Overall, the projected positive trend predominated in GFED regions situated in central and southern Africa, and central and southern Asia. In contrast, the Americas, Australia, and Europe demonstrated no significant trend, as illustrated in Fig. 647.

Formatted: Line spacing: Multiple 1,36 li

Formatted: Font: Not Bold





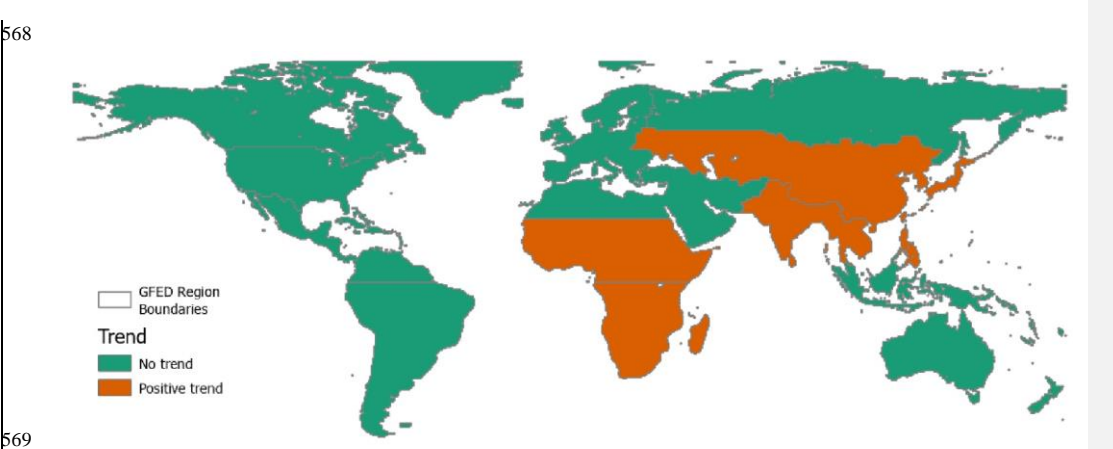


Figure 67: Variation in the direction of trend of interannual variability for burnt areas across different GFED regions. Where (a) shows the direction of the trend and (b) shows the spatial

3.5 Seasonal distribution of the strength of relationship (r-square values) between observed and predicted interannuals variability per GFED region.

Our predictive model performed poorly in predicting interannual variability as exhibited by a poor strength of relationship between the predicted trend when compared to the observed (R2= 0.24) (See Fig 6b and Fig A1). This poor relationship was exhibited across most of the GFED regions (R<sup>2</sup> < 0.50), except for the NHSA which showed strong similarities between the predicted trend and observed trend ( $R^2 = 0.55$ ). This observation suggests that the combination of covariates that we incorporated in this model has limited strength in capturing global interannual variability in burnt area. However, the predicted global trend is in sync with previously reported global trends (Jones et al., 2022).

## 3.3 Seasonal Cycle

568

570

571

572

573

574

575 576

577

578

579

580

581

582

583

584

585

586

587

Our analysis results show that the global extent of BA shows an alternating seasonal cycle with strong peaks in February and August (see Fig. 78). The predicted pattern slightly underestimates the burnt area, however, appears to be closely knit with the observed trend (R<sup>2</sup> = 0.54). Like the global interannual trends, the strength of similarity between observed and predicted seasonal cycles varies according to the GFED region with R2 ranging between 0.06 to 0.99 (refer to Fig. 8). The model predicted better in GFED regions that are situated in Southern Africa, South America, Australia and Asia (R2>0.50) (see Fig.

Formatted: Header

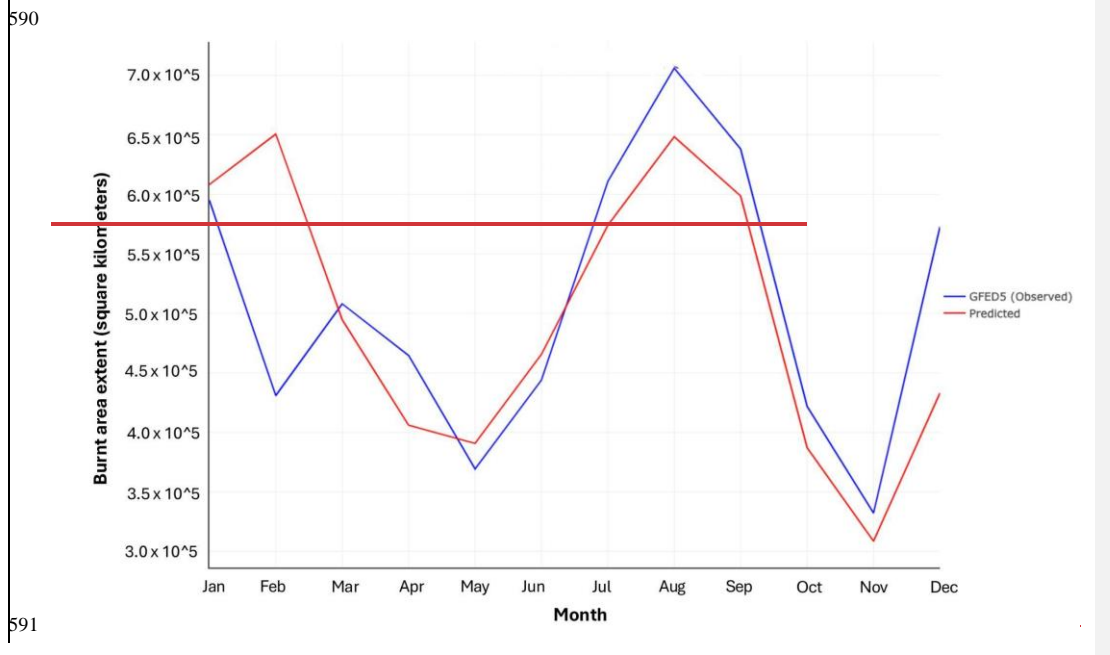
Formatted: Heading 2

Formatted: Line spacing: Multiple 1,36 li

8 and Fig A2). In contrast, poor seasonal predictions were recorded in GFED regions situated in North America, North Africa and Europe as indicated by a poor relationship between observed burnt area and predicted burnt area ( $R^2 < 0.50$ ).

588

589



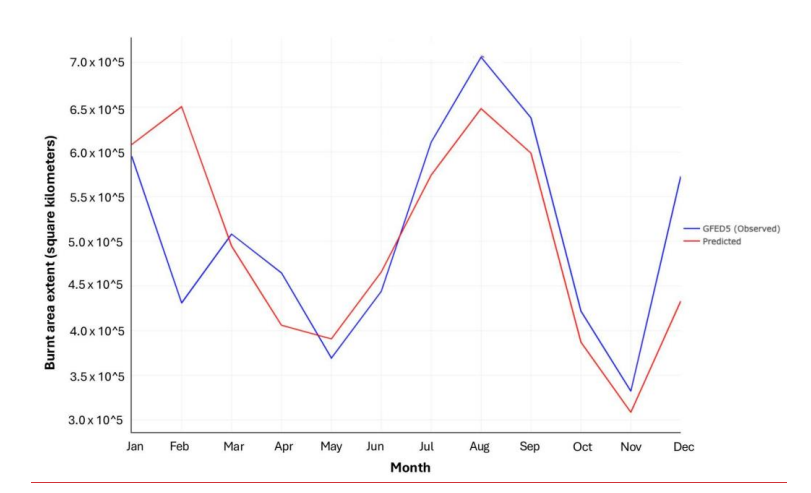


Figure 78: Global seasonal burnt area patterns showing the observed (GFED 5) and predicted burnt area extent.

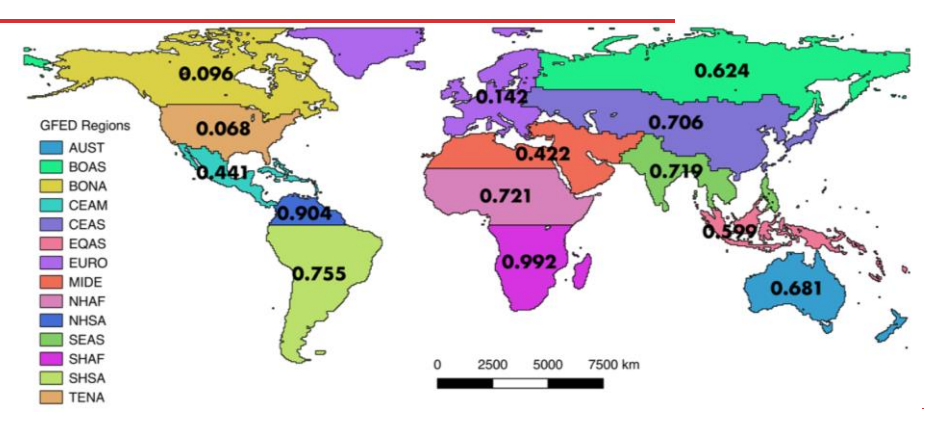


Figure 8: Spatial distribution of r-square values for the relationship between observed and predicted seasonal variability per GFED region.

594

595 596

597

598

599

4 Discussion

Formatted: Line spacing: 1,5 lines, Don't keep with

**Formatted Table** 

Formatted: Header

Formatted: Line spacing: Multiple 1,36 li

38

## 4.1 Main drivers of global burned area

We found a DGVM compatible parsimonious global statistical model made ofthat our candidate variables, namely FWI, PNTC, PTC, TPI, MEPI, HDI, PPN and NDD. Of all the key variables, had strong influence on burnt areas. FWI and PNTC exhibited a strong positive relationship with fire occurrence, underscoring the importance of conducive fire-weather conditions and combustible fuel in driving wildfire occurrence and spread. High PNTC is most likely related to high amounts of flammable vegetation, such as grasses and shrubs. Our findings show that fire weather (~FWI) and fuel availability (~PNTC) influence burnt area extent align with previous studies (Andela et al., 2017; Bistinas et al., 2014; Forkel et al., 2019b; Kuhn-Régnier et al., 2021). (Andela et al., 2017; Bistinas et al., 2019; Kuhn-Régnier et al., 2021). The other studies, however, did focus on the annual burnt area, not the seasonal cycle, which is also crucial to adapt to changes in fire risk.

Our results show that higher PNTC leads to higher burnt area fractions. In contrast, areas with lower non-tree coverPNTC show lower burnt area fractions. Areas with high PNTC typically consist of grasses and shrubs (~ height < 2 m), while areas with low PNTC are often characterized by trees. Grass and shrubs often encourage frequent burning much more than trees (Juli et al., 2017; Wragg et al., 2018). (Juli et al., 2017; Wragg et al., 2018). Conversely, low PNTC indicates high tree cover, which is often less flammable, leading to fewer fires. Though our findings support previous literature indicating that regions with abundant combustible vegetation and favorable fire-weather conditions are prone to frequent burning (Kraaij et al., 2018; Thonicke et al., 2010), (Kraaij et al., 2018; Thonicke et al., 2010), we observed a surprising negative relationship between NDD and burnt area. Previous studies found a positive relationship between NDD and burnt area fractions (Haas et al., 2022), like our single (Haas et al., 2022), like our single-factor plots of NDD and burnt area in Fig A3. This result most probably shows that relationships derived with annual data, as in the other studies mentioned here, cannot simply be transferred to seasonal fire predictions. Studies have shown that the effect of dryness on fire varies depending on vegetation communities in Mediterranean ecosystems (Cardil et al., 2019). Stott (2000) (Cardil et al., 2019). Stott (2000) echoed similar sentiments for tropical environments, indicating the complex relationship between vegetation, dryness and fire. Our efforts to investigate this complex relationship through an interaction term did not significantly improve our model accuracy (~ model 26). Hence, future studies may benefit from further exploring the complex relationship between dryness and vegetation at a global scale, particularly the effect of incorporating polynomial terms on correlated predictors in a linear model.

Our findings revealed that HDI, MEPI and PPN are negatively associated with trends in global fire extent. For HDI, our findings imply that technological advancements, improved surveillance systems, and effective mitigation efforts play a significant role in limiting the extent of burnt areas. Contrary to expectations based on Haas et al. (2022), Haas et al. (2022). PPN, which should correlate with more ignitions, does not appear to increase the burnt area extent (see Fig. 3). In fact, we observed that lower PPN corresponded to larger burnt areas, likely due to the impact of human activities on landscape fragmentation through road construction, and measures to suppress fires in human inhabited spaces to protect properties (Kloster et al., 2010). Saunders et al., (1991) (Kloster et al., 2010). Saunders et al. (1991) observed that the response of fire to changes in PPN is governed by two opposing processes, an increase in population leads to more ignition sources, while

Formatted: Header

Formatted: Line spacing: Multiple 1,36 li

Formatted: Swedish (Sweden)

simultaneously prompting greater fire management efforts to suppress fires. They further highlighted that fire suppression rates are highest in densely populated areas. This suggests that the scale (both spatial and temporal) of analysis may influence nature and extent to which PPN affects burnt area extent. Our results for the effect of PPN have important implications for DGVMs and land surface models. These models differ widely in the assumed effect of PPN, often using a unimodal response simulating BA annually, in some cases distributing the wildfires across seasons in a second step, using rather simplified assumptions (Teckentrup et al., 2019).(Teckentrup et al., 2019). Similarly, we anticipated a positive relationship between MEPI and burnt areas, as MEPI is indicative of ecosystem dryness and flammability. However, our findings revealed a negative relationship, indicating that other factors may be influencing the connection between MEPI and the extent of burnt areas. Our findings are in line with those of Forrest et al. (2024)Forrest et al. (2024) who initially investigated the effect of this index on burnt areas in Europe. Unlike previous global studies that utilized annual GPP, our research employed a more refined measure, MEPI. Future research could benefit from evaluating the relationships between MEPI and burnt areas in other GFED regions and temporal scales.

#### 4.12 Spatial variation in model performance

Our model exhibits stronger performance in predicting the spatial distribution of fires in southern Africa, Australia, and Souths America than in other world regions (See Fig. 4). The stronger performance in these areas is likely due to the well-defined and predictable fire regimes in these regions. Since fire activity here is strongly governed by distinct wet-dry seasonal cycles, which align closely with elimate variables such as precipitation, temperature, and vegetation productivity, factors that fire weather, enabling our model to capture these patterns effectively using linear functions (Archibald, 2016; Van Der Werf et al., 2017). These regions typically exhibit lower interannual variability in fire occurrence, facilitating See Fig. A5), hence better model generalization.

Conversely, our model tends to overpredict fires in the northern hemisphere, particularly in North and Central America, as well as Asia. Performance here declines as fire regimes are more heterogeneous and driven by a combination of biophysical and anthropogenic factors (Chuvieco et al., 2021; Forkel et al., 2019). (Chuvieco et al., 2021; Forkel et al., 2019). High interannual variability in burnt areas in these regions is due to irregular droughts, land use change, and fire suppression policies that make prediction more challenging for linear models. Additionally, the influence of snow cover, freeze-thaw cycles, and varied ignition sources in temperate and boreal regions further complicates seasonal pattern detection (Flannigan et al., 2009). Chuvieco et al., (2021) (Flannigan et al., 2009). Chuvieco et al., (2021) reported about this challenge when building global models. Thus, our findings build upon existing models on global burnt area distribution. What sets our model apart from previous models is its ability to reliably identify global seasonal fire distribution patterns. This simplicity offers a notable advantage, as it facilitates more nuanced interpretation and implementation of DGVMs compared to annual models.

## 4.3 Attribution of global trends

Formatted: Header

Formatted: Line spacing: 1,5 lines, Don't keep with I

Formatted: Line spacing: Multiple 1,36 li

Formatted: Line spacing: 1,5 lines, Don't keep with i

Formatted: Line spacing: Multiple 1,36 li

Our model has contributed novel insights to the existing understanding of the factors influencing global fire trends (Joshi and Sukumar, 2021; Kraaij et al., 2018; Mukunga et al., 2023). Previous research, such as the work by Andela et al. (2017), Previous studies have improved our understanding of drivers of fire but differ in approach and attributional focus for fire trends. For instance, Joshi and Sukumar (2021) employed region-specific multilayer neural networks to reveal spatially varying sensitivities between fire and socio-environmental drivers, providing strong spatial diagnostics but limited transparency on attributions of burnt area trends. Kraaij et al. (2018) provided detailed biome-level attribution of destructive fires by linking drought, fuel state and vegetation context in case studies (e.g., fynbos/plantation complexes), emphasizing vegetation and weather controls at local scales. Mukunga et al. (2023) used random-forest analyses to quantify the added value of human predictors for ignition probability, focusing on anthropogenic controls of ignitions rather than burnt area extent. Building on these approaches, our study contributes novel attributional insight because it explicitly integrates a compact set of DGVM compatible fire-weather and fuel indices (FWI, PTC, TPI, PNTC) with a socio-economic indicator (HDI) within a parsimonious statistical framework for burnt area trends. This allows direct attribution of directional effects (for example, the negative association between HDI and burnt area) across regions. Work by Andela et al. (2017), primarily attributed the decline in global burnt areas to agricultural expansion and intensification. Earl and Simmonds (2018)Earl and Simmonds, (2018) supported this view, adding that increased net primary productivity in Northern Africa also played a significant role. However, our results suggest that human development is a more important driver than agricultural expansion alone. Despite the conventional emphasis on agricultural factors, our attempt to incorporate cropland and rangeland fractions as predictor variables did not substantially enhance our understanding of this trend (model 5 -10, Table 2). Interestingly, our analysis revealed that excluding the HDI from our model and holding it constant to the value of the first year predicted a steady trend that deviates from the observed negative trend in global fire extent and including HDI follows partly followed by a decreasing trend that aligns with the observed trend. (Fig. 5). This highlights the significant influence of HDI in projecting the purported negative global fire trend. HDI is rather broad socioeconomic indicator, which we assume acts as a proxy for factor such as investments and advancements in fire control methods, surveillance, technology, and outreach strategies increasing awareness (Teixeira et al., 2023). Although these Importantly, HDI is not uniform worldwide but varies substantially across regions and levels of socioeconomic development. For instance, in high-HDI countries, greater financial resources, infrastructure, and institutional capacity often translate into stronger investments in fire control technologies, improved surveillance systems, and more effective prevention campaigns. By contrast, in low and middle HDI countries, limited resources and weaker institutional frameworks may constrain fire management capabilities, resulting in greater reliance on natural fire dynamics or less formalized suppression efforts. As many countries continue to develop, it translates improvements in HDI and fire management strategies. Although strategies are often implemented independently and on a smaller scale, their cumulative impact on global fire trends is substantial. Thus, HDI serves as a broad socioeconomic indicator that we assume acts as a proxy for the combined effects of investments, advancements in fire control methods, surveillance, technology, and outreach strategies that increase awareness (Teixeira et al., 2023). Therefore, our model underscores the necessity for global initiatives aimed at enhancing fire control measures through comprehensive awareness campaigns, capacity-building efforts, resource mobilization, and the development and deployment of reliable surveillance technologies. By addressing these factors collectively, we can effectively mitigate the extent and severity of global wildfires, thereby safeguarding ecosystems and human livelihoods.

669

670

671

672

673

674

675

676

677

678

679

680

681

682

683 684

685

686

687

688

689

690

691

692

693

694

695

696

697

698 699

700

701

702

703

704

#### 4.4 Interannual variability

705 706

707

708

709

710

711

712

713

714

715

716

717

718

719

720

721

722

723

724

725

726

727

728

729

730

731

732

733

734

735

736

737

Despite demonstrating the significant role of the HDI in predicting global fire trends, our model struggled to achieve high precision in forecasting interannual variability both globally (see Fig. 5) and within specific GFED regions (see Fig. 54A1). Recognizing that this limitation might stem from an inadequate representation of vegetation (fuel) dynamics, we incorporated FAPAR12 in models 9 to 12 (Table A1) and MEPI in models 11 to 26 (Table A1). Unfortunately, these adjustments did not enhance our ability to predict the interannual variability of wildfires. Studies have found a relationship between increased precipitation in the years preceding the fire season and fire activity in the drier savanna regions of Southern Africa (Shekede et al., 2024). (Shekede et al., 2024). Hence, we also explored the role of previous fuel accumulation on subsequent fire seasons using GPP12 in model 10, respectively. While this approach did not improve global interannual predictions, it showed a slight enhancement in deviance explained (from 0.5357 to 0.5461). This improvement might have been confounded by the effects of the fire-aerosol positive feedback mechanism in Africa (Zhang et al., 2023) (Zhang et al., 2023) and periodic El Niño conditions, which can affect rainfall patterns and lead to drier vegetation conditions, reducing the predictability of fire occurrence, especially with linear models (Shikwambana et al., 2022). (Shikwambana et al., 2022). We note that in the recent comparison of fire-enabled DGVMs in the Fire Model Intercomparison Project (FireMIP) project (Hantson et al. 2020), (Hantson et al., 2020), all models did a poorer job of matching the interannual variability than the spatial patterns by a considerable margin. The seven acceptably-performing models achieved a mean spatial NME (across all data and model comparisons) of 0.84 with respect to spatial patterns, but an NME of 1.15 for interannual variability. Our modelling efforts highlight the complexity of accurately predicting wildfire trends and underscore the need for future research to identify covariates that more effectively capture the interannual variability of fires at a global scale.

# 4.5 Fire seasonality

Globally, our model predicts a notable peak in burnt areas during February and August. (Fig. 8). The February peaks corresponds to dry conditions and fuel accumulation in northern hemisphere regions such as NHSA, NHAF, and MIDE. In contrast, (Fig. A2), with the complementary August peak primarily emanates from tropical occurring in regions characterized by distinct seasonal patterns, particularly in such as SHSA, SHAF, and AUST. Here, Our model predicts this with only two sub annual predictors - the dry season augments the combustibility logarithm of accumulated fuel from the preceding wet season, facilitating fire spread. This observation corroborates earlier studies in the southern hemisphere, which underscore the prevalence of wildfires during prolonged dry spells (Magadzire, 2013; Shekede FWI and MEPI as already demonstrated for Europe by Forrest et al., (2024; Strydom and Savage, 2017). Increased temperatures and desiceated vegetation substantially enhance the likelihood and severity of wildfires during the dry season. Conversely, the onset of the rainy season precipitates a marked reduction in the occurrence of wildfires in these regions.). This underscores the enduring influence of fire weather and vegetation dynamicsgrowth and phenology as principal drivers of seasonal burnt area cycles, with factors such as moisture content in vegetation and soil, as well as humidity, playing pivotal roles in modulating ignition and fire extent within

Formatted: Line spacing: 1,5 lines, Don't keep with

Formatted: Line spacing: Multiple 1,36 li

ecosystems. The seasonal forecasts generated by our model hold significant implications for guiding adaptive strategies, fire management and prevention at both regional and global scale.

The findings of this study exhibit robustness in capturing the global seasonal evelescycle ( $R^2 = 0.536$ , See Fig.7), facilitated by the inclusion of monthly variables such as the MEPI and the logarithm of FWI, which are pivotal in delineating seasonal fire patterns. While the seasonal predictions demonstrate reliability across most GFED regions globally, but notable exceptions were observed in North America, the Middle East and Mediterranean North Africa, and Europe (R2 <0.50, See Fig.8). This discrepancy could be attributed to the intricate climatic conditions inherent to these regions, which influence fires in a manner that eludes simple linear modelling. For instance, tropical regions with clear-cut wet and dry seasons tend to exhibit more regular fire cycles, largely governed by seasonal shifts in precipitation, temperature, and vegetation growth. These predictable patterns make them well-suited to linear modelling approaches (Van Der Werf et al., 2017). (Van Der Werf et al., 2017). contrast, extra-tropical areas in the northern hemisphere experience more irregular and less seasonally driven fire activity. Here, the interaction of drought events, land management, and socio-economic drivers introduces variability that weakens model performance (Chuvieco et al., 2021; Forkel et al., 2019b). (Chuvieco et al., 2021; Forkel et al., 2019), Additionally, varied ignition sources in temperate and boreal zones disrupt consistent seasonal fire patterns (Flannigan et al., 2009). (Flannigan et al., 2009). Given the parsimonious design of our model, with only ~eight predictors and only two of those on a monthly time step, we think that the model's performance is acceptable. For Furthermore, this acceptable seasonal performance fills a gap in the available global fire models. To our knowledge there are no such models which are strongly data-constrained (i.e statistically fitted as opposed to empirical or processes-based) and which predict the seasonal cycle. The closest is SIMFIRE, which is fitted to observed data but which calculates annual burnt area and then distributes throughout the year using a prescribed seasonal cycle based on observed data (Rabin et al., 2017). So, whilst the work presented is not yet integrated into a DGVM, it represents a significant advance in this direction. This is particularly important given the comparatively poor performance of global fire models in predicting the seasonal concentration of burnt area (Hantson et al., 2020, Table 3). However, for certain regions, it might be possible to increase model performance by implementing further region-specific predictors and relationships. Accurate predictions regarding the seasonal dynamics of diverse GFED regions can facilitate the identification of temporal windows when fires are prevalent, thereby furnishing valuable insights for simulating carbon emissions in DGVMs.

# 4.6 Model limitations and excluding drivers of burnt area

738

739

740 741

742

743

744

745

746

747

748

749

750

751

752

753

754

755

756

757

758

759

760

761

762

763

764

765

766

767

768

769

770

771

Several covariates initially considered, such as landcover variables (~PCC, PPS, PRC, PGC), vegetation (~FAPAR) and socioeconomic (~RD), did not make it to the final model (See Table A1) despite their potential relevance identified in previous studies (Forkel et al., 2019; Hantson et al., 2015; Knorr et al., 2014; Pausas and Keeley, 2021; Perkins et al., 2022).(Forkel et al., 2019; Hantson et al., 2015; Knorr et al., 2014; Pausas and Keeley, 2021; Perkins et al., 2022). The differences in our findings are related to differences in the statistical or modelling approach and the fact that most of these studies addressed annual BA patterns, not seasonal variations. Nevertheless, these other factors can clearly also be important for understanding

Formatted: Header

Formatted: English (United States)

Formatted: Line spacing: 1,5 lines, Don't keep with I

Formatted: Line spacing: Multiple 1,36 li

Formatted: English (United States)

fire dynamics, e.g., influencing fuel availability, landscape structure, and ignition sources. For instance, grazing lands can significantly impact fire behavior by altering fuel types and continuity, with areas used for grazing potentially reducing fuel loads (Davies et al., 2010; Strand et al., 2014). (Davies et al., 2010; Strand et al., 2014). Similarly, FAPAR indicates vegetation health and productivity, affecting fuel moisture content and thus fire risk (Pausas and Ribeiro, 2013). (Pausas and Ribeiro, 2013). However, these factors are apparently indirectly represented by the final model, as they are correlated to the driver variables in the final model. FAPAR, for example, is generally highly correlated with GPP. Furthermore, RD is associated with human-caused ignitions and fire suppression capabilities (Forkel et al., 2019b). (Forkel et al., 2019). However, it was excluded here because its contributions were already effectively represented by HDI and PPN, which capture broader socioeconomic conditions and infrastructure impacts. Apart from that, Haas et al., (2022) Apart from that, Haas et al. (2022) observed a shift in the direction of contribution for covariates when PPN and RD are used together. -Considering that we may not have future projections for RD unlike PPN, including the issue of collinearity, we decided to retain only PPN in our model. Furthermore, our attempt to include RD in our models 21, 23 and 24 (Table A1) yielded marginal improvements, which were not different from when we excluded it in model 25. Overall, the decision to exclude most of these covariates was aimed at reducing redundancy and multicollinearity, ensuring a balance between model complexity and predictive power. By focusing on more comprehensive variables with high explanatory power, the final model achieves robust explanatory power. However, the often-small differences in the deviance explained and the NME between different models imply that vegetation-fire modelers might also pick a slightly different set of variables for DGVM integration without using much predictive power.

While our research represents relevant efforts in developing a streamlined model capable of accurately capturing seasonal variations in global fire distribution, it's important to acknowledge certain limitations. The selection of covariates and the statistical model was constrained by the necessity for integration within DGVMs applied to predict future dynamics, potentially omitting some previously identified key predictors (~lightning frequency, gridded livestock densities) and modelling techniques (~ Random Forest, Neural networks, XgBoost, CatBoost) for global fires (Forkel et al., 2019b; Joshi and Sukumar, 2021; Mukunga et al., 2023; Zhang et al., 2023; Zhang et al., 2023; Zhang et al., 2023). (Forkel et al., 2019; Joshi and Sukumar, 2021; Mukunga et al., 2023; Zhang et al., 2023) are interannual variability across many parts of the world. Future investigations should aim to explore the inclusion of other established predictors and methodologies in global fire modelling once they become easily compatible with DGVM integration. Despite these challenges, our study possesses intrinsic value, and the developed model stands as a relatively simple tool for informing global seasonal fire predictions.

## 4.7 Next steps for DGVM integration, future directions and model improvements

To integrate the model presented here into a DGVM and enable future predictions, the remotely sensed variables of vegetation state (PTC, PNTC and MEPI) must be replaced with equivalent variables from the DGVM. -DGVMs include GPP and the cover fractions of vegetation types required to calculate PTC, PNTC and MEPI, so these variables provide a robust and universal coupling strategy to capture the effect of vegetation on burnt area. areas. However, all model results are imperfect and biased to some degree, so the DGVM variables will not correspond perfectly with the remotely sensed ones used for model

Formatted: English (United States)

training. -This error will propagate to the burnt area calculation and so this discrepancy should be investigated. -In the likely event that this discrepancy is not small, the GLM should be refitted using the model-calculated variables to implicitly account for biases in the DGVM simulation, although the burnt area estimated will still be dependent on the DGVM's skill to capture certain dynamics and states. However, we note that our comparatively restricted variable set and simple GLM approach will be more straightforward to integrate and less sensitive to errors in the DGVM simulated state than machine learning approaches with larger suites of predictor variables. For example Son et al., (2024)For example Son et al. (2024) achieved excellent correspondence with observed data using an advanced recursive neural network which was partially integrated into the JSBACH DGVM. However, only the fuel predictor was taken from the prognostically simulated JSBACH model state, other high importance dynamic predictors (including PFTplant functional type cover fractions and both absolute values and anomalies of LAI and water content of four soil layers) are all determined from fixed input data - remotely sensed of climate reanalysis. So Thus, in this case, the quality of the results from hypothetical full integration will be dependent on the ability of JSBACH to simulate many more variables correctly. -The model presented here is tailored for integration into a DGVM by using only a few variables which can be robustly predicted, and, as a simple GLM in contrast to more complex machine learning methods, is less prone to overfitting and relying on correlations in the data which may not hold in the DGVM predicted state. Furthermore, the new model includes seasonal variations in burned area, which are not captured by all existing fire modules within DGVMs (Hantson et al., 2020).

823 <u>modules within DGVMs (Hants</u>
824
825 In comparison to the vegetation

808

809

810

811

812

813

814

815

816

817

818

819

820

821

822

826

827

828

829

830

831

832

833

834

835

836

837

838 839 In comparison to the vegetation variables, the inclusion of the other variables (FWI, HDI, PPN, NDD, TPI) is trivial as they can either be prescribed input variables or can be calculated from the climate input. -Finally, to build a fully coupled vegetation-fire model, it is then necessary to include the effects of the simulated fire on the vegetation. -For this step we can utilise the mortality and combustion components of fire models already available and integrated into DGVMs, for example the BLAZE model (Rabin et al., 2017) or the appropriate equations in SPITFIRE (Thonicke et al., 2010). These parameterizations may need to be adjusted to account for the different simulated burnt area. (Rabin et al., 2017) or the appropriate equations in SPITFIRE (Thonicke et al., 2010). These parameterizations may need to be adjusted to account for the different simulated burnt areas.

### 5. Conclusions

We sought to build a parsimonious statistical model for global seasonal burnt areas that can be integrated into a DGVM. The specific objectives were to 1) to improve our understanding of major drivers of global burnt area dynamics, 2) to leverage a GLM for predicting global burnt areas using DGVM integrable predictors and 3) to evaluate the interannual and seasonal eyeles of burnt area extent, both globally and regionally.

We present a parsimonious statistical model specifically tailored for global burnt areas, with the goal of integration into DGVMs. FWI, PTC, TPI and PNTC were positively related to BA, while MEPI, HDI, PPN, and NDD were negatively related

Formatted: Line spacing: 1,5 lines, Don't keep with

to BA. Our findings highlight the significance of socio-economic advancements, particularly those improving fire management strategies, as evidenced by the negative trend in global fire extent predicted through the inclusion of the HDI as a crucial socio-economic predictor in our model. While our parsimonious model exhibited limitations in predicting the interannual variability of global fires, it demonstrated commendable accuracy in forecasting the spatial (NME = 0.72). The strength of similarity between observed and predicted seasonal cycles varied according to the GFED region with  $R^2$  ranging between 0.06 to 0.99. Its standout performance laid in capturing the seasonal variability, especially in regions often characterized by distinct wet and dry seasons, notably southern Africa ( $R^2$ =0.72 to 0.99), Australia ( $R^2$ 68) and South America ( $R^2$ =0.75 to 0.90). Our predicted interannual variability exhibited poor strength of relationship between the predicted trend when compared to the observed ( $R^2$ =0.24)

We hope that our research outcomes will stimulate a more rigorous implementation of global fire models within DGVM frameworks. This, in turn, will contribute to a deeper understanding of the intricate dynamics of global fire patterns and enhance our capacity to effectively manage and mitigate the consequences of evolving fire regimes in the face of ongoing global changes.

We present a parsimonious statistical model to simulate global burnt area on a monthly timestep thus including seasonal variations. This is an important advance as representation of the seasonal cycle is a weakness in global fire models, both in and out of DGVMs, and across different model types. Notably, this representation of the seasonal cycle was achieved with only two sub annual predictor variables. We found the drivers FWI, TPI, and PNTC are positively associated with BA, whereas MEPI, HDI, PPN, and NDD exhibit negative relationships, and PTC showed a unimodal response with strongest effect at intermediate tree cover. The diversity of these drivers underscores the multifaceted influence of both climatic and socioeconomic drivers on fire dynamics. Our model explicitly accommodates these drivers, capturing how variations in climate, vegetation productivity, and human development interact to modulate fire occurrence and extent. Notably, the use of HDI to represent societal development as a proxy for fire management capacity and the transition away from fire-dependent agricultural practices provides a coarse but global socioeconomic driver beyond GDP and population density. Including this in DGVMs can improve fire, vegetation and human feedbacks, particularly with respect to Shared Socioeconomic Pathways (SSPs, O'Neill et al., 2017) or other scenarios.

Overall, the model developed in this study has demonstrated strong performance in simulating global burned area patterns. It holds potential for integration into DGVMs to enhance the representation of fire dynamics, albeit it remains to be tested how well the model performs when remote-sensing-derived vegetation and land cover variables are replaced with those simulated by a DGVM.

Code and data availability

Formatted: Line spacing: Multiple 1,36 li

875

878

879

880

881

882

883

884

885 886

887

888

893 894

895

896

897

898

899

900

901

The code used in this analysis, model fitting, and plotting is available at https://doi.org/10.5281/zenodo.14177016. Data used for model fitting are available at https://doi.org/10.5281/zenodo.14110150.

#### Author contribution

BK contributed to conceptualization of the model and data analysis and model fitting. MF and TH supported developing the statistical framework and interpreting the results. BK drafted the manuscript, with input from MF and TH.

# Acknowledgements

This project has received funding from the German Research Foundation (DFG) grant "Fire in the Future: Interactions with Ecosystems and Society (FURNACES) project" under grant number HI 1538/14-1. BK received a salary from FURNACES.

## Competing interests

The authors declare that they have no known competing financial interests or personal relationships that could have influenced the work reported in this paper.

## Appendices

Table A1: Results of modelling attempts using different combinations of predictor variables using a progressive inclusion of covariates approach. For Normalized Mean Error (NME), higher values are represented by warmer colours (with red indicating the highest error), while lower values appear in cooler colours (green indicating the lowest error). In contrast, for Deviance Explained, higher values are shown in cooler colours (green indicating better performance), and lower values in warmer colours (red indicating poorer performance). An optimal model is indicated by a combination of cooler colours for both metrics, whereas a combination of warmer colours suggests poor model performance.

Model	Formulae	Deviance explained	NME
model 1	glm(burnt ~ FWI + GPP + HDI + PTC + RD)	0.3548030	0.7472088
model 2	glm(burnt ~ FWI + GPP + HDI + PTC + RD + PGC)	0.3699393	0.7495652
model 3	$glm(burnt \sim FWI + GPP + HDI + PTC + RD + PNTC)$	0.5298061	0.7208771
model 4	glm(burnt ~ FWI + GPP + HDI + PTC + RD + PNTC + FAPAR)	0.5312036	0.7188448

Formatted: Header

Formatted: Don't keep with next

Formatted: Line spacing: Multiple 1,36 li

Formatted: Line spacing: Multiple 1,36 li

Formatted: Line spacing: Multiple 1,15 li

Formatted: Font color: Auto

Formatted: Font color: Auto

Formatted: Line spacing: Multiple 1,15 li

Formatted: Font color: Auto

Formatted: Line spacing: Multiple 1,15 li

Formatted: Font color: Auto

Formatted: Line spacing: Multiple 1,15 li

Formatted: Font color: Auto

Formatted: Font color: Auto

Formatted: Line spacing: Multiple 1,15 li

model 5	glm(burnt ~ FWI + GPP + HDI + PTC + RD + PNTC + FAPAR + PCC)	0.5312697	0.7191269
model 6	glm(burnt ~ FWI + GPP + HDI + PTC + RD + PNTC + FAPAR + PCC + PPS)	0.5328183	0.7195616
model 7	glm(burnt ~ FWI + GPP + HDI + PTC + RD + PNTC + FAPAR + PCC + PRC)	0.5313813	0.7193946
model 8	glm(burnt ~ FWI + GPP + HDI + PTC + RD + PNTC + FAPAR + PCC + PGC)	0.5349288	0.7190611
model 9	glm(burnt ~ FWI + GPP + HDI + PTC + RD + PNTC + FAPAR + PCC + FAPAR12 + PGC)	0.5359802	0.7181930
model	glm(burnt ~ FWI + GPP12 + HDI + poly(PTC, 2) + PNTC + FAPAR + PCC + FAPAR12 + PGC + PPN_)	0.5295939	0.7172668
model 11	glm(burnt ~ FWI + MEPI + HDI + poly(PTC, 2) + RD + PNTC + FAPAR12 + PGC + PS)	0.5579946	0.7193546
model 12	glm(burnt ~ FWI + MEPI + HDI + poly(PTC, 2) + RD + PNTC + FAPAR12 + PS)	0.5571164	0.7192122
model 13	glm(burnt ~ FWI + MEPI + HDI*PCC + PGC + RD + poly(PTC, 2) + PNTC + PS)	0.5569187	0.7214560
model	glm(burnt ~ FWI + MEPI + HDI*PGC + RD + poly(PTC, 2) + PNTC+ PS)	0.5570586	0.7222061
model 15	glm(burnt ~ FWI + MEPI + HDI*PRC + RD + poly(PTC, 2) + PNTC + PS)	0.5664789	0.7154708
model 16	glm(burnt ~ FWI + MEPI*PNTC + HDI + RD + poly(PTC, 2) + PS)	0.5563012	0.7215202
model 17	glm(burnt ~ FWI + MEPI + HDI + RD + poly(PTC, 2) + PNTC + PS + NDD)	0.5681926	0.7191069
model 18	glm(burnt ~ FWI + MEPI + HDI + RD + poly(PTC, 2) + PNTC* PS + NDD + TPI)	0.5711503	0.7167015
model 19	glm(burnt ~ FWI + MEPI + HDI + RD + poly(PTC, 2) + PNTC* PS + NDD + PGC + FAPAR12)	0.5709692	0.7175149
Model 20	glm(burnt ~ FWI + MEPI + HDI + poly(PTC, 2) + PNTC* PS + NDD + FAPAR12)	0.5677209	0.7182814
Model 21	glm(burnt ~ FWI + MEPI + HDI + poly(PTC, 2) + RD + PNTC*PS + NDD + TPI + PPN	0.5714474	0.7170576
Model 22	glm(burnt ~ FWI + MEPI + HDI + poly(PTC, 2)+ PNTC*PS + NDD + TPI + PPN	0.5705348	0.7177887
Model 23	glm(burnt ~ FWI + MEPI+ HDI + poly(PTC, 2) + RD + PNTC*PS + NDD+ TPI+ PPN	0.5714474	0.7170576
Model 24	glm(burnt ~ FWI + MEPI + HDI + poly(PTC, 2) + RD + PNTC*PS + NDD + TPI + PPN + AAP	0.5720048	0.7173093
Model 25	glm(burnt ~ FWI + MEPI + HDI + poly(PTC, 2) + PNTC + PPN + NDD + TPI	0.5682776	0.7186160

**Formatted Formatted Formatted Formatted** Formatted Formatted **Formatted Formatted Formatted** Formatted Formatted **Formatted Formatted Formatted Formatted Formatted Formatted** Formatted **Formatted Formatted Formatted Formatted** Formatted **Formatted Formatted Formatted Formatted Formatted Formatted Formatted** Formatted **Formatted** 

**Formatted** 

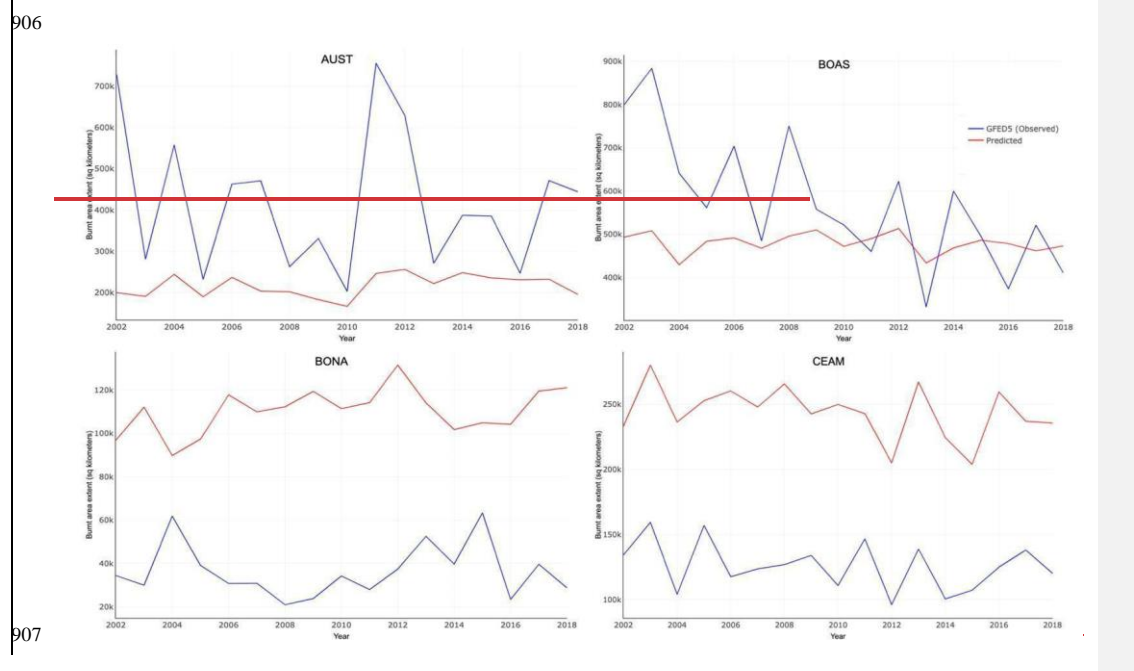
**Formatted** 

Formatted
Formatted
Formatted
Formatted
Formatted
Formatted
Formatted

48

Model	glm(burnt ~ FWI + MEPI + HDI + poly(PTC, 2)* NDD + NTC + PPN + NTC	0.5687439	0.7194855	
26	+ TPI			ĺ

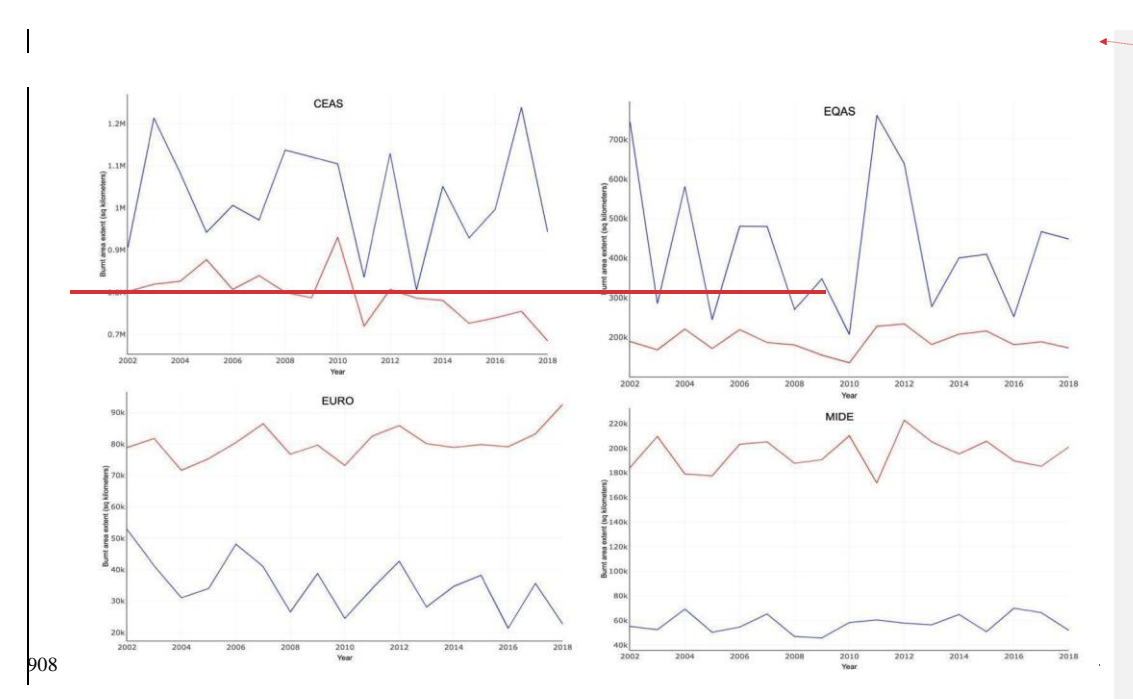
Table A2: Mann-Kendall test results for trend analysis across GFED regions from 2002 to 2018.



Formatted: Header

Formatted: Font color: Auto

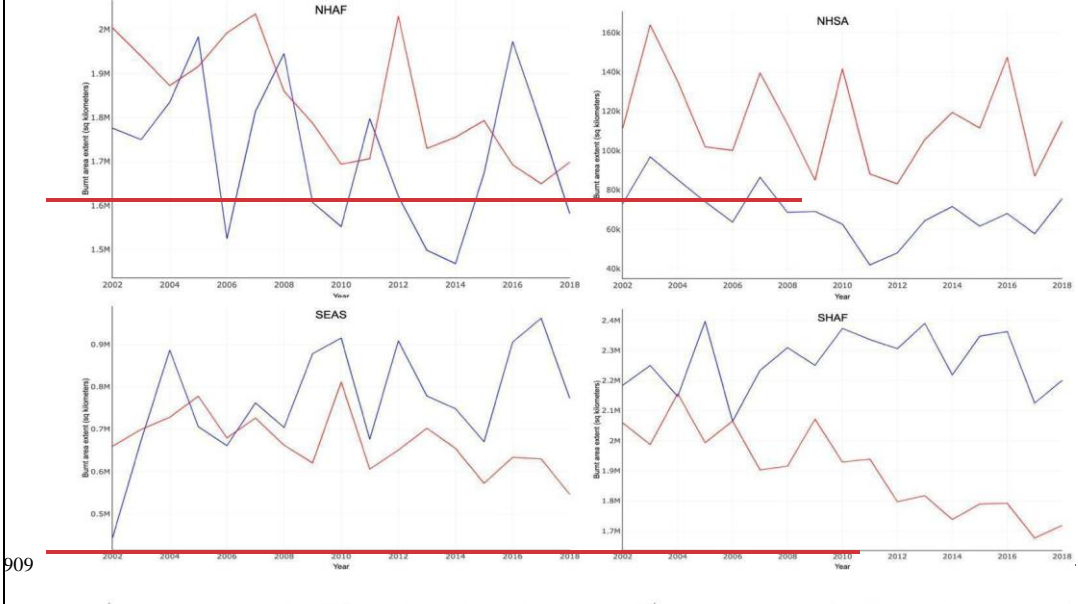
Formatted: Line spacing: Multiple 1,15 li

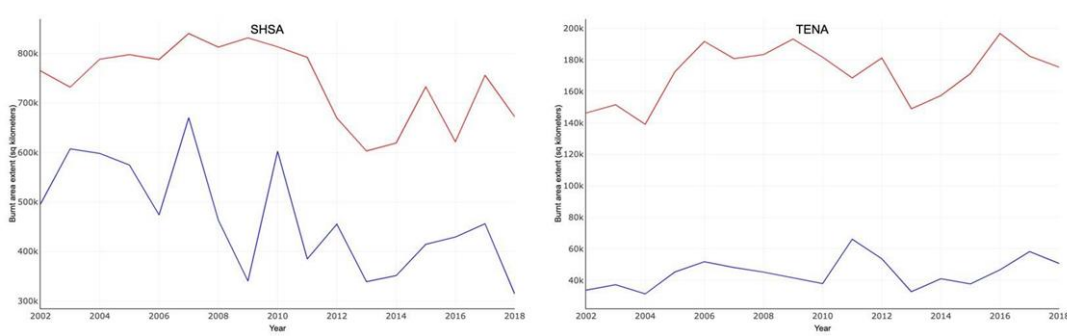


Formatted Table

Formatted: Header





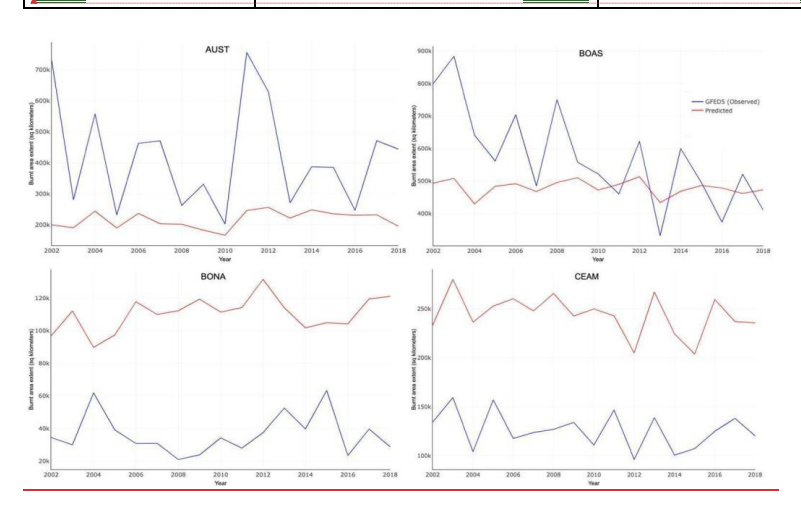


The GFED regions include Boreal North America (BONA), Temperate North America (TENA), Central America (CEAM), Northern Hemisphere South America (NHSA), Southern Hemisphere South America (SHSA), Europe (EURO), Middle East (MIDE), Northern Hemisphere Africa (NHAF), Southern Hemisphere Africa (SHAF), Boreal Asia (BOAS), Central Asia (CEAS), Southeast Asia (SEAS), Equatorial Asia (EQAS) and Australia and New Zealand (AUST). Regions with significant trends are bold (NHAF, SHAF, CEAS, SEAS); the remaining ten regions show insignificant trends.

Formatted: Line spacing: Multiple 1,36 li

Formatted: Font: Not Bold

Region	Sen's slope	P-value
BONA	558.354	0.1082
<u>TENA</u>	895.8292	0.4338
<u>CEAM</u>	<u>-1963.035</u>	<u>0.1494</u>
NHSA	<u>-1601.363</u>	<u>0.387</u>
SHSA	<u>-9119.019</u>	0.0529
<u>EURO</u>	<u>189.2956</u>	<u>0.387</u>
MIDE	202.3893	<u>0.9016</u>
NHAF	<u>-22329.83</u>	0.0026
SHAF	<u>-28205.43</u>	0.0001
BOAS	<u>-1560.25</u>	0.1494
CEAS	<u>-8342.713</u>	<u>0.0011</u>
<u>SEAS</u>	<u>-9671.238</u>	0.0034
EQAS	<u>69.04606</u>	<u>0.9671</u>
AUST	1141.46	0.3434



Formatted: Header

Formatted: Font color: Auto

Formatted: Line spacing: Multiple 1,15 li

Formatted: Font color: Auto

Formatted: Line spacing: Multiple 1,15 li

Formatted: Font color: Auto

Formatted: Line spacing: Multiple 1,15 li

Formatted: Font color: Auto

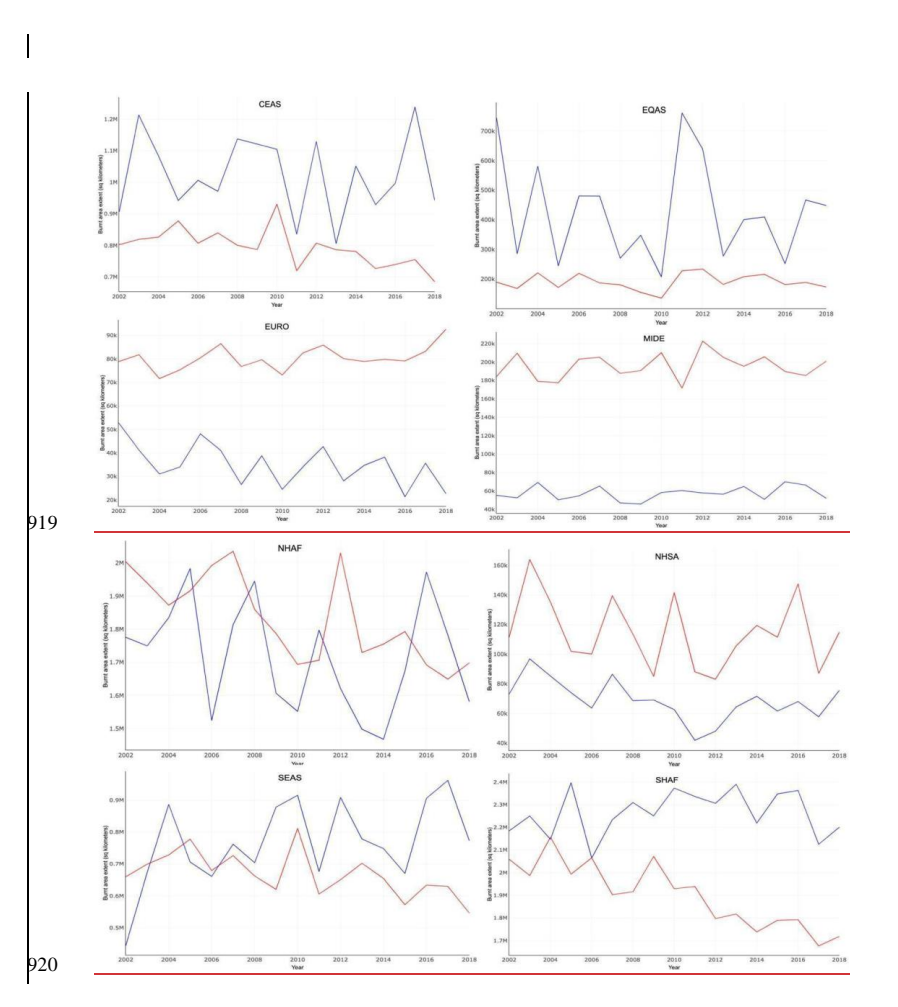
Formatted: Line spacing: Multiple 1,15 li

Formatted: Font color: Auto

Formatted: Line spacing: Multiple 1,15 li

**Formatted Table** 

52





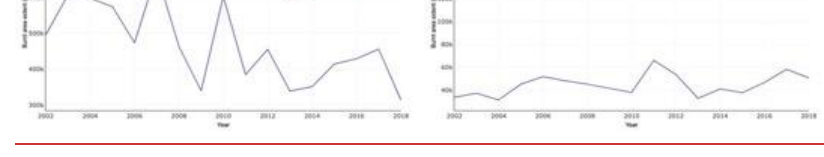
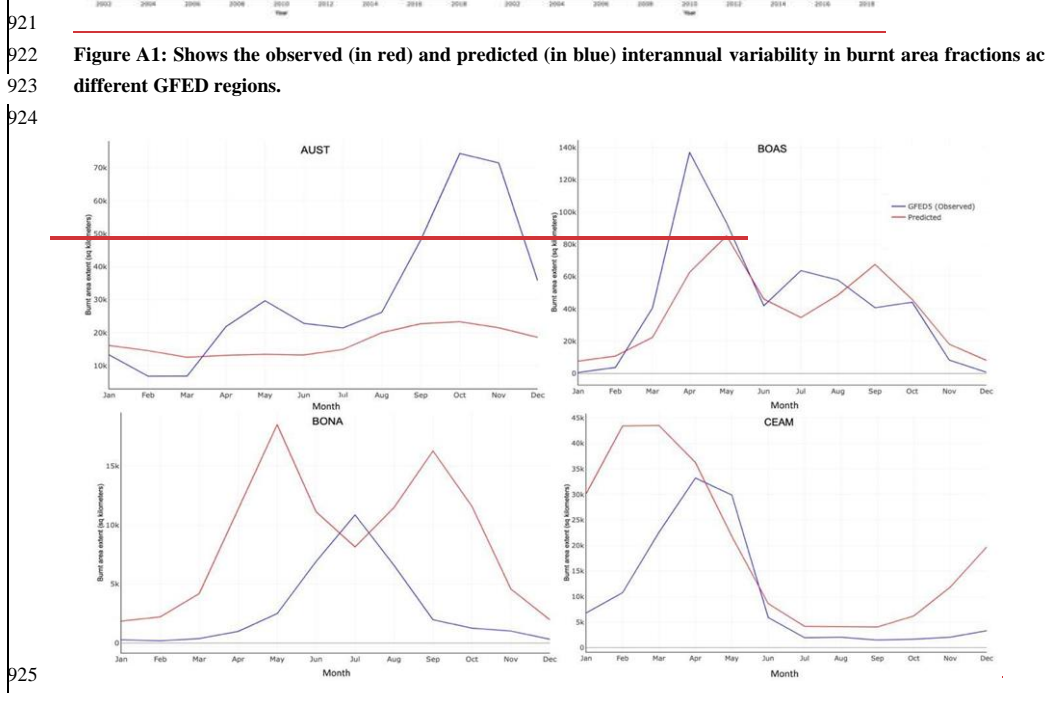
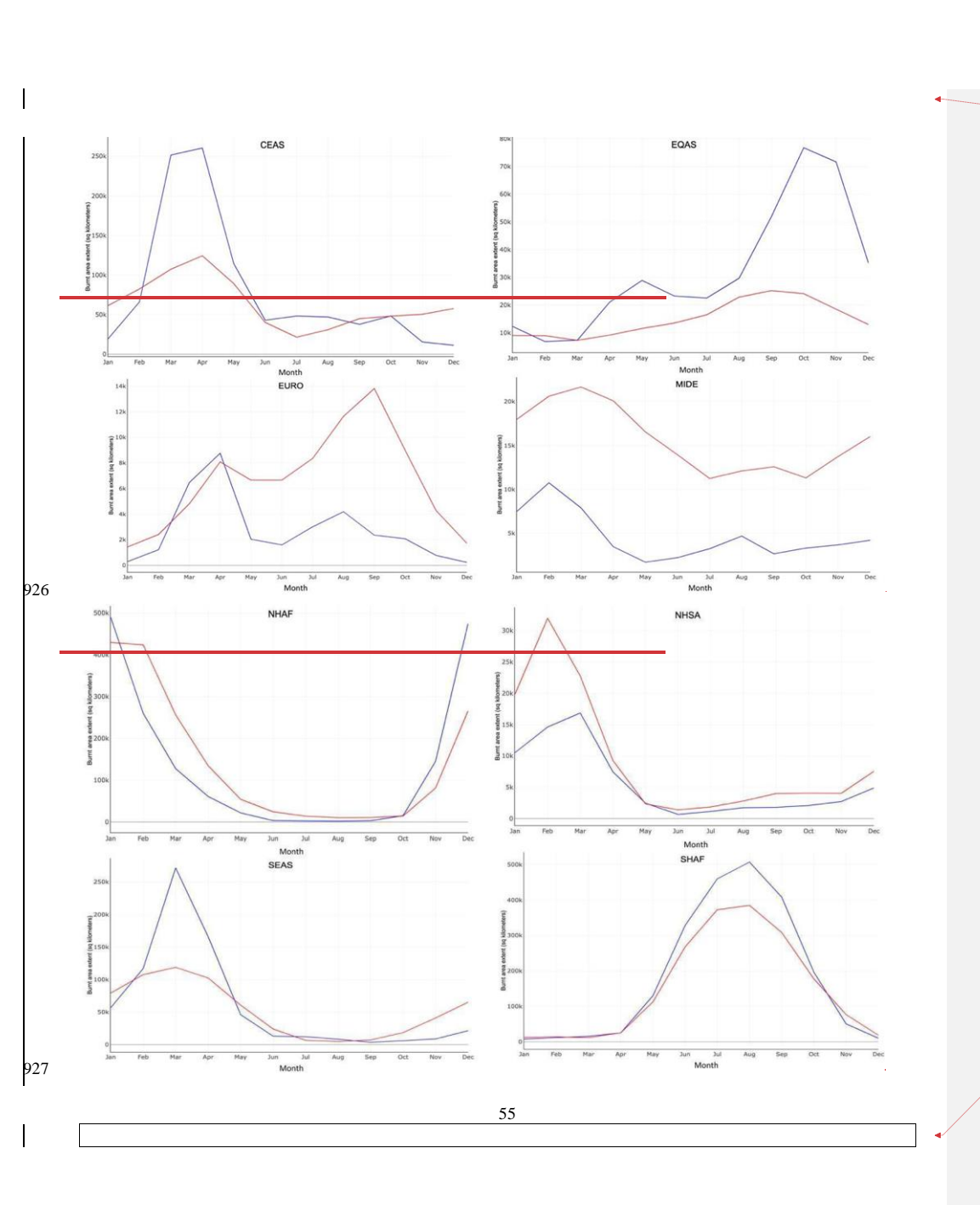
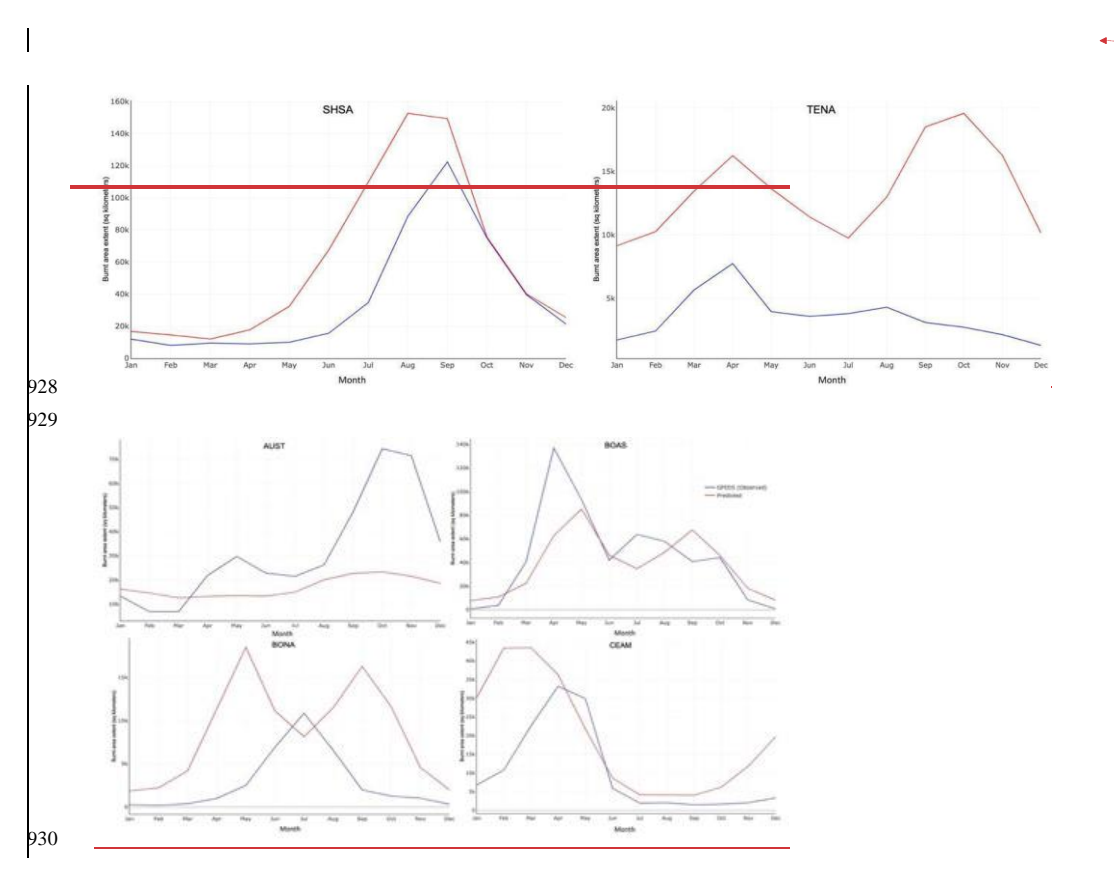


Figure A1: Shows the observed (in red) and predicted (in blue) interannual variability in burnt area fractions across different GFED regions.









Formatted Table

Formatted: Header

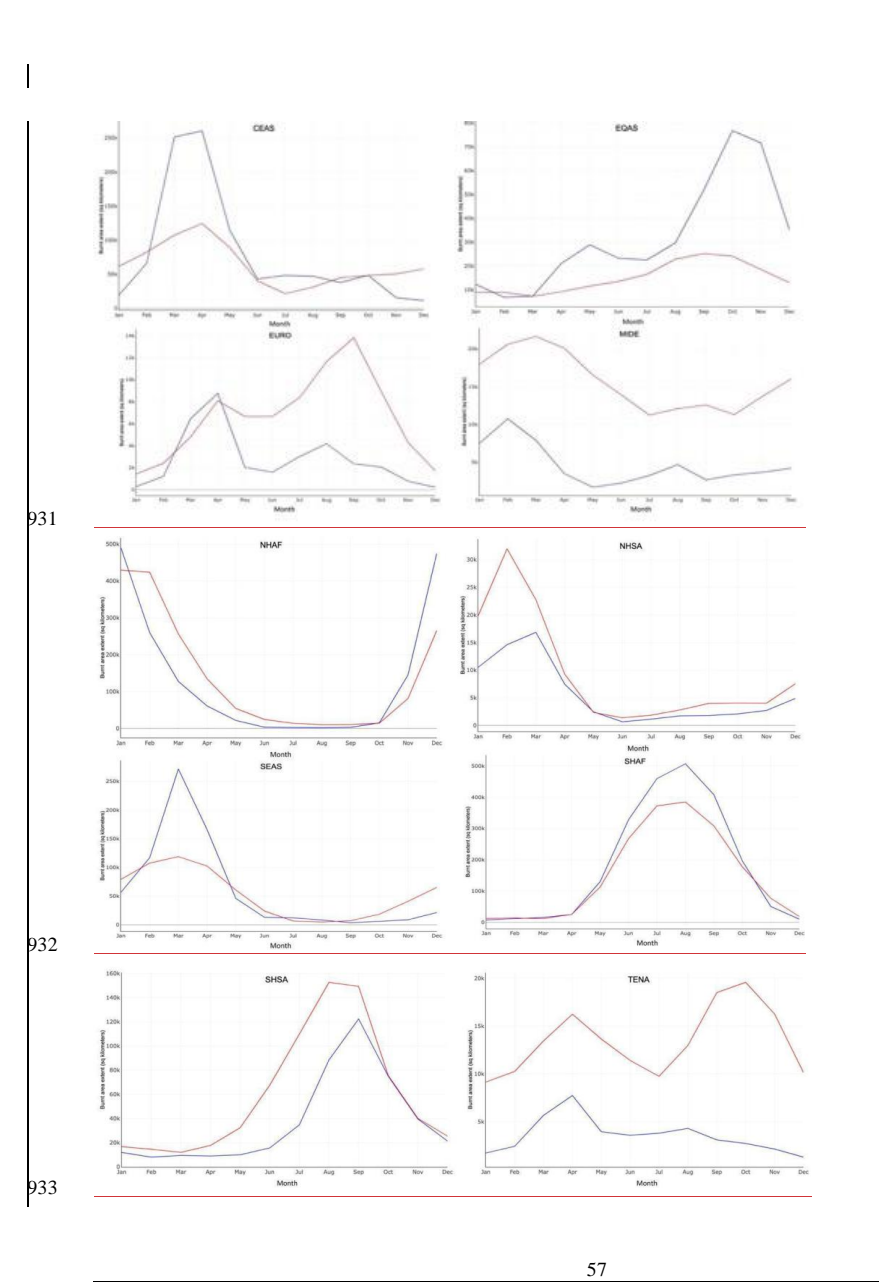
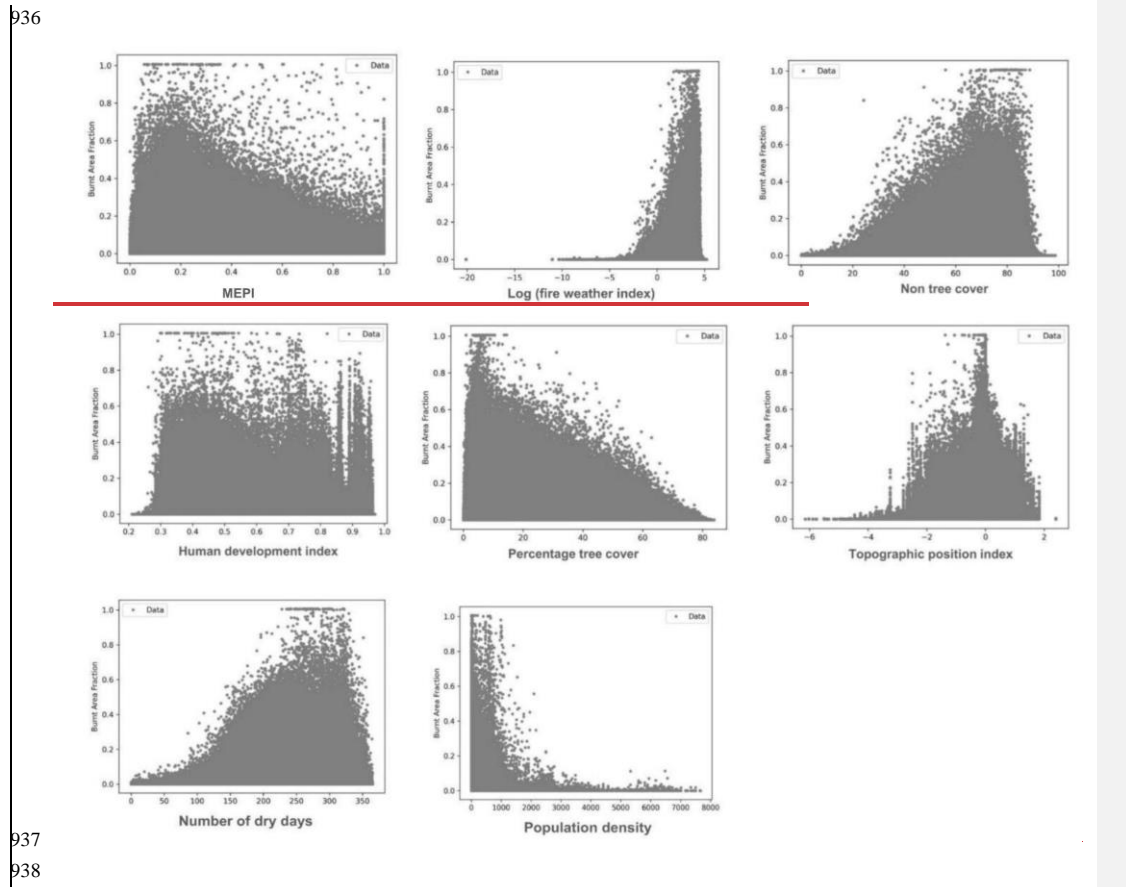


Figure A2: Shows the observed (in red) and predicted (in blue) seasonal variability in burnt area fractions across different GFED regions.

935



Formatted: Header

Formatted: Line spacing: Multiple 1,36 li



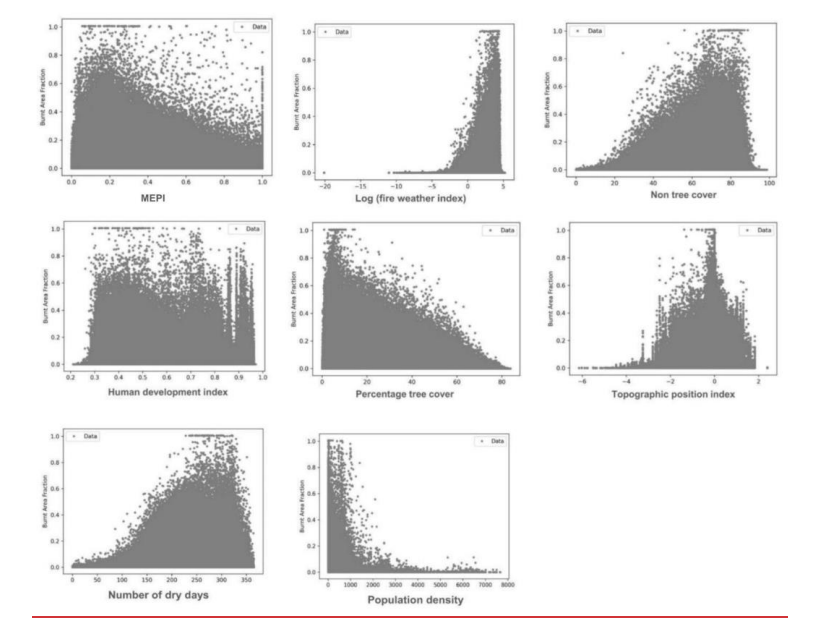


Figure A3: Scatter plots illustrating single-factor relationships between burnt area fraction and various environmental and socio-economic variables: GPP Index, Fire Weather Index, Percentage Non-Tree Cover, Human Development Index, Percentage Tree Cover, Topographic Position Index, Percentage Dry Days, Road Density, Precipitation Seasonality and Annual Precipitation Index. The plots highlight distinct patterns, such as the negative correlation between percentage tree cover and burnt area fraction, and the positive correlation between number of dry days and burnt area fraction.

Region	Sen's slope	P-value
BONA	558.354	0.1082
TENA	895.8292	0.4338
CEAM	-1963.035	0.1494

Formatted: Line spacing: Multiple 1,36 li

**Formatted Table** 

Formatted: Header



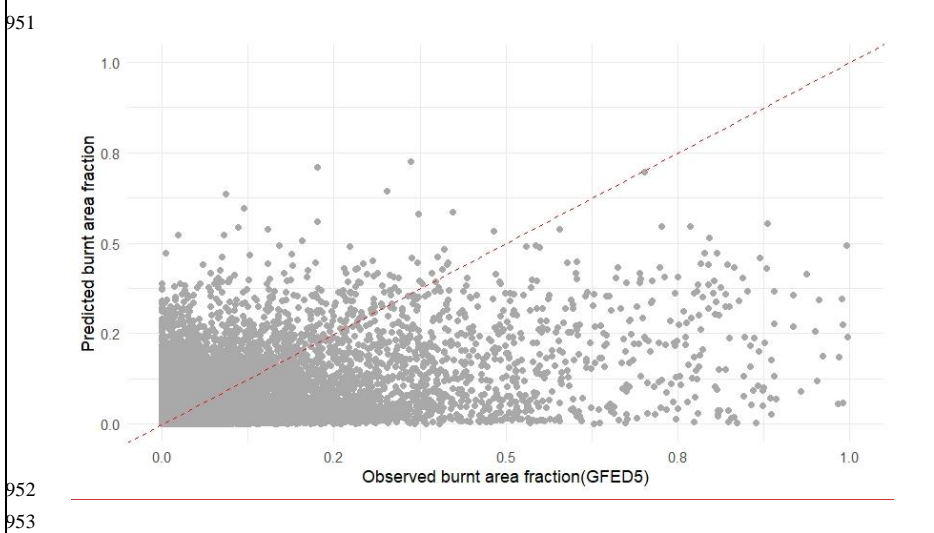


Figure A4: Scatter plots illustrating the relationships between observed burnt area fraction (GFED5) and predicted burnt area fraction for the period between 2002 and 2018.



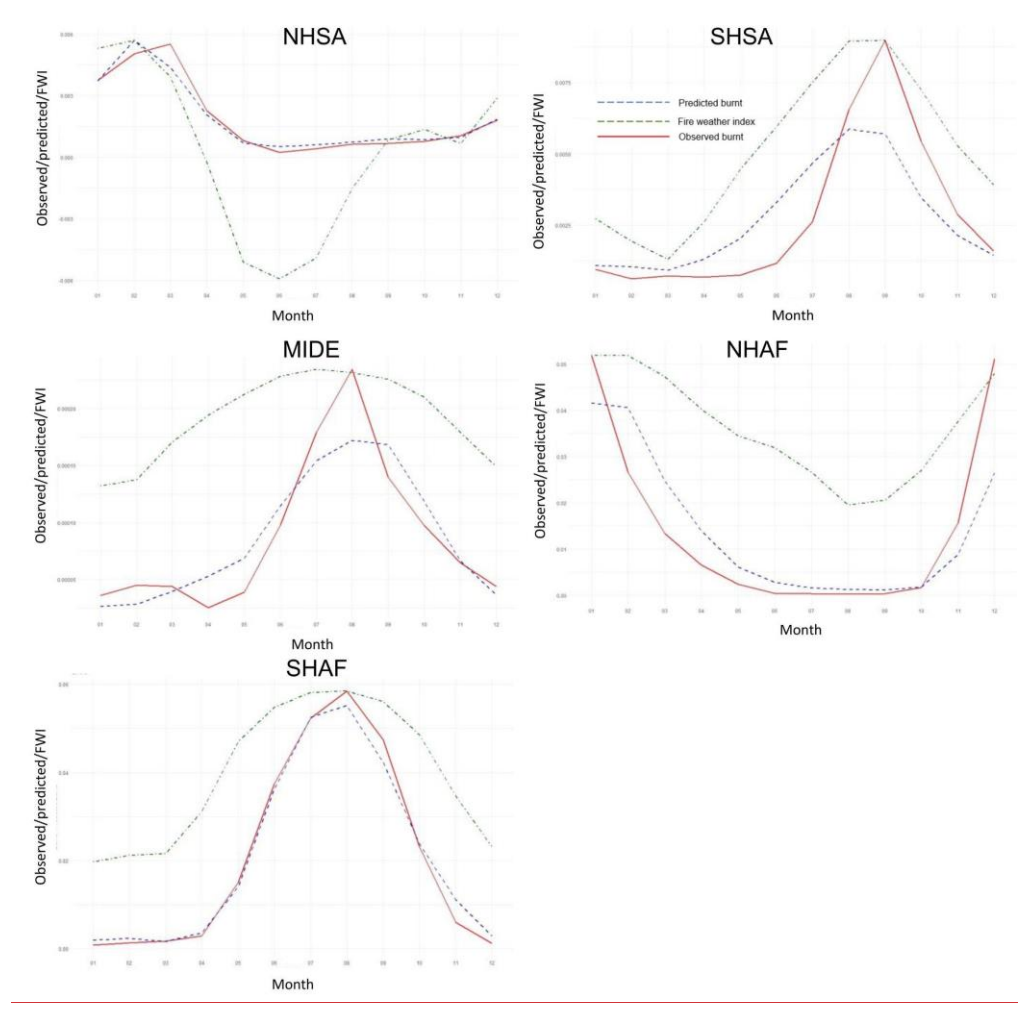


Figure A5. Shows the observed burnt area (in red), predicted burnt (in blue) seasonal variability in burnt area, fire weather index (in green) across GFED regions that have distinct seasonal patterns.

BOAS	<del>-1560.25</del>	<del>0.1494</del>	
CEAS	<del>-8342.713</del>	0.0011	
SEAS	<del>-9671,238</del>	0.0034	
EQAS	<del>69.04606</del>	<del>0.9671</del>	
AUST	<del>1141.46</del>	0.3434	

Table A2: Mann-Kendall test results for trend analysis across GFED regions from 2002 to 2018. Regions with significant trends are bold (NHAF, SHAF, CEAS, SEAS); the remaining ten regions show insignificant trends.

#### References

962

963

964

965

966

967

985

- Aldersley, A., Murray, S.J., Cornell, S.E., 2011. Global and regional analysis of climate and human drivers of wildfire. Sci.
- 968 Total Environ. 409, 3472 3481.
- Andela, N., Morton, D.C., Giglio, L., Chen, Y., van der Werf, G.R., Kasibhatla, P.S., DeFries, R.S., Collatz, G.J., Hantson, S.,
- Archibald, S., 2016. Managing the human component of fire regimes: lessons from Africa. Philos. Trans. R. Soc. B Biol. Sci.
- 971 371, 20150346. https://doi.org/10.1098/rstb.2015.0346.
- Bergado, J.R., Persello, C., Reinke, K., Stein, A., 2021. Predicting wildfire burns from big geodata using deep learning. Saf-
- 973 Sci. 140, 105276.
- 974 Bistinas, I., Harrison, S.P., Prentice, I.C., Pereira, J.M.C., 2014. Causal relationships versus emergent patterns in the global
- 975 controls of fire frequency. Biogeosciences 11, 5087–5101.
- P16 Blouin, K.D., Flannigan, M.D., Wang, X., Kochtubajda, B., 2016. Ensemble lightning prediction models for the province of
- 977 Alberta, Canada. Int. J. Wildland Fire 25, 421 432.
- 978 Bowman, D.M., Kolden, C.A., Abatzoglou, J.T., Johnston, F.H., van der Werf, G.R., Flannigan, M., 2020. Vegetation fires in
- 979 the Anthropocene. Nat. Rev. Earth Environ. 1, 500 515.
- Bowman, D.M., O'Brien, J.A., Goldammer, J.G., 2013. Pyrogeography and the global quest for sustainable fire management.
- 981 Annu. Rev. Environ. Resour. 38, 57-80.
- Bowman, D.M., Williamson, G.J., Abatzoglou, J.T., Kolden, C.A., Cochrane, M.A., Smith, A.M., 2017. Human exposure and
- 983 sensitivity to globally extreme wildfire events. Nat. Ecol. Evol. 1, 0058.
- 984 Brown, P.T., Hanley, H., Mahesh, A., Reed, C., Strenfel, S.J., Davis, S.J., Kochanski, A.K., Clements, C.B., 2023. Climate
  - warming increases extreme daily wildfire growth risk in California. Nature 621, 760-766.
- Callen, T., 2008. What is gross domestic product. Finance Dev. 45, 48–49.

Formatted: Header

Formatted: Font color: Auto

Formatted: Line spacing: Multiple 1,15 li

Formatted: Font color: Auto

Formatted: Line spacing: Multiple 1,15 li

Formatted: Font color: Auto

Formatted: Line spacing: Multiple 1,15 li

Formatted: Font color: Auto

Formatted: Line spacing: Multiple 1,15 li

Formatted: Font color: Auto

Formatted: Line spacing: Multiple 1,15 li

Formatted: Line spacing: Multiple 1,36 li

Formatted: Font: Not Bold

Formatted: Line spacing: 1,5 lines, Don't keep with I

- 987 Cardil, A., Vega-García, C., Ascoli, D., Molina-Terrén, D.M., Silva, C.A., Rodrigues, M., 2019. How does drought impact
- burnt area in Mediterranean vegetation communities? Sci. Total Environ. 693, 133603.
- 989 Carmona-Moreno, C., Belward, A., Malingreau, J. P., Hartley, A., Garcia-Alegre, M., Antonovskiy, M., Buchshtaber, V.,
- 990 Pivovarov, V., 2005. Characterizing interannual variations in global fire calendar using data from Earth observing satellites.
- 991 Glob. Change Biol. 11, 1537-1555.
- 992 Cary, G.J., Keane, R.E., Gardner, R.H., Lavorel, S., Flannigan, M.D., Davies, I.D., Li, C., Lenihan, J.M., Rupp, T.S., Mouillot,
  - F., 2006. Comparison of the Sensitivity of Landscape fire succession Models to Variation in Terrain, Fuel Pattern, Climate
- 994 and Weather, Landsc. Ecol. 21, 121–137. https://doi.org/10.1007/s10980-005-7302-9
- 995 Chen, Y., Hall, J., Van Wees, D., Andela, N., Hantson, S., Giglio, L., Van Der Werf, G.R., Morton, D.C., Randerson, J.T.,
  - 2023. Multi-decadal trends and variability in burnt area from the fifth version of the Global Fire Emissions Database (GFED5).
- 997 Earth Syst. Sci. Data 15, 5227-5259.
- 998 Chuvieco, E., Pettinari, M.L., Koutsias, N., Forkel, M., Hantson, S., Turco, M., 2021. Human and climate drivers of global
- 999 biomass burning variability. Sci. Total Environ. 779, 146361.
- 1000 Clarke, H., Tran, B., Boer, M.M., Price, O., Kenny, B., Bradstock, R., 2019. Climate change effects on the frequency,
- 1001 seasonality and interannual variability of suitable prescribed burning weather conditions in south-eastern Australia. Agric. For.
- 1002 Meteorol. 271, 148 157.

993

996

- 1003 CoreTeam, Rd., 2014. Vienna: R foundation for statistical computing, 2014.
- 1004 Cunningham, C.X., Williamson, G.J., Bowman, D.M.J.S., 2024. Increasing frequency and intensity of the most extreme
- 1005 wildfires on Earth, Nat. Ecol. Evol. 8, 1420 1425, https://doi.org/10.1038/s41559-024-02452-2
- Door Davies, K.W., Bates, J.D., Svejcar, T.J., Boyd, C.S., 2010. Effects of long term livestock grazing on fuel characteristics in
- 1007 rangelands: an example from the sagebrush steppe. Rangel. Ecol. Manag. 63, 662 669.
- 1008 de Jong, M.C., Wooster, M.J., Kitchen, K., Manley, C., Gazzard, R., McCall, F.F., 2016. Calibration and evaluation of the
- 1009 Canadian Forest Fire Weather Index (FWI) System for improved wildland fire danger rating in the United Kingdom. Nat.
- 1010 Hazards Earth Syst. Sci. 16, 1217 1237.
- 1011 DeWilde, L., Chapin, F.S., 2006. Human Impacts on the Fire Regime of Interior Alaska: Interactions among Fuels, Ignition
- 1012 Sources, and Fire Suppression. Ecosystems 9, 1342—1353. https://doi.org/10.1007/s10021-006-0095-0
- Doerr, S.H., Santín, C., 2016. Global trends in wildfire and its impacts: perceptions versus realities in a changing world. Philos.
- 1014 Trans. R. Soc. B Biol. Sci. 371, 20150345.
- 1015 Dormann, C.F., Elith, J., Bacher, S., Buchmann, C., Carl, G., Carré, G., Marquéz, J.R.G., Gruber, B., Lafourcade, B., Leitao,
- 1016 P.J., 2013. Collinearity: a review of methods to deal with it and a simulation study evaluating their performance. Ecography
- 1017 36, 27 46
- 1018 Dwyer, E., Pinnock, S., Grégoire, J. M., Pereira, J.M.C., 2000. Global spatial and temporal distribution of vegetation fire as
- 1019 determined from satellite observations. Int. J. Remote Sens. 21, 1289–1302.

- 1020 Earl, N., Simmonds, I., 2018. Spatial and temporal variability and trends in 2001–2016 global fire activity. J. Geophys. Res.
- 1021 Atmospheres 123, 2524 2536.
- 1022 Fang, L., Yang, J., Zu, J., Li, G., Zhang, J., 2015. Quantifying influences and relative importance of fire weather, topography,
- 1023 and vegetation on fire size and fire severity in a Chinese boreal forest landscape. For. Ecol. Manag. 356, 2 12.
  - Flannigan, M.D., Krawchuk, M.A., de Groot, W.J., Wotton, B.M., Gowman, L.M., 2009. Implications of changing climate for
- 1025 global wildland fire. Int. J. Wildland Fire 18, 483-507.
- 1026 Forkel, M., Andela, N., Harrison, S.P., Lasslop, G., Van Marle, M., Chuvieco, E., Dorigo, W., Forrest, M., Hantson, S., Heil,
- 1027 A., 2019a. Emergent relationships with respect to burnt area in global satellite observations and fire-enabled vegetation models.
- 1028 Biogeosciences 16, 57, 76.
- 1029 Forkel, M., Dorigo, W., Lasslop, G., Chuvieco, E., Hantson, S., Heil, A., Teubner, I., Thonicke, K., Harrison, S.P., 2019b.
- 1030 Recent global and regional trends in burnt area and their compensating environmental controls. Environ. Res. Commun. 1,
- 1031 <del>051005.</del>

1024

- 1032 Forrest, M., Hetzer, J., Billing, M., Bowring, S.P., Kosczor, E., Oberhagemann, L., Perkins, O., Warren, D., Arrogante Funes,
- 1033 F., Thonicke, K., 2024. Understanding and simulating cropland and non-cropland burning in Europe using the BASE (Burnt
- 1034 Area Simulator for Europe) model. EGUsphere 2024, 1 55.
- 1035 Fosberg, M.A., Cramer, W., Brovkin, V., Fleming, R., Gardner, R., Gill, A.M., Goldammer, J.G., Keane, R., Koehler, P.,
- 1036 Lenihan, J., 1999. Strategy for a fire module in dynamic global vegetation models. Int. J. Wildland Fire 9, 79 84.
- 1037 Gallardo, M., Gómez, I., Vilar, L., Martínez-Vega, J., Martín, M.P., 2016. Impacts of future land use/land cover on wildfire
- 1038 occurrence in the Madrid region (Spain). Reg. Environ. Change 16, 1047–1061.
- 1039 Haas, O., Prentice, I.C., Harrison, S.P., 2022. Global environmental controls on wildfire burnt area, size, and intensity. En viron.
- 1040 Res. Lett. 17, 065004.
- 1041 Hantson, S., Andela, N., Goulden, M.L., Randerson, J.T., 2022. Human ignited fires result in more extreme fire behavior and
- 1042 ecosystem impacts. Nat. Commun. 13, 2717.
- 1043 Hantson, S., Arneth, A., Harrison, S.P., Kelley, D.I., Prentice, I.C., Rabin, S.S., Archibald, S., Mouillot, F., Arnold, S.R.,
- 1044 Artaxo, P., 2016. The status and challenge of global fire modelling. Biogeosciences 13, 3359–3375.
- Hantson, S., Kelley, D.I., Arneth, A., Harrison, S.P., Archibald, S., Bachelet, D., Forrest, M., Hickler, T., Lasslop, G., Li, F.,
- 1046 Mangeon, S., Melton, J.R., Nieradzik, L., Rabin, S.S., Prentice, I.C., Sheehan, T., Sitch, S., Teckentrup, L., Voulgarakis, A.,
- 1047 Yue, C., 2020. Quantitative assessment of fire and vegetation properties in simulations with fire enabled vegetation models
- 1048 from the Fire Model Intercomparison Project. Geosci. Model Dev. 13, 3299–3318. https://doi.org/10.5194/gmd-13-3299-2020
- 1049 Hantson, S., Lasslop, G., Kloster, S., Chuvieco, E., 2015. Anthropogenic effects on global mean fire size. Int. J. Wildland Fire
- 1050 <del>24, 589 596.</del>
- 1051 Jain, P., Barber, Q.E., Taylor, S., Whitman, E., Acuna, D.C., Boulanger, Y., Chavardès, R.D., Chen, J., Englefield, P.,
- 1052 Flannigan, M., 2024. Canada Under Fire-Drivers and Impacts of the Record-Breaking 2023 Wildfire Season. Authorea Prepr.

- 1053 Jones, M.W., Abatzoglou, J.T., Veraverbeke, S., Andela, N., Lasslop, G., Forkel, M., Smith, A.J., Burton, C., Betts, R.A., van 1054
  - der Werf, G.R., 2022. Global and regional trends and drivers of fire under climate change. Rev. Geophys. 60, e2020RG000726.
- 1055 Joshi, J., Sukumar, R., 2021. Improving prediction and assessment of global fires using multilayer neural networks. Sci. Rep.
- 1056 11, 3295.
- 1057 Juli, G., Jon, E., Dylan, W., 2017. Flammability as an ecological and evolutionary driver. J. Ecol. 105.
- 1058 Kelley, D.I., Prentice, I.C., Harrison, S.P., Wang, H., Simard, M., Fisher, J.B., Willis, K.O., 2013. A comprehensive
- 1059 benchmarking system for evaluating global vegetation models. Biogeosciences 10, 3313-3340.
- 1060 Kelly, L.T., Fletcher, M. S., Menor, I.O., Pellegrini, A.F., Plumanns-Pouton, E.S., Pons, P., Williamson, G.J., Bowman, D.M.,
- 1061 2023, Understanding Fire Regimes for a Better Anthropocene, Annu, Rev. Environ, Resour, 48,
- 1062 Kendall, M., 1975. Multivariate analysis. Charles Griffin.
- 1063 Kloster, S., Mahowald, N.M., Randerson, J.T., Thornton, P.E., Hoffman, F.M., Levis, S., Lawrence, P.J., Feddema, J.J.,
- 1064 Oleson, K.W., Lawrence, D.M., 2010. Fire dynamics during the 20th century simulated by the Community Land Model.
- 1065 Biogeosciences 7, 1877 1902.
- 1066 Kloster, S., 2017. A human driven decline in global burnt area. Science 356, 1356–1362.
- 1067 Knorr, W., Arneth, A., Jiang, L., 2016. Demographic controls of future global fire risk. Nat. Clim. Change 6, 781-785.
- 1068 Knorr, W., Kaminski, T., Arneth, A., Weber, U., 2014, Impact of human population density on fire frequency at the global
- 1069 scale. Biogeosciences 11, 1085-1102.
- 1070 Koubi, V., 2019. Sustainable development impacts of climate change and natural disaster. Backgr. Pap. Prep. Sustain. Dev.
- 1071 Outlook.
- 1072 Kraaii, T., Baard, J.A., Arndt, J., Vhengani, L., Van Wilgen, B.W., 2018. An assessment of climate, weather, and fuel factors
- 1073 influencing a large, destructive wildfire in the Knysna region, South Africa, Fire Ecol. 14, 1-12.
- 1074 Krawchuk, M.A., Moritz, M.A., Parisien, M. A., Van Dorn, J., Hayhoe, K., 2009. Global pyrogeography: the current and
- 1075 future distribution of wildfire. PloS One 4, e5102.
- 1076 Kuhn-Régnier, A., Voulgarakis, A., Nowack, P., Forkel, M., Prentice, I.C., Harrison, S.P., 2021. The importance of antecedent
- 1077 vegetation and drought conditions as global drivers of burnt area. Biogeosciences 18, 3861-3879. https://doi.org/10.5194/bg-
- 1078 18-3861-2021
- 1079 Larsen, W.A. and McCleary, S.J., 1972. The use of partial residual plots in regression analysis. Technometrics, 14(3), pp.781-
- 1080
- 1081 Le Page, Y., Pereira, J.M.C., Trigo, R., Da Camara, C., Oom, D., Mota, B., 2008. Global fire activity patterns (1996-2006)
- 1082 and climatic influence: an analysis using the World Fire Atlas. Atmospheric Chem. Phys. 8, 1911 1924.
- 1083 Lehsten, V., Arneth, A., Spessa, A., Thonicke, K., Moustakas, A., 2016. The effect of fire on tree grass coexistence in
- 1084 savannas: a simulation study. Int. J. Wildland Fire 25, 137-146.

- 1085 Magadzire, N., 2013. Reconstruction of a fire regime using MODIS burnt area data: Charara Safari Area, Zimbabwe.
- 1086 Stellenbosch: Stellenbosch University.
- 1087 Mann, H.B., 1945. Nonparametric tests against trend. Econom. J. Econom. Soc. 245 259.
- 1088 MacCarthy J, Tyukavina A, Weisse MJ, Harris N, Glen E. Extreme wildfires in Canada and their contribution to global loss
- in tree cover and carbon emissions in 2023. Global Change Biology. 2024;30(6):e17392.
- 1990 Morvan, D., 2011. Physical phenomena and length scales governing the behaviour of wildfires: a case for physical modelling.
- 1091 Fire Technol. 47, 437-460.
- 1992 Mukunga, T., Forkel, M., Forrest, M., Zotta, R. M., Pande, N., Schlaffer, S., Dorigo, W., 2023. Effect of Socioeconomic
- 1093 Variables in Predicting Global Fire Ignition Occurrence. Fire 6, 197.
- 1994 Nolan, R.H., Anderson, L.O., Poulter, B., Varner, J.M., 2022. Increasing threat of wildfires: the year 2020 in perspective: A
- 1095 Global Ecology and Biogeography special issue. Glob. Ecol. Biogeogr. 31, 1898—1905. https://doi.org/10.1111/geb.13588
- 1096 O'brien, R.M., 2007. A caution regarding rules of thumb for variance inflation factors. Qual. Quant. 41, 673–690.
- 1997 Oliveira, S., Pereira, J.M., San-Miguel-Ayanz, J., Lourenço, L., 2014. Exploring the spatial patterns of fire density in Southern
- 1098 Europe using Geographically Weighted Regression, Appl. Geogr. 51, 143–157.
- 1099 Parisien, M. A., Parks, S.A., Krawchuk, M.A., Flannigan, M.D., Bowman, L.M., Moritz, M.A., 2011. Scale-dependent
- 100 controls on the area burnt in the boreal forest of Canada, 1980 2005. Ecol. Appl. 21, 789 805. https://doi.org/10.1890/10-
- 1101 <del>0326.1</del>
- 102 Pausas, J.G., Keeley, J.E., 2021. Wildfires and global change. Front. Ecol. Environ. 19, 387–395.
- Pausas, J.G., Ribeiro, E., 2013. The global fire productivity relationship. Glob. Ecol. Biogeogr. 22, 728-736.
- 104 Pechony, O., Shindell, D.T., 2010. Driving forces of global wildfires over the past millennium and the forthcoming century.
- 1105 Proc. Natl. Acad. Sci. 107, 19167 19170.
- 106 Perkins, O., Matej, S., Erb, K., Millington, J., 2022. Towards a global behavioural model of anthropogenic fire: The
- 107 spatiotemporal distribution of land-fire systems. Socio-Environ. Syst. Model. 4, 18130-18130.
- 108 Perry, G.L.W., 1998, Current approaches to modelling the spread of wildland fire: a review, Prog. Phys. Geogr. 22, 222 245.
- 109 Pfeiffer, M., Spessa, A., Kaplan, J.O., 2013. A model for global biomass burning in preindustrial time: LPJ LMfire (v1. 0).
- 1110 Geosci, Model Dev. 6, 643 685.
- 1111 Rabin, S.S., Melton, J.R., Lasslop, G., Bachelet, D., Forrest, M., Hantson, S., Kaplan, J.O., Li, F., Mangeon, S., Ward, D.S.,
- 1 2 2017. The Fire Modelling Intercomparison Project (FireMIP), phase 1: Experimental and analytical protocols with detailed
- 1113 model descriptions. Geosci. Model Dev. 10, 1175–1197.
- 1 A Robinne, F. N., Burns, J., Kant, P., Flannigan, M., Kleine, M., de Groot, B., Wotton, D.M., 2018. Global fire challenges in a
- 1115 warming world. IUFRO.
- 116 Saha, M.V., Scanlon, T.M., D'Odorico, P., 2019. Climate seasonality as an essential predictor of global fire activity. Glob.
- 1117 Ecol. Biogeogr. 28, 198 210.

- 1 18 Saunders, D.A., Hobbs, R.J., Margules, C.R., 1991. Biological Consequences of Ecosystem Fragmentation: A Review-
- 1119 Conserv. Biol. 5, 18 32. https://doi.org/10.1111/j.1523-1739.1991.tb00384.x
- 1 20 Son, R., Stacke, T., Gayler, V., Nabel, J. E. M. S., Schnur, R., Alonso, L., Requena Mesa, C., Winkler, A. J., Hantson, S.,
- 121 Zaehle, S., Weber, U., and Carvalhais, N.: Integration of a Deep Learning Based Fire Model Into a Global Land Surface
- 122 Model, Journal of Advances in Modelling Earth Systems, 16, e2023MS003710, https://doi.org/10.1029/2023MS003710, 2024.
- 1123 Shekede, M.D., Kusangaya, S., Chavava, C.B., Gwitira, I., Chemura, A., 2024. A two-decade analysis of the spatial and
- 1 temporal variations in burnt areas across Zimbabwe. PLOS Clim. 3, e0000201.
- 1125 Shikwambana, L., Kganyago, M., Xulu, S., 2022, Analysis of wildfires and associated emissions during the recent strong
  - ENSO phases in Southern Africa using multi-source remotely-derived products. Geocarto Int. 37, 16654-16670.
- 1127 Stott, P., 2000. Combustion in tropical biomass fires: a critical review, Prog. Phys. Geogr. Earth Environ, 24, 355–377.
- 1|128 https://doi.org/10.1177/030913330002400303
- 129 Strand, E.K., Launchbaugh, K.L., Limb, R.F., Torell, L.A., 2014. Livestock grazing effects on fuel loads for wildland fire in
- 1130 sagebrush dominated ecosystems. J. Rangel. Appl. 1, 35 57.
- 1131 Strydom, S., Savage, M.J., 2017. Potential impacts of climate change on wildfire dynamics in the midlands of KwaZulu-Natal,
- 1132 South Africa, Clim. Change 143, 385-397.
- 1133 Teckentrup, L., Harrison, S.P., Hantson, S., Heil, A., Melton, J.R., Forrest, M., Li, F., Yue, C., Arneth, A., Hickler, T., Sitch,
- 1134 S., Lasslop, G., 2019. Response of simulated burnt area to historical changes in environmental and anthropogenic factors: a
- 1 35 comparison of seven fire models. Biogeosciences 16, 3883-3910. https://doi.org/10.5194/bg-16-3883-2019
- 1136 Teixeira, J.C.M., Burton, C., Kelly, D.I., Folberth, G.A., O'Connor, F.M., Betts, R.A., Voulgarakis, A., 2023. Representing
- 1 37 socio-economic factors in the INFERNO global fire model using the Human Development Index. Biogeosciences Discuss.
- 1138 <del>2023, 1-27.</del>

1140

1126

- 139 Thonicke, K., Spessa, A., Prentice, I.C., Harrison, S.P., Dong, L., Carmona Moreno, C., 2010. The influence of vegetation,
  - fire spread and fire behaviour on biomass burning and trace gas emissions: results from a process-based model. Biogeosciences
- 1141 <del>7, 1991 2011.</del>
- 1 42 Vilar, L., Herrera, S., Tafur García, E., Yebra, M., Martínez-Vega, J., Echavarría, P., Martín, M.P., 2021. Modelling wildfire
- 1 43 occurrence at regional scale from land use/cover and climate change scenarios. Environ. Model. Softw. 145, 105200.
- 1 44 Wragg, P.D., Mielke, T., Tilman, D., 2018. Forbs, grasses, and grassland fire behaviour. J. Ecol. 106, 1983 2001.
- 1145 Wu, C., Venevsky, S., Sitch, S., Mercado, L.M., Huntingford, C., Staver, A.C., 2021. Historical and future global burnt area
- 1 146 with changing climate and human demography. One Earth 4, 517 530.
- 147 Xi, D.D., Taylor, S.W., Woolford, D.G., Dean, C.B., 2019. Statistical models of key components of wildfire risk. Annu. Rev.
- 1148 Stat. Its Appl. 6, 197 222.
- 1 49 Zhang, Y., Mao, J., Ricciuto, D.M., Jin, M., Yu, Y., Shi, X., Wullschleger, S., Tang, R., Liu, J., 2023. Global fire modelling
- 1 | 150 and control attributions based on the ensemble machine learning and satellite observations. Sci. Remote Sens. 7, 100088.

- Aldersley, A., Murray, S.J., Cornell, S.E., 2011. Global and regional analysis of climate and human drivers of wildfire. Sci.
- 1152 <u>Total Environ. 409, 3472–3481.</u>
- Andela, N., Morton, D.C., Giglio, L., Chen, Y., van der Werf, G.R., Kasibhatla, P.S., DeFries, R.S., Collatz, G.J., Hantson, S.,
- Kloster, S., 2017. A human-driven decline in global burned area. Science 356, 1356–1362.
- Archibald, S., 2016. Managing the human component of fire regimes; lessons from Africa. Philos. Trans. R. Soc. B Biol. Sci.
- 1 1 1 56 371, 20150346. https://doi.org/10.1098/rstb.2015.0346
- Australian Government, 2020. Estimating greenhouse gas emissions from bushfires in Australia's temperate forests: focus on
- 158 2019-20 (Technical Update), Australian Government, Department of Industry, Science, Energy and Resources.
- 1159 Bergado, J.R., Persello, C., Reinke, K., Stein, A., 2021. Predicting wildfire burns from big geodata using deep learning. Saf.
- 1160 Sci. 140, 105276.
- Bistinas, I., Harrison, S.P., Prentice, I.C., Pereira, J.M.C., 2014. Causal relationships versus emergent patterns in the global
- controls of fire frequency. Biogeosciences 11, 5087–5101.
- Blouin, K.D., Flannigan, M.D., Wang, X., Kochtubajda, B., 2016. Ensemble lightning prediction models for the province of
- 1164 Alberta, Canada. Int. J. Wildland Fire 25, 421–432.
- Bowman, D.M., Kolden, C.A., Abatzoglou, J.T., Johnston, F.H., van der Werf, G.R., Flannigan, M., 2020. Vegetation fires in
- the Anthropocene. Nat. Rev. Earth Environ. 1, 500–515.
- Bowman, D.M., O'Brien, J.A., Goldammer, J.G., 2013. Pyrogeography and the global quest for sustainable fire management.
- 1168 Annu. Rev. Environ. Resour. 38, 57–80.
- Bowman, D.M., Williamson, G.J., Abatzoglou, J.T., Kolden, C.A., Cochrane, M.A., Smith, A.M., 2017. Human exposure and
- sensitivity to globally extreme wildfire events. Nat. Ecol. Evol. 1, 0058.
- Brown, P.T., Hanley, H., Mahesh, A., Reed, C., Strenfel, S.J., Davis, S.J., Kochanski, A.K., Clements, C.B., 2023. Climate
- 1172 warming increases extreme daily wildfire growth risk in California. Nature 621, 760–766.
- 1173 Callen, T., 2008. What is gross domestic product. Finance Dev. 45, 48–49.
- 174 Canadell, J.G., Meyer, C.P., Cook, G.D., Dowdy, A., Briggs, P.R., Knauer, J., Pepler, A., Haverd, V., 2021. Multi-decadal
- increase of forest burned area in Australia is linked to climate change. Nat. Commun. 12, 6921.
- 1176 Cardil, A., Vega-García, C., Ascoli, D., Molina-Terrén, D.M., Silva, C.A., Rodrigues, M., 2019. How does drought impact
- burned area in Mediterranean vegetation communities? Sci. Total Environ. 693, 133603.
- 1178 Carmona-Moreno, C., Belward, A., Malingreau, J.-P., Hartley, A., Garcia-Alegre, M., Antonovskiy, M., Buchshtaber, V.,
- 1179 Pivovarov, V., 2005. Characterizing interannual variations in global fire calendar using data from Earth observing satellites.
- 1180 Glob. Change Biol. 11, 1537–1555.
- 181 Cary, G.J., Keane, R.E., Gardner, R.H., Lavorel, S., Flannigan, M.D., Davies, I.D., Li, C., Lenihan, J.M., Rupp, T.S., Mouillot,
- 182 F., 2006. Comparison of the Sensitivity of Landscape-fire-succession Models to Variation in Terrain, Fuel Pattern, Climate
- and Weather. Landsc. Ecol. 21, 121–137. https://doi.org/10.1007/s10980-005-7302-9

- 184 Chen, Y., Hall, J., Van Wees, D., Andela, N., Hantson, S., Giglio, L., Van Der Werf, G.R., Morton, D.C., Randerson, J.T.,
- 185 2023. Multi-decadal trends and variability in burned area from the fifth version of the Global Fire Emissions Database
- 1186 (GFED5). Earth Syst. Sci. Data 15, 5227–5259.
- 187 Chuvieco, E., Pettinari, M.L., Koutsias, N., Forkel, M., Hantson, S., Turco, M., 2021. Human and climate drivers of global
- biomass burning variability. Sci. Total Environ. 779, 146361.
- Il89 Clarke, H., Tran, B., Boer, M.M., Price, O., Kenny, B., Bradstock, R., 2019. Climate change effects on the frequency,
- 1 90 seasonality and interannual variability of suitable prescribed burning weather conditions in south-eastern Australia. Agric. For.
- 1191 <u>Meteorol. 271, 148–157.</u>
- 192 Copernicus Climate Change Service, 2021. Downscaled bioclimatic indicators for selected regions from 1979 to 2018 derived
- 1 193 <u>from reanalysis. https://doi.org/10.24381/CDS.FE90A594</u>
- 1194 CoreTeam, Rd., 2014. Vienna: R foundation for statistical computing, 2014.
- 195 Cunningham, C.X., Williamson, G.J., Bowman, D.M.J.S., 2024. Increasing frequency and intensity of the most extreme
- 1196 wildfires on Earth. Nat. Ecol. Evol. 8, 1420–1425. https://doi.org/10.1038/s41559-024-02452-2
- 197 Curasi, S.R., Melton, J.R., Arora, V.K., Humphreys, E.R., Whaley, C.H., 2024. Global climate change below 2° C avoids large
- 198 end century increases in burned area in Canada. Npj Clim. Atmospheric Sci. 7, 228.
- 199 Dantas De Paula, M., Gómez Giménez, M., Niamir, A., Thurner, M., Hickler, T., 2020. Combining European Earth
- 1200 Observation products with Dynamic Global Vegetation Models for estimating Essential Biodiversity Variables. Int. J. Digit.
- 1201 Earth 13, 262–277. https://doi.org/10.1080/17538947.2019.1597187
- 1202 Davies, K.W., Bates, J.D., Svejcar, T.J., Boyd, C.S., 2010. Effects of long-term livestock grazing on fuel characteristics in
- rangelands: an example from the sagebrush steppe. Rangel. Ecol. Manag. 63, 662–669.
- de Jong, M.C., Wooster, M.J., Kitchen, K., Manley, C., Gazzard, R., McCall, F.F., 2016. Calibration and evaluation of the
- 1205 Canadian Forest Fire Weather Index (FWI) System for improved wildland fire danger rating in the United Kingdom. Nat.
- 1206 Hazards Earth Syst. Sci. 16, 1217–1237.
- 1207 DeWilde, L., Chapin, F.S., 2006. Human Impacts on the Fire Regime of Interior Alaska: Interactions among Fuels, Ignition
- 1208 Sources, and Fire Suppression. Ecosystems 9, 1342–1353. https://doi.org/10.1007/s10021-006-0095-0
- 1209 DiMiceli, C.M., Carroll, M.L., Sohlberg, R.A., Huang, C., Hansen, M.C., Townshend, J.R., 2011. Annual global automated
- MODIS vegetation continuous fields (MOD44B) at 250 m spatial resolution for data years beginning day 65, 2000–2010,
- 1211 collection 5 percent tree cover. Univ. Md. Coll. Park MD USA 2011.
- 1212 Doerr, S.H., Santín, C., 2016. Global trends in wildfire and its impacts: perceptions versus realities in a changing world. Philos.
- 1213 Trans. R. Soc. B Biol. Sci. 371, 20150345.
- 1214 Dormann, C.F., Elith, J., Bacher, S., Buchmann, C., Carl, G., Carré, G., Marquéz, J.R.G., Gruber, B., Lafourcade, B., Leitão,
- 1215 P.J., 2013. Collinearity: a review of methods to deal with it and a simulation study evaluating their performance. Ecography
- 1216 <u>36, 27–46.</u>

- 1217 Dwyer, E., Pinnock, S., Grégoire, J.-M., Pereira, J.M.C., 2000. Global spatial and temporal distribution of vegetation fire as
- determined from satellite observations. Int. J. Remote Sens. 21, 1289–1302.
- 1219 Earl, N., Simmonds, I., 2018. Spatial and temporal variability and trends in 2001–2016 global fire activity, J. Geophys. Res.
- 1220 <u>Atmospheres 123, 2524–2536.</u>
- Fang, L., Yang, J., Zu, J., Li, G., Zhang, J., 2015. Quantifying influences and relative importance of fire weather, topography,
- and vegetation on fire size and fire severity in a Chinese boreal forest landscape. For. Ecol. Manag. 356, 2–12.
- Flannigan, M.D., Krawchuk, M.A., de Groot, W.J., Wotton, B.M., Gowman, L.M., 2009. Implications of changing climate for
- 1224 global wildland fire. Int. J. Wildland Fire 18, 483–507.
- 1225 Forkel, M., Andela, N., Harrison, S.P., Lasslop, G., Van Marle, M., Chuvieco, E., Dorigo, W., Forrest, M., Hantson, S., Heil,
- 1226 A., 2019. Emergent relationships with respect to burned area in global satellite observations and fire-enabled vegetation
- 1227 <u>models. Biogeosciences 16, 57–76.</u>
- 1228 Forrest, M., Hetzer, J., Billing, M., Bowring, S.P., Kosczor, E., Oberhagemann, L., Perkins, O., Warren, D., Arrogante-Funes,
- 1229 F., Thonicke, K., 2024. Understanding and simulating cropland and non-cropland burning in Europe using the BASE (Burnt
- 1230 Area Simulator for Europe) model. EGUsphere 2024, 1–55.
- 1231 Fosberg, M.A., Cramer, W., Brovkin, V., Fleming, R., Gardner, R., Gill, A.M., Goldammer, J.G., Keane, R., Koehler, P.,
- Lenihan, J., 1999. Strategy for a fire module in dynamic global vegetation models. Int. J. Wildland Fire 9, 79–84.
- 1233 Gallardo, M., Gómez, I., Vilar, L., Martínez-Vega, J., Martín, M.P., 2016. Impacts of future land use/land cover on wildfire
- 1234 occurrence in the Madrid region (Spain). Reg. Environ. Change 16, 1047–1061.
- Haas, O., Prentice, I.C., Harrison, S.P., 2022. Global environmental controls on wildfire burnt area, size, and intensity. Environ.
- 1236 Res. Lett. 17, 065004.
- Hantson, S., Arneth, A., Harrison, S.P., Kelley, D.I., Prentice, I.C., Rabin, S.S., Archibald, S., Mouillot, F., Arnold, S.R.,
- 1238 Artaxo, P., 2016. The status and challenge of global fire modelling. Biogeosciences 13, 3359–3375.
- Hantson, S., Kelley, D.I., Arneth, A., Harrison, S.P., Archibald, S., Bachelet, D., Forrest, M., Hickler, T., Lasslop, G., Li, F.,
- 1240 2020. Quantitative assessment of fire and vegetation properties in simulations with fire-enabled vegetation models from the
- 1241 Fire Model Intercomparison Project. Geosci. Model Dev. 13, 3299–3318.
- 1242 Hantson, S., Lasslop, G., Kloster, S., Chuvieco, E., 2015. Anthropogenic effects on global mean fire size. Int. J. Wildland Fire
- 1243 24, 589–596
- 1244 Jain, P., Barber, Q.E., Taylor, S., Whitman, E., Acuna, D.C., Boulanger, Y., Chavardès, R.D., Chen, J., Englefield, P.,
- 1245 Flannigan, M., 2024. Canada Under Fire-Drivers and Impacts of the Record-Breaking 2023 Wildfire Season. Authorea Prepr.
- Jones, M.W., Abatzoglou, J.T., Veraverbeke, S., Andela, N., Lasslop, G., Forkel, M., Smith, A.J., Burton, C., Betts, R.A., van
- der Werf, G.R., 2022. Global and regional trends and drivers of fire under climate change. Rev. Geophys. 60, e2020RG000726.
- 1248 Joshi, J., Sukumar, R., 2021. Improving prediction and assessment of global fires using multilayer neural networks. Sci. Rep.
- 249 <u>11, 3295.</u>

- 1250 Juli, G., Jon, E., Dylan, W., 2017. Flammability as an ecological and evolutionary driver. J. Ecol. 105.
- 1251 Kelley, D.I., Prentice, I.C., Harrison, S.P., Wang, H., Simard, M., Fisher, J.B., Willis, K.O., 2013. A comprehensive
- benchmarking system for evaluating global vegetation models. Biogeosciences 10, 3313–3340.
- Kelly, L.T., Fletcher, M.-S., Menor, I.O., Pellegrini, A.F., Plumanns-Pouton, E.S., Pons, P., Williamson, G.J., Bowman, D.M.,
- 1254 <u>2023. Understanding Fire Regimes for a Better Anthropocene. Annu. Rev. Environ. Resour. 48.</u>
- 1255 Kendall, M., 1975. Multivariate analysis. Charles Griffin.
- 1256 Klein Goldewijk, K., Beusen, A., Doelman, J., Stehfest, E., 2017. Anthropogenic land use estimates for the Holocene–HYDE
- 1257 3.2. Earth Syst. Sci. Data 9, 927–953.
- 1258 Kloster, S., Mahowald, N.M., Randerson, J.T., Thornton, P.E., Hoffman, F.M., Levis, S., Lawrence, P.J., Feddema, J.J.,
- 1259 Oleson, K.W., Lawrence, D.M., 2010. Fire dynamics during the 20th century simulated by the Community Land Model.
- 1260 <u>Biogeosciences 7, 1877–1902.</u>
- 1261 Knorr, W., Arneth, A., Jiang, L., 2016. Demographic controls of future global fire risk. Nat. Clim. Change 6, 781–785.
- 1262 Knorr, W., Kaminski, T., Arneth, A., Weber, U., 2014. Impact of human population density on fire frequency at the global
- 1263 <u>scale. Biogeosciences 11, 1085–1102.</u>
- 1264 Koubi, V., 2019. Sustainable development impacts of climate change and natural disaster. Backgr. Pap. Prep. Sustain. Dev.
- 1265 Outlook
- 1266 Kraaij, T., Baard, J.A., Arndt, J., Vhengani, L., Van Wilgen, B.W., 2018. An assessment of climate, weather, and fuel factors
- 1267 <u>influencing a large, destructive wildfire in the Knysna region, South Africa. Fire Ecol. 14, 1–12.</u>
- 1268 Krawchuk, M.A., Moritz, M.A., Parisien, M.-A., Van Dorn, J., Hayhoe, K., 2009. Global pyrogeography: the current and
- 1269 <u>future distribution of wildfire. PloS One 4, e5102.</u>
- 1270 Kuhn-Régnier, A., Voulgarakis, A., Nowack, P., Forkel, M., Prentice, I.C., Harrison, S.P., 2021. The importance of antecedent
- 1271 vegetation and drought conditions as global drivers of burnt area. Biogeosciences 18, 3861–3879.
- 1272 Le Page, Y., Morton, D., Bond-Lamberty, B., Pereira, J.M.C., Hurtt, G., 2015. HESFIRE: a global fire model to explore the
- role of anthropogenic and weather drivers. Biogeosciences 12, 887–903.
- Lehsten, V., Arneth, A., Spessa, A., Thonicke, K., Moustakas, A., 2016. The effect of fire on tree-grass coexistence in
- 1275 savannas: a simulation study. Int. J. Wildland Fire 25, 137–146.
- 1276 MacCarthy, J., Tyukavina, A., Weisse, M.J., Harris, N., Glen, E., 2024. Extreme wildfires in Canada and their contribution to
- global loss in tree cover and carbon emissions in 2023. Glob. Change Biol. 30, e17392. https://doi.org/10.1111/gcb.17392
- 1278 Mann, H.B., 1945. Nonparametric tests against trend. Econom. J. Econom. Soc. 245–259.
- Morvan, D., 2011. Physical phenomena and length scales governing the behaviour of wildfires: a case for physical modelling.
- 1280 Fire Technol. 47, 437–460.
- 1281 Mukunga, T., Forkel, M., Forrest, M., Zotta, R.-M., Pande, N., Schlaffer, S., Dorigo, W., 2023. Effect of Socioeconomic
- Variables in Predicting Global Fire Ignition Occurrence. Fire 6, 197.

Formatted Table

71

- Nolan, R.H., Anderson, L.O., Poulter, B., Varner, J.M., 2022. Increasing threat of wildfires: the year 2020 in perspective: A
- 1284 Global Ecology and Biogeography special issue. Glob. Ecol. Biogeogr. 31, 1898–1905. https://doi.org/10.1111/geb.13588
- Nurrohman, R.K., Kato, T., Ninomiya, H., Végh, L., Delbart, N., Miyauchi, T., Sato, H., Shiraishi, T., Hirata, R., 2024. Future
- 1286 prediction of Siberian wildfire and aerosol emissions via the improved fire module of the spatially explicit individual-based
- dynamic global vegetation model. EGUsphere 2024, 1–56.
- 1288 O'brien, R.M., 2007. A Caution Regarding Rules of Thumb for Variance Inflation Factors. Qual. Quant. 41, 673-690.
- 1289 <u>https://doi.org/10.1007/s11135-006-9018-6</u>
- 1290 Oliveira, S., Pereira, J.M., San-Miguel-Ayanz, J., Lourenço, L., 2014. Exploring the spatial patterns of fire density in Southern
- Europe using Geographically Weighted Regression. Appl. Geogr. 51, 143–157.
- 1992 O'Neill, B.C., Kriegler, E., Ebi, K.L., Kemp-Benedict, E., Riahi, K., Rothman, D.S., van Ruijven, B.J., van Vuuren, D.P.,
- Birkmann, J., Kok, K., Levy, M., Solecki, W., 2017. The roads ahead: Narratives for shared socioeconomic pathways
- 1294 describing world futures in the 21st century. Glob. Environ. Change 42, 169–180
- 1295 <u>https://doi.org/10.1016/j.gloenvcha.2015.01.004</u>
- Parisien, M.-A., Parks, S.A., Krawchuk, M.A., Flannigan, M.D., Bowman, L.M., Moritz, M.A., 2011. Scale-dependent
- 1297 controls on the area burned in the boreal forest of Canada, 1980–2005. Ecol. Appl. 21, 789–805. https://doi.org/10.1890/10-
- 1298 0326.1
- Pausas, J.G., Keeley, J.E., 2021. Wildfires and global change. Front. Ecol. Environ. 19, 387–395.
- Pausas, J.G., Ribeiro, E., 2013. The global fire–productivity relationship. Glob. Ecol. Biogeogr. 22, 728–736.
- Pechony, O., Shindell, D.T., 2010. Driving forces of global wildfires over the past millennium and the forthcoming century.
- 1302 Proc. Natl. Acad. Sci. 107, 19167–19170.
- 1803 Perkins, O., Matej, S., Erb, K., Millington, J., 2022. Towards a global behavioural model of anthropogenic fire: The
- spatiotemporal distribution of land-fire systems. Socio-Environ. Syst. Model. 4, 18130–18130.
- 1805 Perry, G.L.W., 1998. Current approaches to modelling the spread of wildland fire: a review. Prog. Phys. Geogr. 22, 222–245.
- 1B06 Pfeiffer, M., Spessa, A., Kaplan, J.O., 2013. A model for global biomass burning in preindustrial time: LPJ-LMfire (v1. 0).
- 1307 <u>Geosci. Model Dev. 6, 643–685.</u>
- Rabin, S.S., Melton, J.R., Lasslop, G., Bachelet, D., Forrest, M., Hantson, S., Kaplan, J.O., Li, F., Mangeon, S., Ward, D.S.,
- 1809 2017. The Fire Modeling Intercomparison Project (FireMIP), phase 1: Experimental and analytical protocols with detailed
- model descriptions. Geosci. Model Dev. 10, 1175–1197.
- 1311 Robinne, F.-N., Burns, J., Kant, P., Flannigan, M., Kleine, M., de Groot, B., Wotton, D.M., 2018. Global fire challenges in a
- 1312 warming world, IUFRO.
- 1\(\beta\)13 Running, S., Zhao, M., 2021. MODIS/Terra gross primary productivity gap-filled 8-day L4 global 500m SIN grid V061.
- NASA EOSDIS Land Process. Distrib. Act. Arch. Cent. DAAC Data Set MOD17A2HGF-061.

- 1815 Saha, M.V., Scanlon, T.M., D'Odorico, P., 2019. Climate seasonality as an essential predictor of global fire activity. Glob.
- 1316 <u>Ecol. Biogeogr. 28, 198–210.</u>
- 1317 Santoro, M., Cartus, O., 2023. ESA Biomass Climate Change Initiative (Biomass\_cci): Global datasets of forest above-ground
- 1318 biomass for the years 2010, 2017, 2018, 2019 and 2020, v4. No Title.
- 1319 Saunders, D.A., Hobbs, R.J., Margules, C.R., 1991. Biological Consequences of Ecosystem Fragmentation: A Review.
- 1320 Conserv. Biol. 5, 18–32. https://doi.org/10.1111/j.1523-1739.1991.tb00384.x
- 1821 Shekede, M.D., Kusangaya, S., Chavava, C.B., Gwitira, I., Chemura, A., 2024. A two-decade analysis of the spatial and
- temporal variations in burned areas across Zimbabwe. PLOS Clim. 3, e0000201.
- 1823 Shikwambana, L., Kganyago, M., Xulu, S., 2022. Analysis of wildfires and associated emissions during the recent strong
- 1324 ENSO phases in Southern Africa using multi-source remotely-derived products. Geocarto Int. 37, 16654–16670.
- 1825 Son, R., Stacke, T., Gayler, V., Nabel, J.E.M.S., Schnur, R., Alonso, L., Requena-Mesa, C., Winkler, A.J., Hantson, S., Zaehle,
- 1326 S., Weber, U., Carvalhais, N., 2024. Integration of a Deep-Learning-Based Fire Model Into a Global Land Surface Model. J.
- 1327 Adv. Model. Earth Syst. 16. https://doi.org/10.1029/2023ms003710
- 1328 Stott, P., 2000. Combustion in tropical biomass fires: a critical review. Prog. Phys. Geogr. Earth Environ. 24, 355–377.
- 1329 https://doi.org/10.1177/030913330002400303
- 1330 Strand, E.K., Launchbaugh, K.L., Limb, R.F., Torell, L.A., 2014. Livestock grazing effects on fuel loads for wildland fire in
- 1331 <u>sagebrush dominated ecosystems. J. Rangel. Appl. 1, 35–57.</u>
- 1832 Teckentrup, L., Harrison, S.P., Hantson, S., Heil, A., Melton, J.R., Forrest, M., Li, F., Yue, C., Arneth, A., Hickler, T., Sitch,
- 1333 S., Lasslop, G., 2019. Response of simulated burned area to historical changes in environmental and anthropogenic factors: a
- 1334 comparison of seven fire models. Biogeosciences 16, 3883–3910. https://doi.org/10.5194/bg-16-3883-2019
- 1835 Teixeira, J.C.M., Burton, C., Kelly, D.I., Folberth, G.A., O'Connor, F.M., Betts, R.A., Voulgarakis, A., 2023. Representing
- 1336 socio-economic factors in the INFERNO global fire model using the Human Development Index. Biogeosciences Discuss.
- 1337 2023, 1–27.
- 1338 Thonicke, K., Spessa, A., Prentice, I.C., Harrison, S.P., Dong, L., Carmona-Moreno, C., 2010. The influence of vegetation,
- fire spread and fire behaviour on biomass burning and trace gas emissions: results from a process-based model. Biogeosciences
- 1340 7, 1991–2011.
- 1B41 UCLouvain, 2017. ESA Climate Change Initiative-Land Cover. ESA CCI Land Cover Time-Ser.-Clim. Res. Data Package
- 1342 CRDP.
- 1343 Uddin, G.E., 2023. Human Development Index: A regional perspective. Int. J. Dev. Manag. Rev. 18, 125–140.
- 1844 Van Der Werf, G.R., Randerson, J.T., Giglio, L., Van Leeuwen, T.T., Chen, Y., Rogers, B.M., Mu, M., Van Marle, M.J.,
- 1\(\beta 45\) Morton, D.C., Collatz, G.J., 2017. Global fire emissions estimates during 1997–2016. Earth Syst. Sci. Data 9, 697–720.
- 1B46 Villarreal, S., Vargas, R., 2021. Representativeness of FLUXNET Sites Across Latin America. J. Geophys. Res.

73

1347 <u>Biogeosciences 126, e2020JG006090. https://doi.org/10.1029/2020JG006090</u>

1349	Wu, C., Venevsky, S., Sitch, S., Mercado, L.M., Huntingford, C., Staver, A.C., 2021. Historical and future global burned area	
1350	with changing climate and human demography. One Earth 4, 517–530.	
1351	Xi, D.D., Taylor, S.W., Woolford, D.G., Dean, C.B., 2019. Statistical models of key components of wildfire risk. Annu. Rev.	
1352	Stat. Its Appl. 6, 197–222.	
1353	Yang, H., Ciais, P., Santoro, M., Huang, Y., Li, W., Wang, Y., Bastos, A., Goll, D., Arneth, A., Anthoni, P., Arora, V.K.,	
1354	Friedlingstein, P., Harverd, V., Joetzjer, E., Kautz, M., Lienert, S., Nabel, J.E.M.S., O'Sullivan, M., Sitch, S., Vuichard, N.,	
1355	Wiltshire, A., Zhu, D., 2020. Comparison of forest above-ground biomass from dynamic global vegetation models with	
1356	spatially explicit remotely sensed observation-based estimates. Glob. Change Biol. 26, 3997–4012.	
1357	https://doi.org/10.1111/gcb.15117	
1358	Zhang, Y., Mao, J., Ricciuto, D.M., Jin, M., Yu, Y., Shi, X., Wullschleger, S., Tang, R., Liu, J., 2023. Global fire modelling	
1359	and control attributions based on the ensemble machine learning and satellite observations. Sci. Remote Sens. 7, 100088.	
1360	•	Formatted: Line spacing: Multiple 1,36 li
ı		. 3

Wragg, P.D., Mielke, T., Tilman, D., 2018. Forbs, grasses, and grassland fire behaviour. J. Ecol. 106, 1983–2001.

74

1348

Formatted: Header